



Call: H2020-SC5-2014-two-stage

Topic: SC5-01-2014

PRIMAVERA

Grant Agreement 641727



**PRocess-based climate sIMulation: AdVances in high resolution modelling and
European climate Risk Assessment**

Deliverable D10.4

***Scientific input for risk assessments for policy makers and
end-users***

Deliverable Title	Scientific input for risk assessments for policy makers and end users		
Brief Description	<p>For each use case construct a narrative, or storyline, of relevant meteorological events in current and future climate. These will include a statistical description and an underpinning scientific assessment on physical mechanisms causing the events and the ability of models to simulate those events. It will also include processing of output from PRIMAVERA models to user-relevant meteorological variables (for both policymakers and end users). The information will be complemented by information on local vulnerability and impact of events from WP11.</p>		
WP number	10		
Lead Beneficiary	David Brayshaw (UREAD)		
Contributors	<p>Alexander J. Baker (UREAD) Dragana Bojovic (BSC) Louis-Philippe Caron (BSC) Paula Gonzalez (UREAD) Rob Groenland (KNMI) Galina Guentchev (Met Office) Rein Haarsma (KNMI) Kevin Hodges (UREAD) Dimitris Kapetanakis (KNMI) Phillip Kreussler (BSC) Eveline van der Linden (KNMI) Julia Lockwood (Met Office) Erika Palin (Met Office) Malcolm Roberts (Met Office) Reinhard Schiemann (UREAD) Balakrishnan Solaraju Murali (BSC) Antonello Squintu (KNMI) Gustav Strandberg (SMHI) Gerard van der Schrier (KNMI) Benoît Vannière (UREAD) Pier Luigi Vidale (UREAD)</p>		
Creation Date	21/1/2020		
Version Number	5		
Version Date	30/6/2020		
Deliverable Due Date	30/6/2020		
Actual Delivery Date	30/6/2020		
Nature of the Deliverable	X	<p>R - Report P - Prototype D - Demonstrator O - Other</p>	
Dissemination Audience	X	<p>PU - Public</p> <p>PP - Restricted to other programme participants, including the Commission services</p> <p>RE - Restricted to a group specified by the consortium, including the Commission services</p> <p>CO - Confidential, only for members of the consortium, including the Commission services</p>	

Version	Date	Modified by	Comments
0	21/1/2020	D Brayshaw	Proposed outline
1	21/2/2020	D Brayshaw	Revised outline
2	29/5/2020	D Brayshaw	First (incomplete) draft
3	18/6/2020	D Brayshaw	Second draft
4	29/6/2020	D Brayshaw	Draft for submission
5	30/6/2020	D Brayshaw	Submitted version

Table of Contents

1	Executive Summary	12
1.1	<i>Scope.....</i>	12
1.2	<i>Agriculture and health.....</i>	13
1.3	<i>Insurance</i>	14
1.4	<i>Energy.....</i>	16
1.5	<i>Water</i>	17
1.6	<i>Transport.....</i>	17
2	Project Objectives	19
3	Detailed Report	20
3.1	<i>AMOC storylines and their impact on heatwaves and European agriculture and health</i>	20
3.2	<i>Impacts on the insurance sector from tropical cyclones, post-tropical cyclones and extratropical cyclones</i>	41
3.3	<i>Blocking, jets and consequences for wind power.....</i>	80
3.4	<i>Precipitation and the water sector</i>	111
3.5	<i>Management of low-temperature and high-temperature conditions in the transport sector</i>	
	116	
4	Lessons Learnt	146
5	Links Built	148
5.1	<i>Outside PRIMAVERA</i>	148
5.2	<i>Between PRIMAVERA workpackages</i>	149
6	References	150

List of Tables

Table 1: Correlations of maximum lifetime IKE (for the period from 1950-2050) with associated maximum wind speed, IKE area and minimum MSLP for the northern hemisphere.	49
Table 2: Temperature thresholds chosen by Vajda et al. (2011) as representative of hazardous conditions for European transport.....	118
Table 3 Summary of models analysed with approximate native horizontal resolutions at mid latitudes (50°N).....	125

List of Figures

Figure 1: Ocean heat transport at 26°N. The line shows 10-day filtered data. There is a decrease in northward heat transport after 2008-2009 of 0.17PW. Data from Bryden et al. (2020).....	21
Figure 2: Observed difference in temperature at 5m depth (2016 minus 2008 values). Surface waters are 2°C cooler over 8 years in the midocean region south of Iceland Figure from Bryden et al. (2020).	22
Figure 3: A comparison of time series from a climate simulation of the CM2.6 climate model, showing a decrease in sub-polar sea-surface temperature (dark blue) with a warming of the surface waters in the Gulf Stream region (red), along with a decrease in the overturning strength (light blue). The two regions are defined as in the inset. Figure from Caesar et al. (2018).	23
Figure 4: Composit analysis of surface heat flux over the North Atlantic (left) and sea-level pressure (right) using an index for central-eastern European surface air temperature. Positive values of the surface heat flux correspond to a release of heat and to anomalously high ocean surface temperature.....	24
Figure 5: Schematic picture of the atmospheric response to a cold anomaly in sea-surface temperature. The SST anomaly is depicted as the blue-ish area on the light blue surface. The black lines represent the change in geopotential height in response to the cooling of the air temperatures (blue lines). The bottom panel shows the enhance baroclinicity along the polar front (pink circles) and the vertical and downstream propagation of eddy activity (pink arrows). This leads to enhancement of the jet (black lines) and establish low and high pressure areas on either sides of the jet.	25
Figure 6: Summer-average sea-surface temperature anomalies and daily maximum air temperature anomalies over land for the 2015 (left). The right panel show the 850mb geopotential height anomaly for this summer. Figure from Duche et al. (2016).....	25
Figure 7: Summer mean climate change in the RCP 4.5 scenario simulations. (a) CMIP 5 model mean summer change (2071-2100) minus (1971-2000) in mean sea-level pressure. (b) As (a), but for the surface air temperature. (c) as (a) but for the turbulent ocean- atmosphere heat flux (positive upward). Figure from Haarsma et al. (2015).....	27

Figure 8: Relation of European climate variables to AMOC variations. (a) Regression (shaded (mm month ⁻¹)) and correlation (contours) of rainfall change onto AMOC change for the (2071–2100)–(1971–2000) inter-model variations. (b) As in (a), but for solar radiation (W m ⁻²). Figure from Haarsma et al. (2015)	27
Figure 9: The surface temperature warming by 2050 based on the Hadley Centre climate model (part of the Primavera suite of models) for various resolutions in ocean and atmosphere. The ‘warming hole’, the much less steep increase in warming – or even a decrease in warming – is stronger in the model configurations with a high-resolution ocean model.	29
Figure 10: Top: soil moisture content (m) climate change signal (future–present) in Europe for (a) spring and (b) summer in the high-resolution model. Bottom: (c–d) same but for difference in climate change signal between the high- and standard-resolution model. Figure from Van der Linden et al. (2019).	31
Figure 11: Climate change signal (future – present) of total cloud cover and surface solar radiation (top panel) and daily mean surface air temperature and soil moisture storage for T159 (dashed lines) and T799 (solid lines). Values are smoothed with a 20-day running mean filter and averaged over central-western Europe. Figure from Van der Linden et al. (2019).....	32
Figure 12: Density distributions of soil moisture anomalies over central-western Europe in April-June at low-resolution (upper left) and high-resolution (upper right). The lower panels show the same, but for the July-September season. The vertical black lines indicate the drought thresholds based on the 20 th percentile of present-day soil moisture anomaly distributions. Figure from Van der Linden et al. (2019). .	32
Figure 13: Discharge of the river Rhine at Lobith (the Netherlands) for the nine driest years on record. Data from Rijkswaterstaat	33
Figure 14: The Z500 level (contours) and SST (colour) as anomalies from the long-term mean for winter 1920/1921 (top), spring 1921 (middle) and summer 1921 (bottom), based on the 20th Century Reanalysis.	34
Figure 15: The 1921 storm track density anomaly for the northern hemisphere based on the 20th Century Reanalysis (left) and a reconstruction of individual storms based on synoptic charts from Erida (1922).....	34
Figure 16: Impact analysis following the categories defined by Stahl et al. (2016) for the 1921 drought vs. time, for (from top to bottom) the Netherlands, United Kingdom, Belgium, Czech Republic, Germany.	40
Figure 17: Specific impacts for ‘water supply’ (left panel) and ‘Agriculture and livestock farming’ (right panel) for each of the five analysed countries.	40
Figure 18 Insurance loss events during 2017. Source: Munich Re NatCatSERVICE.	42
Figure 19 Timeseries of various metrics of insurance loss arising from natural hazards: top panel – number of loss events; middle panel – overall losses and insured losses; bottom panel – loss events worldwide, comparing the nominal overall losses (losses recorded at the time) with inflation-adjusted (blue line) and normalised (GDP-adjusted; purple line) losses. Source: Munich Re NatCatSERVICE.....	43

Figure 20: Example of a wind speed field selected by the tracker. The storm centre as detected by the tracker is represented by the green dot. The 18 ms-1 isotachs are highlighted in yellow. All the grid points located within the isotachs are taken into consideration when calculating IKE.....	47
Figure 21: Scatter plot of storm area above 18 ms-1 wind speed threshold ("IKE area") against wind speed associated with maximum lifetime IKE of all the storms in the entire northern hemisphere from 1950-2050. IKE values are colour-coded for both resolutions, LR (circles) and HR (triangles). Regression lines are drawn in solid for LR and in dashed for HR. The regressions for the storms attributed to the WNP and NA are shown in blue and red, respectively. The dashed ellipses show an approximation of constant IKE values across the scatter plot.	48
Figure 22: Distribution of TCP5 in (a) observations and (b) in PRIMAVERA models. Solid curves stand for LR and dashed curve stands for HR.....	56
Figure 23: Composite of the 200 strongest tropical cyclones in the low-resolution AMIP configuration of each PRIMAVERA model over the period 1950-1965 [first row] and 2035-2050 [second row] and their difference.	57
Figure 24: Same as Figure 23 but for high-resolution AMIP simulations.....	57
Figure 25: Distribution in cumulative frequency of precipitation associated with all tropical vortices and averaged in a 5-degree radial cap for (a) 1950-1965, (b) 2035-2050 and (c) their difference normalised by the global mean surface temperature change. Plain curves stand for low-resolution and dashed curves for high-resolution.	58
Figure 26: Distribution of loss index from storms in low resolution (left) and high resolution (right) models. The observed distribution (ERA5) is shown with the thick black line. Note that the vertical axis is normalised by number of winters (approximately 64 years for each model, 35 years for ERA5) and the horizontal axis uses a log scale	64
Figure 27: CDFs of seasonal aggregate loss index from storms in low resolution (left) and high resolution (right) models. The observed distribution (ERA5) is shown in black. The points represent each season in the dataset.	65
Figure 28: Scatter plots of storm severity index against storm area for the low resolution (left) and high resolution (right) models. ERA5 footprints are shown with black filled circles. The black line is used to define 'high intensity, low area' storms (see text).	66
Figure 29: Time series of number of storm days (a) and total storm area (b) per season, for the low resolution models (grey) and ERA5 (black). c) and d) as above, but for the high resolution models. . Note that for the models were more than one ensemble member was available, only the first member has been analysed. Also the MPI-ESM1-2-HR model for the future period has been omitted from (a) and (b) due to an issue with the time coordinate in the sfcWindmax data (currently under investigation)	67
Figure 30: Track density—historical biases and model agreement. (a) multi-reanalysis mean, (b,c) highresSST-present and (d,e) hist-1950. Unit is cyclone transits per year per unit area (within a 5° geodesic radius of storm centres).	75

Figure 31: Track density—climate change response and model agreement. (a,b) highresSST-future minus highresSST-present and (c,d) highres-future minus hist-1950. Unit is cyclone transits per year per unit area (within a 5° geodesic radius of storm centres)	75
Figure 32: Interannual variability in (left) the number of extratropical transition events and (right) the percentage of tropical cyclones undergoing extratropical transition in the North Atlantic simulated by atmosphere-land-only simulations, compared with reanalyses. Legends show climatological mean values over the reanalysis period for (red) the multi-reanalysis mean, (solid black) low- and (dashed black) high-resolution ensemble means.....	76
Figure 33: As Figure 32 for the fully coupled simulations.....	77
Figure 34: Historical climate relative proportions of cyclone structures at time of landfall over Europe. Symmetrical (Sym.) / asymmetrical (Asym.) warm-core (WC) / cold-core (CC).....	78
Figure 35: Future climate relative proportions of cyclone structures at time of landfall over Europe. Symmetrical (Sym.) / asymmetrical (Asym.) warm-core (WC) / cold-core (CC).....	78
Figure 36: EOF1 and 2 patterns corresponding to the EOF decomposition of cold season filtered 850hPa zonal wind. Corresponding explained variances are indicated on top, in between parenthesis. Black contours are 850 hPa zonal wind historical mean for a qualitative comparison and are plotted every 2 m/s. Panels correspond to: a) ERA interim analysis (from Gonzalez et al. 2019), b) HadGEM3-GC3.1 model at MM (top) and HM (bottom) resolutions; c) CMCC-CM2 model at HR4 (top) and VHR4 (bottom) resolutions; and d) MPI-ESM1.2 model at HR (top) and XR (bottom) resolutions.....	83
Figure 37: Summary plot of the EOF analysis applied to filtered 850hPa zonal wind. The x axis presents the variance explained by EOF1 and the y axis for EOF2. Diagonal dashed lines correspond to different amounts of variance accumulated by the two. The black dot represents the values obtained for ERA-I and individual GCMs are included as different coloured dots: HadGEM3-GC3.1 in blue, CMCC-CM2 in green and MPI-ESM1.2 in red.....	83
Figure 38: Cold season coefficients of determination (R^2) between 10-day filtered 850 hPa zonal wind over the North Atlantic sector and the EOF-MLR estimated fields. a) Corresponds to ERA-I and b) to the CMIP5 multi-model mean (MMM), both adapted from Gonzalez et al. 2019. Individual PRIMAVERA GCMs are included as follows, with low and high resolutions respectively: c) and f) HadGEM3-GC3.1, d) and g) CMCC-CM2 and e) and h) MPI-ESM1.2.....	85
Figure 39: As Figure 38 but for European sector 10m wind speeds.....	86
Figure 40: (a) Multi-model mean (MMM) GCM-based change for the 10-day filtered 850 hPa zonal wind field (left) and the EOF-MLR estimated fields (right) in m/s. The black contours represent the historical MMM mean field plotted every 2 m/s. (Adapted from Gonzalez et al. 2019). Similar plot for individual PRIMAVERA GCMs are presented as: b) and e) HadGEM3-GC3.1; c) and f) CMCC-CM2; d) and g) MPI-ESM1.2. Colour scales vary with each dataset.	87

Figure 41: As in Figure 40 but for European sector 500hPa wind speeds.....	88
Figure 42: As in Figure 40 but for European sector 10m wind speeds.....	89
Figure 43: Distribution of 880 GW PV (left) and 440 GW wind turbines (right) over Europe in 2050, produced with the CLIMIX model with a spatial resolution of 0.11° latitude-longitude (figure from Ravestein et al. 2018).....	92
Figure 44: Difference (in pp) between the average PVpot in the summer (JJA) under 2050 weather conditions in each scenario and those under observed weather conditions (in 1981-2010) . The upper two represent the sNAO positive phase, the lower two the negative sNAO phase. The moderate and high global warming scenarios are shown on the left and right, respectively.....	93
Figure 45: Difference (in pp) the average Wpot at 80 m in the summer (JJA) under 2050 weather conditions in each scenario with those under observed weather conditions (in 1981-2010). The upper two represent the sNAO positive phase, the lower two the negative sNAO phase. The moderate and high global warming scenarios are shown on the left and right, respectively.....	94
Figure 46: Difference (in pp) between the average PVpot in the winter (DJF) under 2050 weather conditions in each scenario and those under observed weather conditions (in 1981-2010) . The upper two represent the sNAO positive phase, the lower two the negative NAO phase. The moderate and high global warming scenarios are shown on the left and right, respectively weather conditions in each scenario and those under observed weather conditions (in 1981-2010) . The upper two represent the NAO positive phase, the lower two the negative sNAO phase. The moderate and high global warming scenarios are shown on the left and right, respectively.....	95
Figure 47: Difference (in pp) the average Wpot at 80 m in the winter (DJF) under 2050 weather conditions in each scenario with those under observed weather conditions (in 1981-2010). The upper two represent the NAO positive phase, the lower two the negative NAO phase. The moderate and high global warming scenarios are shown on the left and right, respectively.....	96
Figure 48: Presenting the Wpot, PVpot, and HDD percentage differences between the three lowest production months in winter and the average of the respective months over both NAO phases.....	99
Figure 49: Probability of observing low wind days given the occurrence of winter blocking. Top panels correspond to ATL blocking and bottom panels to GRL blocking. a) and d) present the probabilities corresponding to ERA-I, b) and e) those for the LR version of HadGEM3-GC3.1, and c) and f) to the HR version of the same model. Purple shades indicate an exceedance with respect to the climatological probability, which is 20% by definition.....	102
Figure 50: Probability of observing low temperature days given the occurrence of winter blocking. Top panels correspond to ATL blocking and bottom panels to GRL blocking. a) and d) present the probabilities corresponding to ERA-I, b) and e) those for the LR version of HadGEM3-GC3.1, and c) and f) to the HR version of the same model. Green shades indicate an exceedance with respect to the climatological probability, which is 20% by definition.....	103

Figure 51: Probability of the joint occurrence of low wind and low temperature days given the presence of winter blocking. Top panels correspond to ATL blocking and bottom panels to GRL blocking. a) and d) present the probabilities corresponding to ERA-I, b) and e) those for the LR version of HadGEM3-GC3.1, and c) and f) to the HR version of the same model. Probabilities are expressed as differences with respect to the climatological value, which varies for each country. Purple shades indicate an exceedance with respect to the climatological probability.....	104
Figure 52: Projected changes in MOHC winter regional blocking statistics from the comparison of the highresSST-present and highresSST-future scenarios. Top panel presents percent changes in duration and bottom panel in frequency [%].....	105
Figure 53: Projected probability of observing low wind days given the occurrence of winter regional blocking in MOHC under the highresSST-future scenario. a) ATL blocking in the LR version; b) ATL blocking in the HR version; GRL blocking in the LR version; d) GRL blocking in the HR version.....	106
Figure 54: Projected probabilities of observing cold days given the occurrence of winter regional blocking in MOHC under the highresSST-future scenario. a) ATL blocking in the LR version; b) ATL blocking in the HR version; GRL blocking in the LR version; d) GRL blocking in the HR version.....	107
Figure 55: Projected probabilities of observing joint LW and CE days given the occurrence of winter regional blocking in MOHC under the highresSST-future scenario. a) ATL blocking in the LR version; b) ATL blocking in the HR version; GRL blocking in the LR version; d) GRL blocking in the HR version.....	108
Figure 56. Change in average precipitation (%) 2021-2050 compared to 1981-2010 in winter (DJF, left) and summer (JJA, right) for 9 Primavera models.....	112
Figure 57. Change in the annual number of days with daily precipitation above 10 mm (r10mm, (days), left) and in the maximum one-day precipitation (rx1day (%), right); 2021-2050 compared to 1981-2010 for 9 Primavera models.....	113
Figure 58 Frequency of weather patterns during days with minimum temperatures below 0°C; 30 weather patterns defined by Robert Neal.....	120
Figure 59 Weather patterns occurring most frequently during days with minimum temperatures below 0°C in Dublin, Ireland.....	121
Figure 60 Frequency of weather patterns during days with maximum temperature above 25°C in Dublin.....	122
Figure 61 Weather patterns occurring most frequently during days with maximum temperatures above 25°C in Dublin, Ireland.....	123
Figure 62 Frequency of weather patterns during days with maximum temperature above 25°C in London.....	124
Figure 63 Weather pattern 2 occurring frequently during days with maximum temperatures above 25°C in London, Great Britain.....	125
Figure 64 Biases in annual number of Frost Days (FD) as indicated by a set of AMIP low-resolution PRIMAVERA models for 1950-2014, compared to EOBS. All models and observations re-gridded to the HadGEM3-GC31-LM model grid. Negative values indicate areas where modelled numbers of frost days are smaller than those observed.....	126

Figure 65 Biases in annual number of Frost Days (FD) as indicated by a set of AMIP high-resolution PRIMAVERA models for 1950-2014, compared with EOBS. All models and observations re-gridded to the MPI-ESM1-2-XR model grid.....	127
Figure 66 Biases in annual number of Frost Days (FD) as indicated by a set of coupled low-resolution PRIMAVERA models for 1950-2014, compared to EOBS. All models and observations re-gridded to the HadGEM3-GC31-LL model grid.....	128
Figure 67 Biases in annual number of Frost Days (FD) as indicated by a set of coupled high-resolution PRIMAVERA models for 1950-2014, compared with EOBS. All models and observations re-gridded to the MPI-ESM1-2-XR model grid.....	129
Figure 68 Bias improvement between AMIP and coupled low-resolution simulations for 1950-2014; positive values indicate that the coupled models have smaller biases when compared with EOBS; models re-gridded to HadGEM3-GC31-LL	130
Figure 69 Bias improvement between AMIP and coupled high-resolution simulations for 1950-2014; positive values indicate that the coupled models have smaller biases when compared with EOBS; models re-gridded to HadGEM3-GC31-LL	131
Figure 70 Future changes in annual frequency of Frost Days (2015-2050 minus 1980-2014) for coupled simulations from the low- and high-resolution PRIMAVERA models. The EOBS frost days are calculated for the period 1980-2014.....	132
Figure 71 Biases in the frequency of TX32 in PRIMAVERA low-resolution coupled models for 1950-2014 compared with EOBS; Models re-gridded to HadGEM3-GC31-LL grid.....	133
Figure 72 Biases in the frequency of TX32 in PRIMAVERA high-resolution coupled models for 1950-2014 compared with EOBS; Models re-gridded to MPI-ESM1-2-XR grid.....	134
Figure 73 Future changes in frequency of TX32 days as represented by low-resolution PRIMAVERA models, 2015-2050 minus 1980-2014. The EOBS frequency of hot days is also included for comparison (1980-2014)	135
Figure 74 Future changes in frequency of TX32 days as represented by high-resolution PRIMAVERA models, 2015-2050 minus 1980-2014. The EOBS frequency of hot days is also included for comparison (1980-2014)	136
Figure 75 Biases in the frequency of SU in PRIMAVERA low-resolution coupled models for 1950-2014 compared with EOBS; Models re-gridded to HadGEM3-GC31-LL grid.....	137
Figure 76 Biases in the frequency of SU in PRIMAVERA high-resolution coupled models for 1950-2014 compared with EOBS; Models re-gridded to MPI-ESM1-2-XR grid.....	138
Figure 77 Future changes in frequency of SU as represented by low-resolution PRIMAVERA models, 2015-2050 minus 1980-2014; The EOBS frequency of these days is also included for comparison (1980-2014)	139
Figure 78 Future changes in frequency of SU as represented by high-resolution PRIMAVERA models, 2015-2050 minus 1980-2014; The EOBS frequency of these days is also included for comparison (1980-2014)	140

1 Executive Summary

1.1 Scope

This deliverable, D10.4, concerns the use of PRIMAVERA model output data for the construction of scientific risk assessments relating to societally relevant meteorological hazards. In particular, this document seeks to construct a set of scientific narratives which relate the physical climate simulations produced within PRIMAVERA to the sectoral use-cases proposed in deliverable D10.1. It therefore draws upon the work of WP10 and 11 (particularly in deliverable D10.1 and D11.6, and tasks T11.2 and 11.3) wherein key meteorological hazards impacting different sectors (health, agriculture, water, energy, insurance, transport) were discussed and identified in conjunction with users and stakeholders. This deliverable also draws upon the cumulative outputs and analysis from WP1, 2, 3, 5 and 10, focussing particularly on the Stream 1 integrations. Thus, while this present document focusses on the construction of sectorally-relevant scientific narratives associated with present and future climate, it should be read in conjunction with deliverables D10.2 and D10.3 which provide a broader contextual evaluation of the qualities of the PRIMAVERA simulations and the benefits (or otherwise) of increased horizontal resolution.

Not all of the use-cases identified in D10.1 were appropriate for development as scientific narratives or storylines. Instead, five distinct use-cases where there is a clear link between physical climate processes and socio-economic impacts are selected as the focus of this document. These are:

- heatwaves and droughts/health/agriculture;
- cyclones/insurance;
- blocking/jets/energy;
- precipitation/water; and
- extreme temperatures/transport.

Each of these five use-cases is addressed individually in the document that follows. In each use-case, a narrative or a storyline is presented linking the physical nature of the meteorological hazard such as storms or blocking to (a) the simulation of these hazards by the PRIMAVERA models (including projected changes between “present day” and mid-21st century); and (b) the consequences and implications for the relevant sector. Europe is typically the geographical focus of these studies and, as a consequence, Euro-Atlantic meteorology is a central concern (e.g., blocking and mid-latitude storms feature in multiple use-case narratives), but not exclusively (e.g., tropical cyclones pose a threat to European commercial interests, particularly in insurance, while drought with uneven distribution over Europe presents threat to the agricultural sector).

1.2 Agriculture and health

The impacts of climate variability and climate change on agriculture and health are vast and diverse. In this report we limit ourselves only to one aspect of the spectrum of climatic variability: heatwaves and droughts. Summer droughts and heatwaves often go hand-in-hand as dry soils feed back on the radiation balance and further increase surface air temperature.

The combination of droughts and heatwaves are viewed by MunichRe as an explosive combination. In recent years, Europe has seen many devastating heat waves and 2018 was a year where the combination of a drought and hot weather caused massive reductions in crop yields, while forest fires were abundant in Scandinavia. The consequences are billion-dollar losses for agriculture. In some cases, entire harvests have been lost.

Agriculture and forestry are not the only areas to feel the impact of heatwaves and droughts. MunichRe makes clear that these extreme conditions also pose a danger to life and health and cause material damage and business interruption. Shipping and energy are also among the areas of industry affected, for instance if river water levels drop or power plants have to be shut down due to a lack of cooling water. Extreme heat can also have a negative impact on tourism. The insurance sector has seen one particular issue grow in significance in recent years — the increased risk of wildfires.

The aim of this report is not to give an extensive overview of possible droughts that can occur in Europe as the climate warms, nor an in-depth analysis of the changes that catastrophic droughts will hit the continent. Instead we focus on one particular storyline where drought over western and central Europe is related to a persistent anti-cyclone over the British Isles bringing stable conditions and dry weather. In the perspective of Global Climate Models, this high-pressure area is related to a cooling of the northern North Atlantic which is, in its turn, related to a decrease in the Atlantic Meridional Overturning Circulation.

Although there are observations that the strength of the overturning is decreasing as a result of global higher air temperatures, nevertheless, the fate of the overturning is an uncertain factor. The perspective of the modelling community on the future overturning strength depends on which configuration of global climate models is used. The configuration with a spatial resolution of the current CMIP5 model generation shows a decreasing strength of the overturning in response to global warming, but not as strong as the perspective from the latest generation high-resolution climate models provides. This discrepancy is the basis of the storylines presented in this report.

Drought and heat waves impact the society in many ways. In order to sketch the impacts of the combination of a drought and heat wave in the story line on this topic, we revert to an observed situation which has similarities (in terms of drivers) with the drought discussed in the storylines. Based on written reports on impacts of the drought and accompanying heat wave in this year, an overview is made of impacts to society. These impacts are similar as the impacts MunichRe has reported-on for the 2018 drought.

1.3 Insurance

As a large portion of the costs caused by cyclones is insured (Munich Re 2018), insurance companies are highly interested in predicting storm activity and the associated potential damages and losses. Tropical, post-tropical and extratropical cyclones (TCs, PTCs and ETCs) all result in insurance losses in Europe, whether or not their physical impacts are experienced there directly. The ability of PRIMAVERA models to simulate a range of key features of these storms has been evaluated: the representation of integrated kinetic energy (a metric of damage potential) and the precipitation and moisture budget in TCs; the ability of the models to improve (compared with current models) on information that can be processed to create ETC event sets for use in catastrophe modelling; and the ability of models to adequately represent the tropical-to-extratropical transition.

Traditionally, the destructive potential of TCs is estimated using the maximum 1-minute sustained wind speed and their corresponding classification on the Saffir-Simpson scale, or the Accumulated Cyclone Energy index and the Power Dissipation Index. However, all these metrics neglect a key storm component when it comes to estimating damages: the storm size. It is possible that by focusing on such metrics when estimating the probable impact of climate change on TC activity and neglecting a key factor driving losses, our projected changes in TC activity will not be representative of the associated losses. Here, the intensity metric Integrated Kinetic Energy (IKE), which takes into account storm size and correlates more closely with damages than other commonly used metrics, is evaluated in PRIMAVERA models and the effect of resolution is investigated. By using a metric which tracks more closely with insured losses, we aim to make analyses of TC activity in climate models more relevant to the insurance sector. In our study, we showed that storm's IKE is relatively insensitive to model resolution. However, we also showed that the origin of the IKE is very different between a high-resolution (HR) and a low-resolution (LR) model configuration. While in HR, the storms are more intense than in LR, the LR compensates by creating larger storms such that the total IKE is comparable in both cases. However, because there is a larger number of storms and a more realistic geographical distribution in HR, the IKE accumulated over a given season is larger and closer to observed values in the HR. We note that our study was

undertaken using only one GCM, the CNRM-CM6 model, in both LR and HR configurations, using simulations performed in atmosphere-only mode. We are currently extending our analysis to verify whether these results are robust to coupling and whether they apply to other models as well.

Upon landfall, tropical cyclone precipitation, sometimes in association with surge, can be responsible for wide-spread flooding. As exemplified by hurricane Harvey in 2017, freshwater flooding can occur inland, far from coastal areas, where owners are not always insured for such hazards. Evaluating the fidelity of tropical cyclone precipitation in GCMs is of interest for insurance activities in at least two different respects: first, for improving TC flood forecasting, and second, for evaluating how the return period of extreme precipitation events will change in future. First, TC flood forecasting requires to predict accurately tropical cyclone tracks, the amount and distribution of precipitation and how precipitation is integrated in a flood model, and to do so several days ahead to allow time for early warnings. The uncertainty of the evolution of the weather is accounted for by a probabilistic approach, often at the expense of GCMs horizontal resolution. Our analysis of the PRIMAVERA ensemble has investigated, in a systematic way, how tropical cyclone precipitation benefits from increasing GCM resolution. Second, the PRIMAVERA simulations show a large inter-model spread of projections of TC precipitation, which we have been able to relate to the detail of its distribution in the frame of reference of the storm in each model. This work will help to predict with more confidence the change of extreme precipitation associated with tropical cyclones in a future climate.

Other work has created ETC event sets from high-resolution models and explored their potential value in understanding insurance losses. Event sets are used to provide input to catastrophe modelling in the insurance sector, so the interest here is in understanding whether PRIMAVERA models are better than existing sources of climate information at simulating these events. It was found that the higher-resolution set of models show an improvement in distribution of storm losses compared to the low-resolution models, but this does not have much effect on the distribution of seasonal aggregate loss. The low-resolution models, however, tend to produce storms with extremely high losses which dominate a season. These losses are highly uncertain due to the bias correction method. Overall, however, both sets of models compare reasonably well to observations and may therefore be useful for insurers to understand long term windstorm risk. A (re)insurance broker organisation has been testing the footprint data and has found that the results are in line with industry catastrophe models.

Finally, the nature of the tropical-to-extratropical transition of cyclones in different high-resolution models is analysed. Although rare, landfalling PTCs are an important natural hazard for Europe. Historical high-impact European events, such as Debby (1982), Floyd (1999) and Ophelia (2017), brought the potential risks associated with PTCs to the attention of policy-makers, the insurance sector, and the public. Many storms originating in the tropics undergo a complex structural evolution, including

extratropical transition, and the simulation of these processes is expected to benefit from increased horizontal resolution. PRIMAVERA offered an opportunity to move beyond case studies to examine PTC risk systematically across models using objective identification and classification methods.

1.4 Energy

With increases in the penetration of renewable energy sources, the climate sensitivity of the energy systems has also increased significantly. In this context, understanding the impacts of weather and climate variability on the European energy sector, and projecting likely future changes is very relevant and timely. The enhanced resolution of the PRIMAVERA models has been shown to lead to a better representation of different aspects of European weather and climate and are therefore well suited to impact studies.

Research focused on future projections of three dynamical processes that play a fundamental role in conditioning wind speeds –and therefore wind power– over Europe were performed. An analysis of the likely changes in the North Atlantic jet and its impacts on near-surface winter mean wind speeds over Europe revealed a large level of uncertainty in the future changes in these variables, arising both from model spread but also from dramatic changes between horizontal resolutions of the same model. On seasonal-to-interannual timescales, a study exploring the role of the North Atlantic Oscillation (NAO) on the future vulnerability of renewable energy sources was introduced. It showed that even though climate change is likely to impact future renewable energy resources over Europe, these impacts are smaller than the variability induced by the change in NAO and its summer counterpart, especially in the case of wind power. Atmospheric blocking, a much shorter-lived weather-scale phenomena, is known to have large impact on the European energy systems, by promoting very cold events that further enhance winter peak demand. Furthermore, it is shown here that due to its impact on low wind events, it can lead to a double challenge in some countries with significant wind power penetrations. Low temperature, low wind and a combination of the two are all more likely to be observed during winter blocking conditions over a large area of central and northern Europe. Initial projections suggest that winter blocking is likely to become less frequent over Europe, but preliminary results also suggest that these compound low-wind low-temperature events will remain more likely during blocking conditions (as opposed to under “non-blocked” conditions).

The significant levels of uncertainty present in the future projections associated with these energy system-relevant processes suggest that for planning purposes, the focus should be put on designing systems that are resilient to current climate and weather variability. The impacts of such events, however, can still be larger than

under current conditions due to the enhanced sensitivity associated to increases in the penetration of weather-sensitive renewable energy sources.

1.5 Water

The diverse water sector needs information about how precipitation is projected to change in the future. Depending on the branch of the sector different types of precipitation are interesting: short term, long term, seasonal sum or number of precipitation days. It makes a large difference whether the same precipitation amount falls over one day or over a month. Thus, there is not a unique measure to evaluate how changes in precipitation impact the water sector.

In general, average precipitation is projected to increase in northern Europe and decrease in southern Europe. The increase in the north is largest in winter; the decrease in the south is largest in summer. The change in the most extreme precipitation shows a complex pattern. On the large scale, the tendency is that extreme precipitation will increase in the future, also in regions with decreasing average precipitation. Both the amount and intensity of precipitation is projected to change in the future.

Future changes in precipitation mean that the water sector will face new problems. Depending on the region and season water availability will decrease or increase. In a warmer climate less precipitation will fall as snow which has an impact on runoff and stream flows. This means that hydro power usage patterns will have to adapt. In southern Europe, irrigation may have to be limited during the dry season to save water, while in northern Europe measures may have to be taken to handle the increased amounts of water. In addition, extreme precipitation may increase all over Europe, which means that all cities need to be prepared for more flash floods.

Every part of the water sector will need to reflect on their particular vulnerabilities and potential ways to adapt. This section only looks at changes up until 2050, but climate change will continue also in the latter half of this century, which also means that adaptation measure will have to be ongoing.

1.6 Transport

The transport sector is strongly impacted by a variety of weather events, such as high and low temperatures, high winds, excess precipitation, and coastal hazards. Following interactions with users from a transport infrastructure organization, this research focused on evaluation of the simulation of the frequency of low-temperature events (frost days) and the processes leading to their occurrence. In addition, we

explored the representation of, and future changes, in days with temperatures exceeding two high-temperature thresholds (summer days and hot days) identified as leading to pronounced impacts on the transport sector.

The main process leading to the development of extreme high- and low-temperature episodes is a persistent high-pressure blocking feature over or close to an area of interest. These high-pressure features impede the advancement of storms from west to east along the North Atlantic storm track, thus leading to more stagnant (blocked) conditions. Improvements in the representation of some aspects of blocking in the PRIMAVERA models compared with CMIP5, and in the high-resolution PRIMAVERA models compared with the low-resolution PRIMAVERA models, were identified in research from WP2. However, there is less progress in the representation of blocking persistence, which is likely to be important for the occurrence of prolonged hot or cold spells.

The representation of frost days is considered within atmosphere-only (AMIP) and coupled model simulations from five models developed by the MOHC, MPI, ECMWF, EC-Earth Consortium and CMCC modelling centres. The AMIP models underestimate the number of frost days during the historical period, whereas the coupled models predominantly overestimate them. The atmosphere-only results are corroborated by Squintu et al. (2020) who found that the AMIP simulations display “warmer trends in the winter extremes” than those observed, leading to the simulation of too few frost days. Our analyses indicate that the coupled models are characterized by biases of slightly greater magnitude in the frequency of frost days compared to the AMIP simulations. Overall, the PRIMAVERA models project a decrease in the frequency of frost days in the future.

The analyses of the number of hot days focused on the entire European continent. The coupled PRIMAVERA models generally underestimated the frequency of hot days in Spain while overestimating the numbers in south-eastern Europe and Italy. The number of summer days, which were evaluated over Ireland and Great Britain only, were generally underestimated by the PRIMAVERA models during the historical period (1950-2014). The low- and high-resolution PRIMAVERA models projected increases in the frequency of hot and summer days, and also in the areas affected by them. Specifically, the areas affected by hot days are projected to expand northwards in the future.

The balance between high and low temperature extremes is relevant for the management of the associated transport impacts. The type of information provided by our research using the state-of-the-art PRIMAVERA models provide support regarding the projected changes in the balance between these two extremes, which in turn could be considered in weather resilience and climate change adaptation activities in the sector.

2 Project Objectives

With this deliverable, the project has contributed to the achievement of the following objectives (DOA, Part B Section 1.1) WP numbers are in brackets:

No.	Objective	Yes	No
A	To develop a new generation of global high-resolution climate models. (3, 4, 6)		X
B	To develop new strategies and tools for evaluating global high-resolution climate models at a process level, and for quantifying the uncertainties in the predictions of regional climate. (1, 2, 5, 9, 10)		X
C	To provide new high-resolution protocols and flagship simulations for the World Climate Research Programme (WCRP)'s Coupled Model Intercomparison Project (CMIP6) project, to inform the Intergovernmental Panel on Climate Change (IPCC) assessments and in support of emerging Climate Services. (4, 6, 9)		X
D	To explore the scientific and technological frontiers of capability in global climate modelling to provide guidance for the development of future generations of prediction systems, global climate and Earth System models (informing post-CMIP6 and beyond). (3, 4)		X
E	To advance understanding of past and future, natural and anthropogenic, drivers of variability and changes in European climate, including high impact events, by exploiting new capabilities in high-resolution global climate modelling. (1, 2, 5)		X
F	To produce new, more robust and trustworthy projections of European climate for the next few decades based on improved global models and advances in process understanding. (2, 3, 5, 6, 10)	X	
G	To engage with targeted end-user groups in key European economic sectors to strengthen their competitiveness, growth, resilience and ability by exploiting new scientific progress. (10, 11)	X	
H	To establish cooperation between science and policy actions at European and international level, to support the development of effective climate change policies, optimize public decision making and increase capability to manage climate risks. (5, 8, 10)	X	

3 Detailed Report

3.1 AMOC storylines and their impact on heatwaves and European agriculture and health

Gerard van der Schrier, KNMI; Eveline van der Linden (KNMI); Rein Haarsma (KNMI); Balakrishnan Solaraju Murali (BSC); Rob Groenland (KNMI); Dragana Bojovic (BSC)

3.1.1 Introduction

In the last few years, a coherent view developed how large-scale atmospheric circulation responds to climate change (IPCC, 2013). Major elements in this view are a poleward expansion of the Hadley circulation and a poleward shift of the mid-latitude storm tracks. Observations are now showing changes that seem to be consistent with what Global Circulation Models project for a warming climate but the large interannual variability of mid-latitude climate makes it difficult to clearly attribute the rising global temperatures to these circulations. A link between a warming world and atmospheric circulation features that lead to climatic extremes are especially interesting as these climatic extremes have a huge impact on society.

Alteration in the frequency, intensity, spatial extent, or duration of weather and climatic extremes, like heat waves and droughts, will lead to increased stress on human and natural systems and a tendency for serious adverse effects in many places around the world (Lavell et al. 2013), especially if the increase in (climatological) hazard is linked to an increase in (societal) vulnerability. The focus on extreme events in a future climate also fuels the increase in attention for historic extreme events as a detailed historical perspective is interesting from an attribution perspective. A recent example is the analysis of the 1947 heatwave (Harrington et al. 2019).

While consensus grows on large-scale and aggregated aspects of climate, regional effects of circulation changes are much less well understood and a large variation in projections is around which makes it much more difficult to distill a coherent view of how regional effects will change. Given the uncertainty in the response of regional climate to global warming, the development of storylines, or narratives, of climate change has been proposed as an informative way to characterize and communicate future climate projections to stakeholders and policy makers (Zappa, 2019).

The concept of a storyline involves a possible and physically self-consistent future unfolding of global and regional climate events. In a storyline approach, multiple storylines are identified in order to span the uncertainty in the future projections. The focus is not on attributing a probability to the different storylines but on understanding the driving physical factors, the chain of mechanisms involved and the implications at the regional level (Hazeleger et al. 2015; Zappa et al. 2019).

In the storyline of this chapter, a scenario unfolds which couples observed and projected changes in the large-scale ocean circulation to changes in the pressure pattern of the mid-latitude troposphere in the Atlantic sector. The change in pressure distribution is a persistent anti-cyclone over the British Isles and this set-up leads to reduced precipitation and enhanced drying. The impact in terms of physical parameters of this change in pressure is quantified in a high-resolution GCM (Hazeleger et al. 2010). The impact on agriculture and health of the ensuing drought is described by highlighting events in 1920 and 1921. The drought in 1921 can be used as an analogue or worst-case scenario perhaps, of a drought which has its origin in persistently high pressure over the British Isles.

3.1.2 Ocean circulation and effects on the sea surface temperature

A fundamental aspect of global climate is the heat balance. The earth receives much more radiative energy at the equator than at the poles. This is because of the spherical shape of the earth. However, outgoing radiation is much more uniformly distributed over the earth. This situation can only exist if there is a heat transport from equator to poles.

The two heat-distributing engines are the atmosphere and the ocean (Gill, 2016; Trenberth & Caron, 2001; Trenberth & Solomon, 1994). The northward ocean heat transport at 26°N in the Atlantic has been measured since 2004 (Figure 1) and it shows surprisingly large temporal variations (Bryden et al., 2020). Apart from the strong interannual variations – which toppled the view that the ocean was just a very sluggish player in the climate system – the northward heat transport shows a long-term reduction of 0.17PW after 2009. This reduction relates to a slow-down of the Atlantic meridional overturning circulation (AMOC).

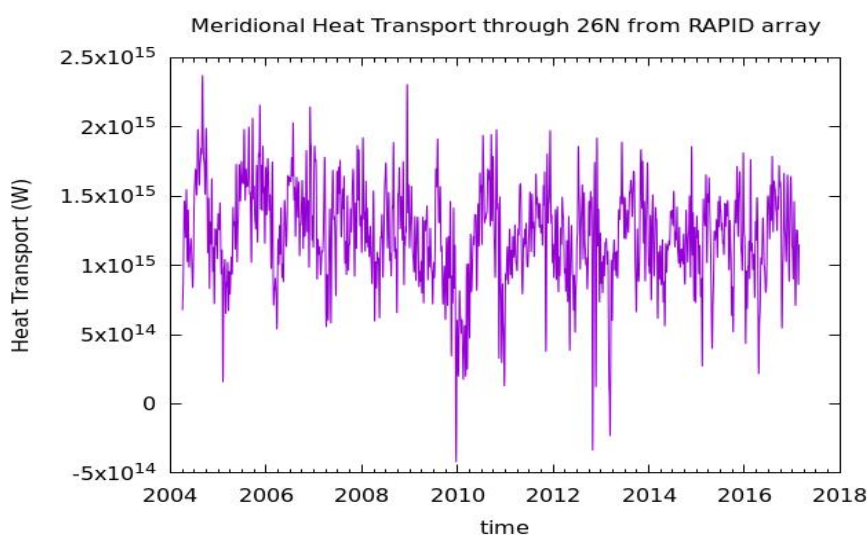


Figure 1: Ocean heat transport at 26°N. The line shows 10-day filtered data. There is a decrease in northward heat transport after 2008-2009 of 0.17PW. Data from Bryden et al. (2020).

The reduced heat transport affects the surface temperatures of the North Atlantic. The slow down in the overturning has cooled (and freshened) the surface of the Atlantic from the Bahamas to Iceland (Figure 2). The cooling peaks south of Iceland where temperatures just below the surface were 2°C cooler in 2016 than they were in 2008 (Bryden et al. 2020).

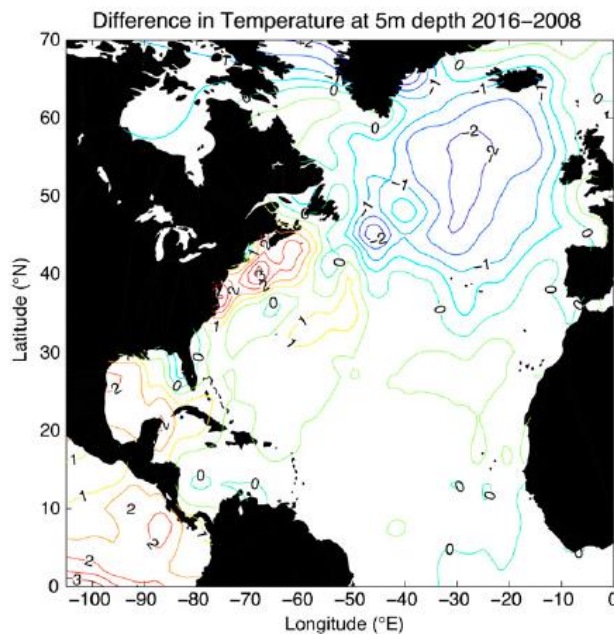


Figure 2: Observed difference in temperature at 5m depth (2016 minus 2008 values). Surface waters are 2°C cooler over 8 years in the midocean region south of Iceland Figure from Bryden et al. (2020).

The cooling of the northern North Atlantic is a ‘fingerprint’ of a decreased overturning. This fingerprint is found in observations and it can be found in climate simulations as well. Caesar et al (2018) use the CMIP5 suite of models to make the link between the fingerprint in sea-surface temperature (SST) and overturning strength explicit, and used observed SST fields to reconstruct the overturning strength to the end of the 19th century. Figure 3 shows a comparison of time series of SST anomalies and the strength of the overturning circulation in one of the models used for this analysis. The graph shows SST anomalies in the subpolar gyre (dark blue) and Gulf Stream region (red), with a time series of the overturning strength (light blue). They conclude that the AMOC has been slowing since the 1950s with superimposed interdecadal natural variability and punctuated by large but brief variations.

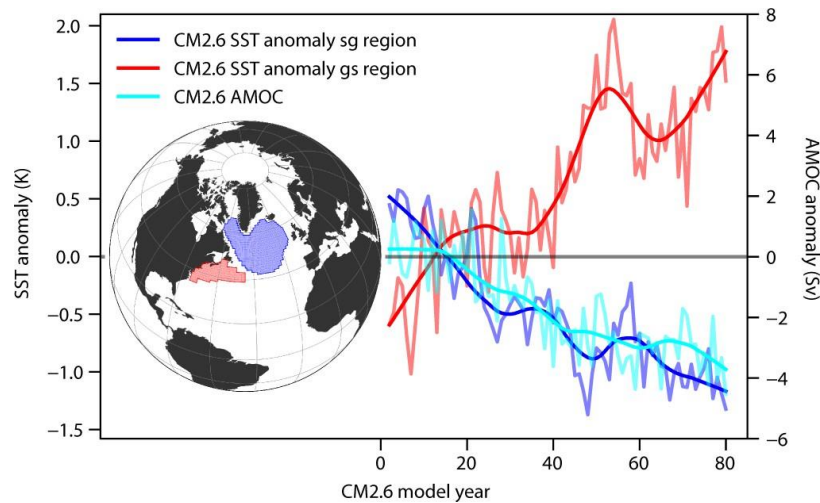


Figure 3: A comparison of time series from a climate simulation of the CM2.6 climate model, showing a decrease in sub-polar sea-surface temperature (dark blue) with a warming of the surface waters in the Gulf Stream region (red), along with a decrease in the overturning strength (light blue). The two regions are defined as in the inset. Figure from Caesar et al. (2018).

3.1.3 A response of the atmosphere to the northern North Atlantic

It is no surprise that the cooling of a vast stretch of ocean at the doorstep of the European continent will have effects on the climate of Europe. Especially since the cold anomaly is upstream as the dominant atmospheric circulation at mid-latitude is eastward. Using the 20th Century Reanalysis, Gosh et al. (2017) investigate the atmospheric response to diabatic heating in the North Atlantic. What they find is a pathway which explains observed multidecadal variations of European summer climate. This pathway bridges variations in the North Atlantic SSTs with the European summer climate through a surface baroclinic pressure response, with a positive pressure anomaly associated with a negative temperature anomaly. The pressure anomaly is located somewhat east of the sea-surface temperature anomaly. Further downstream, this response induces an east-west wave-like pattern in the sea-level pressure field. The pressure response causes warming of Central to Eastern Europe by creating an atmospheric blocking-like situation (Gosh et al. 2017).

Figure 4 (left panel) illustrates this bridge, where a composite of total (sensible and latent) summer surface heat flux anomaly is shown over the ocean surface for the years that a surface air temperature index over central-eastern Europe is negative. The positive values denote heat release from the ocean surface (so a positive sea surface temperature anomaly). The right panel of Figure 4 shows the associated SLP pattern, with a low pressure centre over the British Isles and a wave-train further downstream.

In their analysis, Gosh et al. (2017) find that variations in the strength and sign of the pressure anomaly affect meridional temperature advection strongly. In addition, a positive pressure anomaly is enhanced at higher altitude (500 hPa) which is

reminiscent of a blocking-like situation. Analysis show indeed that a positive pressure anomaly fosters favourable conditions for blockings to occur.

Recently, Gervais et al. (2019) added a second mechanism for how North Atlantic seas surface temperatures affect tropospheric circulation in the Atlantic sector. This mechanism involves the midlatitude jet. This leads to a cooling of the North Atlantic that triggers a direct linear baroclinic response leading to local surface high pressure anomaly shifted downstream of the SST anomaly, and an eddy-forced response. The SST anomaly leads to enhanced baroclinity along the subpolar front, simply because of the steeper temperature gradient in the ocean surface relating to the cooler waters in the sub polar gyre. This enhanced baroclinity fuels the generation of eddy activity that propagates vertically and downstream of the SST anomaly. This eddy activity acts to strengthen the eddy-driven jet. Gervais et al. (2019) show that the jet enhancement leads to the development of barotropic highs and lows on the equatorward and poleward side of the jet enhancement respectively. Figure 5 schematically illustrates the two mechanisms, with the direct linear barotropic response in the upper panel and the transient eddy response, the vertical and downstream propagation of eddy activity in the lower panel.

In a situation where a blocking situation exists, like what Gosh et al. (2017) have found as a response to a SST cold anomaly, the mid-latitude jet is diverted northward. The mechanism of Gervais et al. (2019) indicate that the same SST anomaly then also enhances this jet which further strengthens the high-pressure anomaly. The two mechanisms, triggered by the same sea-surface temperature anomaly, both enhance the strength of the high-pressure system over the British Isles.

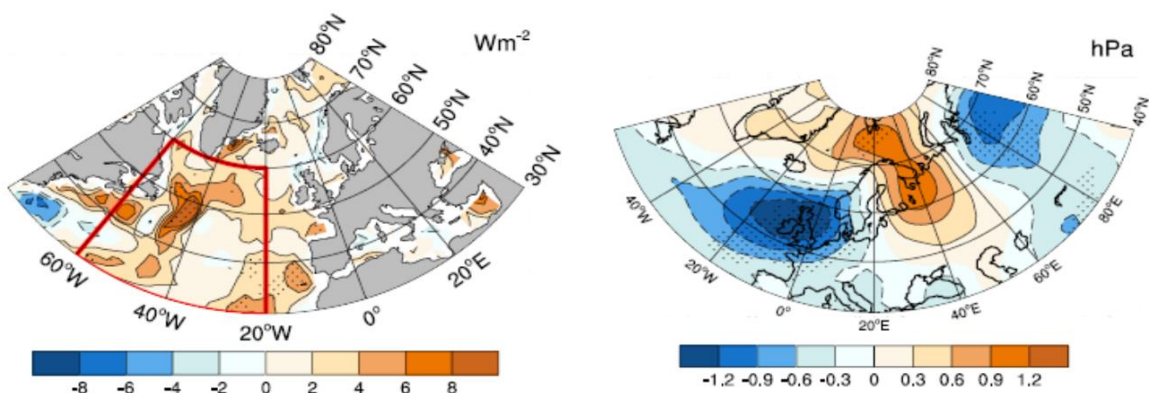


Figure 4: Composite analysis of surface heat flux over the North Atlantic (left) and sea-level pressure (right) using an index for central-eastern European surface air temperature. Positive values of the surface heat flux correspond to a release of heat and to anomalously high ocean surface temperature.

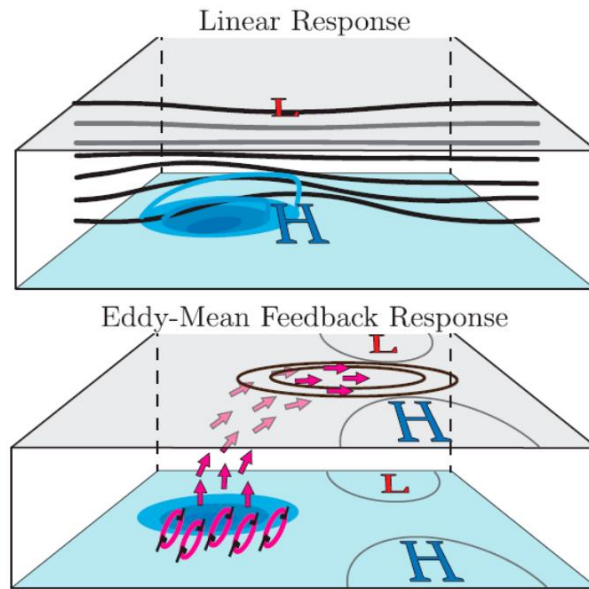


Figure 5: Schematic picture of the atmospheric response to a cold anomaly in sea-surface temperature. The SST anomaly is depicted as the blue-ish area on the light blue surface. The black lines represent the change in geopotential height in response to the cooling of the air temperatures (blue lines). The bottom panel shows the enhanced baroclinicity along the polar front (pink circles) and the vertical and downstream propagation of eddy activity (pink arrows). This leads to enhancement of the jet (black lines) and establish low and high pressure areas on either sides of the jet.

The chain of events, from cold sea surface temperatures in the North Atlantic to a response in the tropospheric pressure patterns has been linked to the exceptionally warm summer of 2015 by Duchez et al. (2016). They note that 2015 has both an exceptionally strong SST anomaly in the North Atlantic and exceptionally high daily maximum temperatures during the summer season (Figure 6). Although a process study of the events leading to this particular event was absent in the study, they do show that similar cold anomalies were present prior or at the onset of major heat waves in Europe since 1980. This indicates that the cold sea surface waters are indeed a factor in establishing these heat waves.

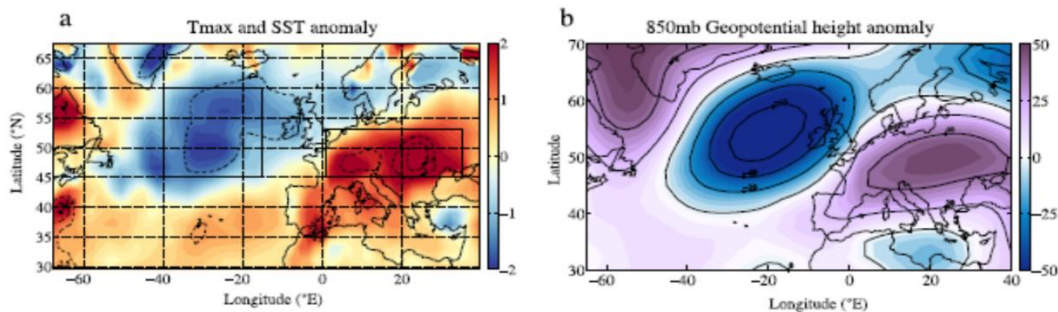


Figure 6: Summer-average sea-surface temperature anomalies and daily maximum air temperature anomalies over land for the 2015 (left). The right panel shows the 850mb geopotential height anomaly for this summer. Figure from Duchez et al. (2016)

ASIDE TO DISCUSS THE DUCHEZ STUDY

The validity of the Duchezi et al. (2016) conclusion has been discussed in the literature. Josey et al. (2019) argue that while a major impact of the 2015 cold anomaly in the northern North Atlantic could have been to act as a precursor to the 2015 European heat wave, more work is needed to understand the causal mechanism by which it affects the atmospheric circulation. They also point to other factors that may have been important for the heat wave development, including remote influences from the Pacific region and changes linked to declining Arctic sea ice and related Arctic amplification of the global warming signal. Local land-based effects, particularly soil moisture content, could also have played a major role and have previously been suggested as a primary factor for the extreme heat wave of 2003.

A second study that is critical on the Duchezi et al. (2016) results is Wehrli et al. (2019). In their simulations they conclude that the atmospheric circulation is a strong driver of the event, while a shift of the radiation balance in response to soil moisture deficits explains a smaller part of the heat-wave. One experiment of Wehrli et al. (2019) is a SST-forced simulation using the observed SST pattern of 2015 as input. They conclude that, on average, this simulation produces air temperatures over Europe that are a bit colder. They argue that the contribution of the ocean anomaly of that year to the event is rather a very small cooling. However, Wehrli et al. (2019) are unsure if the discrepancy with Duchezi et al. (2016) is related to their framework or the employed model.

3.1.4 Model projections

The chain of events described above is based mainly on analysis of observations, reanalyses and model-based process studies. The impact of anomalously cool North Atlantic surface waters, its effect on the troposphere and the role it plays in triggering a heat wave all start with a reduction in the Atlantic Meridional Overturning Circulation.

Climate projects indicate that the reduction in the AMOC is likely to continue as the climate warms. Our changing climate shows its largest increase in temperature at the northern high-latitudes. This area is also the area where the strength of the AMOC is most sensitive to changes in the density of the sea water with a strong overturning requiring high density surface waters. However, the increase in temperature at these latitudes decreases the density of sea water. In addition, higher air temperature allows for a larger amount of water vapour in the air, meaning (for the high latitudes) that the amount of precipitation increases as well. The resulting decrease in salinity of the sea water further decreases the density of the surface waters of the northern North Atlantic.

Haarsma et al. (2015) analyse the slow down of the AMOC and its consequences in the CMIP5 model suite under the RCP4.5 scenario. They find that as the AMOC further decreases in strength in their projection, the models show the appearance of a high-pressure anomaly over the British Isles (Figure 7, left panel). This anomaly is located downstream of an area of reduced North Atlantic warming (Figure 7, middle panel). Associated with this ‘warming hole’ is an area where the turbulent heat release from the ocean to the atmosphere is reduced (Figure 7, right panel).

The oceanic changes and their effects on the pressure distribution reported by Haarsma et al. (2015) have their effects on projected European summers. In their analysis, Haarsma et al. (2015) show that the suite of CMIP5 models point to the ocean-induced pressure response as a dominant contributor to atmospheric circulation change over Europe in response to global warming. A simple regression analysis (Figure 8) reveals that the response of the reduced AMOC and associated reduced ocean-atmosphere heat exchange is a reduction in summer rainfall and an increase in solar radiation is seen (Haarsma et al. 2015).

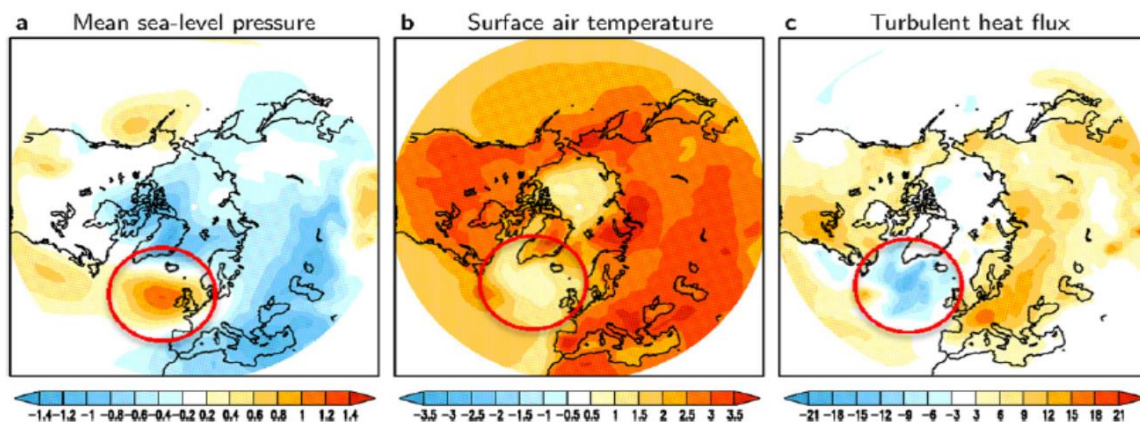


Figure 7: Summer mean climate change in the RCP 4.5 scenario simulations. (a) CMIP 5 model mean summer change (2071–2100) minus (1971–2000) in mean sea-level pressure. (b) As (a), but for the surface air temperature. (c) as (a) but for the turbulent ocean- atmosphere heat flux (positive upward). Figure from Haarsma et al. (2015).

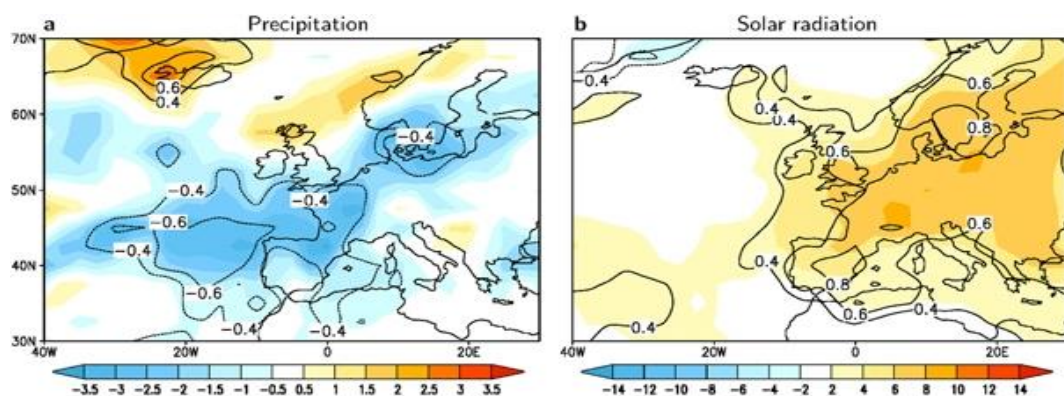


Figure 8: Relation of European climate variables to AMOC variations. (a) Regression (shaded (mm month^{-1})) and correlation (contours) of rainfall change onto AMOC change for the (2071–2100)–(1971–2000) inter-model variations. (b) As in (a), but for solar radiation (W m^{-2}). Figure from Haarsma et al. (2015)

The analysis of Haarsma et al. (2015) on the CMIP5 model suite is contrasted by the Roberts et al. (2020) analysis who analyzed the latest generation high-resolution global climate models in the framework of the H2020 Primavera project.

In their analysis, Roberts et al. (2020) find that the decline in the Atlantic Meridional Overturning Circulation, and related heat transport, tends to become stronger as model resolution is enhanced, particularly when the ocean resolution is increased from non-eddy to eddy-present and eddy-rich. Although this generation of models is still not perfect, the high resolution simulations show improvements in representing the water properties compared to their low resolution counterparts. The increase in realism in these simulations adds to the confidence in these models to reliably model future variations in the AMOC.

The future climate projections of these models for the period 2015-2050 show that the overturning circulation tends to decline more rapidly in the higher resolution models by more than 20% compared to the control state, which is related to both the mean state and to the subpolar gyre contribution to deep water formation. Such large declines in AMOC are not seen in resolutions more typical of the current generation of climate models (Roberts et al. 2020).

The stronger slow-down of the high-resolution models is shown in Figure 9 which shows the ‘warming hole’ of the future climate projections. The warming hole is stronger in the high resolution models than in their equivalents with a lower (more CMIP5-like) resolution. These simulations suggest an enhanced change for Northern Hemisphere climate for a future climate.

The two different perspectives on the fate of the overturning circulation, one based on the CMIP5 model suite and one based on the latest generation of high-resolution climate models, provide the basis of a bifurcation in the story line. The chain of events in the two storylines will be similar but the severity of drought and heat waves, and their impacts on society, will differ.

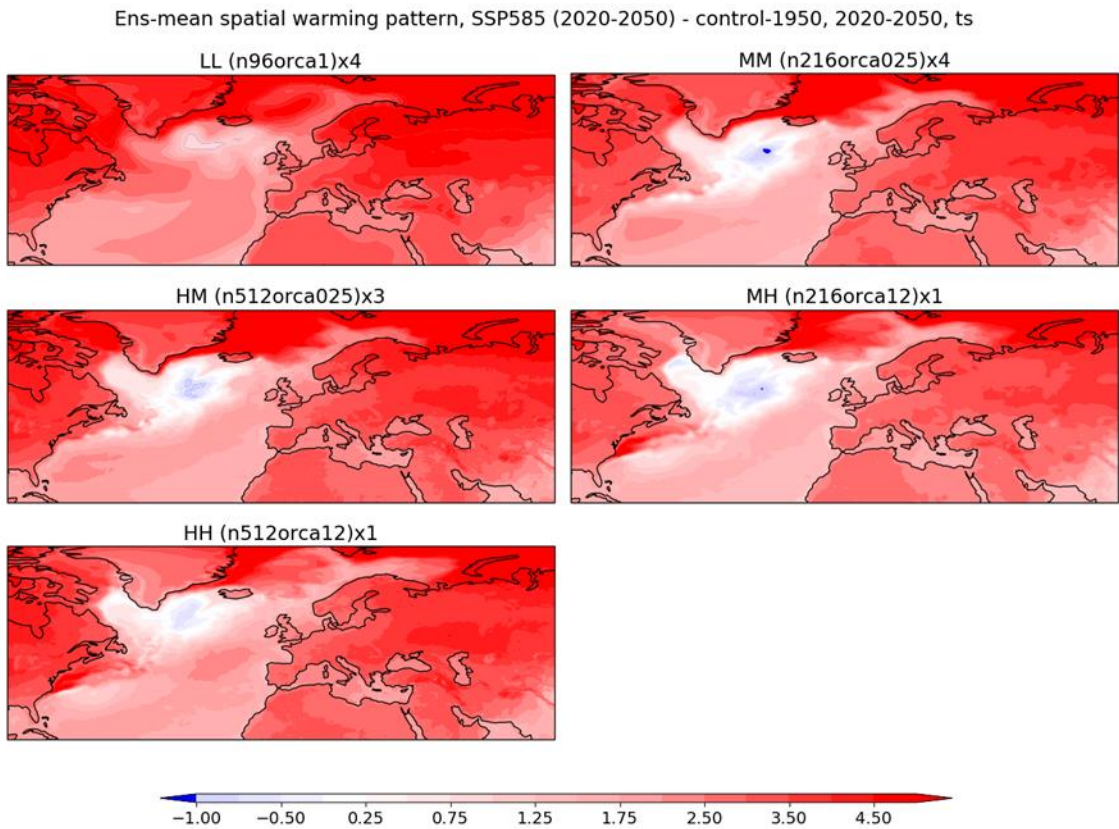


Figure 9: The surface temperature warming by 2050 based on the Hadley Centre climate model (part of the Primavera suite of models) for various resolutions in ocean and atmosphere. The ‘warming hole’, the much less steep increase in warming – or even a decrease in warming – is stronger in the model configurations with a high-resolution ocean model.

3.1.5 Future drought and heat in response to the slow-down of the overturning

The impact of model resolution on the quantitative estimate of decrease in the future overturning circulation has its impacts on projections of future drought and heat waves. Van der Linden et al. (2019) looked into the impact of model resolution on the magnitude and seasonality of future soil-drying in central-western Europe. They used the EC-Earth global climate model (Hazeleger et al. 2011) to study two 30-year periods representative of the start and end of the 21st century under low-to-moderate greenhouse gas forcing (RCP4.5). In central-western Europe, at high spatial resolution (~25 km) soil drying is more severe and starts earlier in the season than at standard resolution (~112 km). The differences in the projected large-scale atmospheric circulation and local soil moisture feedbacks lead to enhanced evapotranspiration in spring and reduced precipitation in summer. Furthermore, in the high-resolution model the stronger anticyclonic anomaly over the British Isles extends over central-western Europe and supports soil drying. The resulting drier future land induces stronger soil moisture feedbacks that amplify drying conditions in

summer. These effects on soil moisture are illustrated in Figure 10, where the climate signal in soil moisture content (future–present) in Europe is shown for spring and summer in the high-resolution model. The difference between the high and the low resolution model configurations is given in the lower panels of Figure 10. These lower panels clearly indicate the weaker signal in soil moisture drying in the lower resolution models.

There is also a second effect Van der Linden et al. (2019) observe: a more realistic position of the storm track at high model resolution leads to reduced biases in precipitation and temperature in the present-day climatology, which act to amplify future changes in evapotranspiration in spring.

The effects of a stronger drying of the soils in the high-resolution models also impact on the occurrence of heat waves. The soil-moisture-limited evapotranspiration in summer promotes sensible heating of the boundary layer. This is required balance the amount of solar radiation. The shift from latent heat to sensible heat in satisfying the radiation balance has two effects: the air temperature must rise to accommodate the rise in sensible heat and relative humidity decreases leading to less cloudy conditions. The combination of these effects lead to an increase in dry summer days and more incoming solar radiation. As a result a series of consecutive hot and dry summers appears in the future high-resolution climate. These effects are illustrated in Figure 11 and show the typical seasonal cycle averaged over the 30-years of simulations.

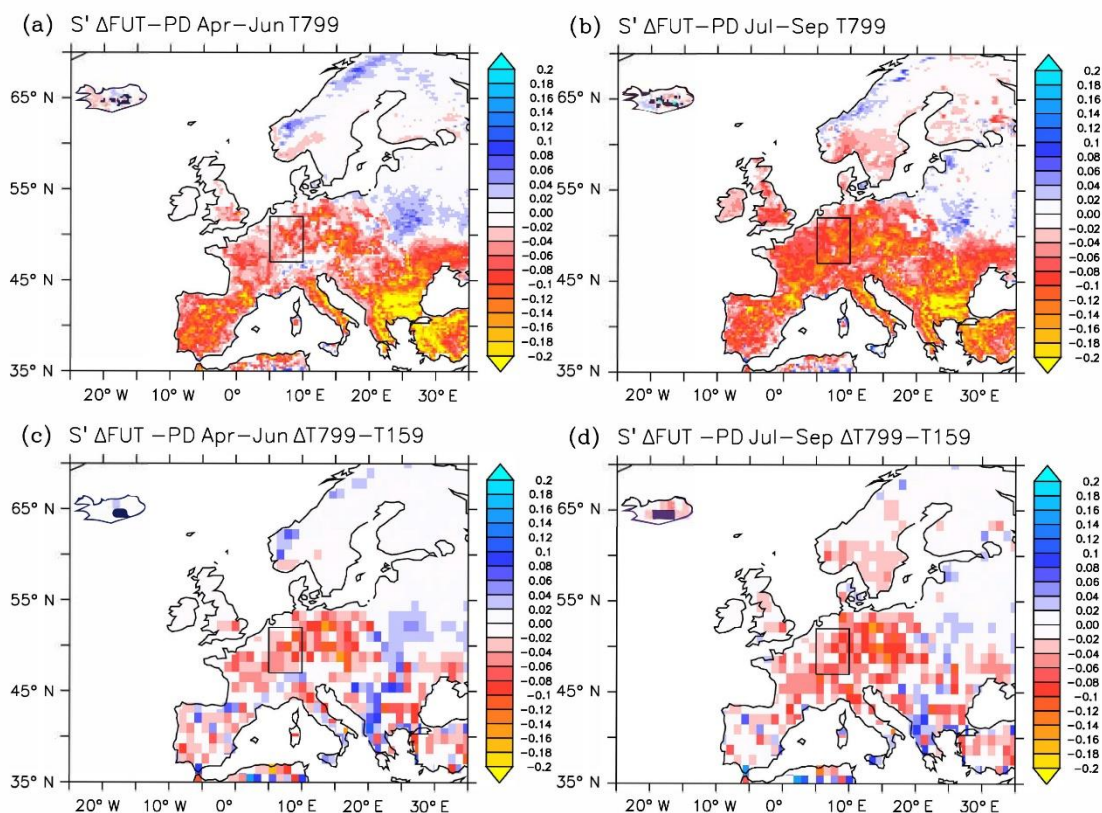


Figure 10: Top: soil moisture content (m) climate change signal (future–present) in Europe for (a) spring and (b) summer in the high-resolution model. Bottom: (c–d) same but for difference in climate change signal between the high- and standard-resolution model. Figure from Van der Linden et al. (2019).

Another effect Van der Linden et al. (2019) observe in their climate simulations, is that the seasonality of the signal changes. Figure 12 provides density plots of soil moisture anomalies for spring and summer, for the high-resolution and low-resolution model configurations and for the rectangular box indicated in black lines in figure 10. While the low-resolution model does not really show a change in soil moisture anomalies in spring between the future and the present climate, the high-resolution model version shows that low soil moisture is much more common in a future climate. Apparently, drying sets-in much earlier in the year in the high-resolution model than in the low-resolution model. This has its effects on summer drought as well. As soil moisture is a conservative quantity, the lack of soil moisture which is built-up in spring persists into the summer and the summer drying adds to these deficits. While both the low-resolution and the high-resolution models indicate future summer drying, the overall effects in the high-resolution model are more dramatic (Figure 12).

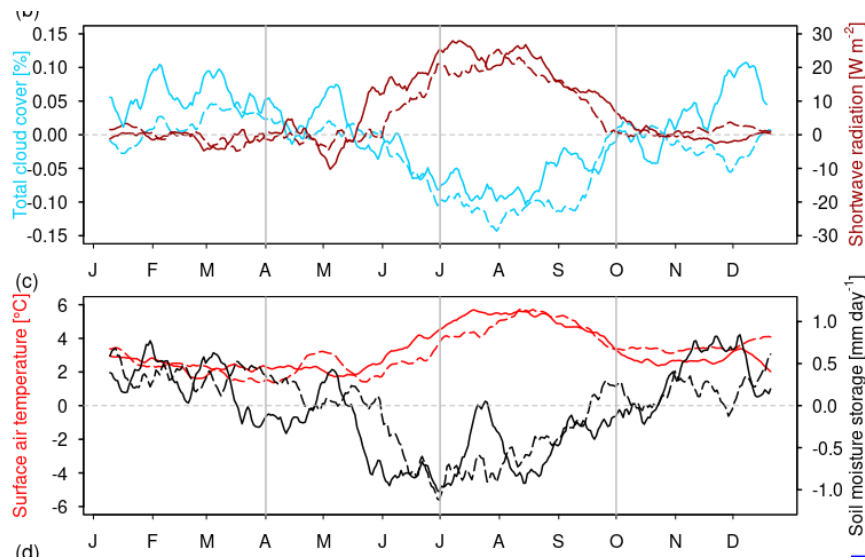


Figure 11: Climate change signal (future – present) of total cloud cover and surface solar radiation (top panel) and daily mean surface air temperature and soil moisture storage for T159 (dashed lines) and T799 (solid lines). Values are smoothed with a 20-day running mean filter and averaged over central-western Europe. Figure from Van der Linden et al. (2019).

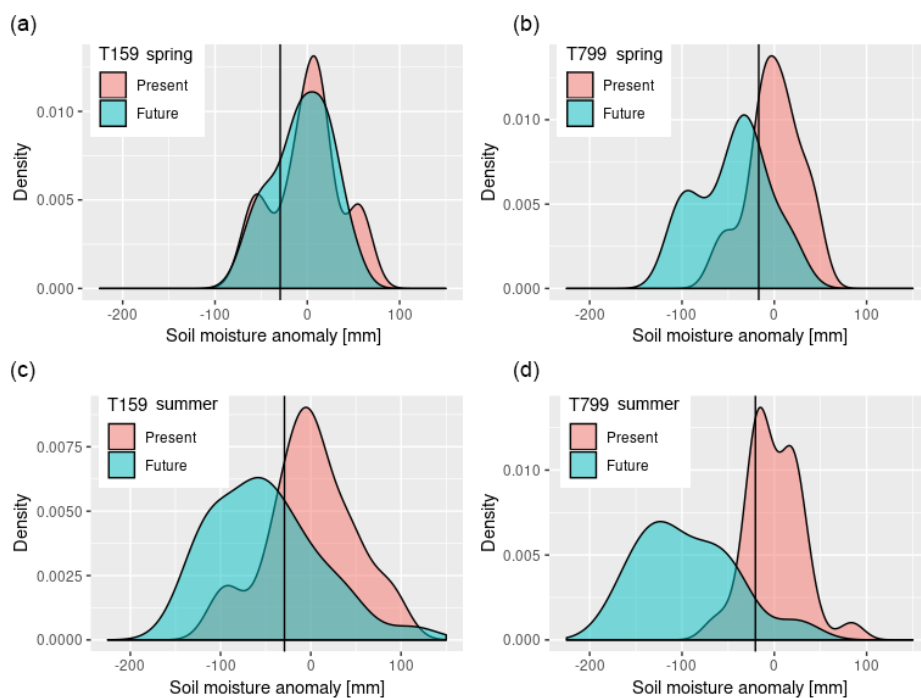


Figure 12: Density distributions of soil moisture anomalies over central-western Europe in April-June at low-resolution (upper left) and high-resolution (upper right). The lower panels show the same, but for the July-September season. The vertical black lines indicate the drought thresholds based on the 20th percentile of present-day soil moisture anomaly distributions. Figure from Van der Linden et al. (2019).

3.1.6 Assessment of impacts

The impacts of the chain of events from a reduction in the AMOC to a persistent anti-cyclone over the British Isles which favours dry and sunny weather in spring and

summer – bringing in drought and heat waves – is illustrated by looking for an analogy. The analogy is selected on the basis of having sustained high-pressure area over (roughly) the British Isles. While there are several examples of years which are characterized by such circulation pattern, and which are also a droughty year, the year we select for the impact study is 1921. This year is the driest year on record for western Europe (van der Schrier et al. 2006), although none of its seasons actually tops the ranks of driest on record. Figure 13 illustrates the exceptional nature of 1921 in terms of discharge of the Rhine river at the point where it enters the Netherlands. Using this metric, the year 1921 (dark blue line) ranks first in driest years ever using this metric. Not only is the discharge in summer among the lowest but the discharge throughout the spring was exceptionally low.

An analysis of the circulation is provided by van der Schrier et al. (2020) (Figure 14). This figure shows that a SST anomaly is present in the North Atlantic. It also shows important ridge/block features diverting the zonal Atlantic moisture flux from reaching central Europe and providing enhanced stability from winter 1920/1921 into the summer of 1921. While the Z500 maxima changes with seasons, the main driver is always the same. The blocking nature of the anti-cyclone over the British Isles is evident in a storm track density analysis using the 20th Century Reanalysis (Figure 15) which shows an enhanced intensity south of Greenland and over Iceland and a reduction over the central North Atlantic, the British Isles and into central and eastern Europe. The decrease in storm tracks entering the European interior is also found in a period publication of prof. Erida (1922) (Figure 15)

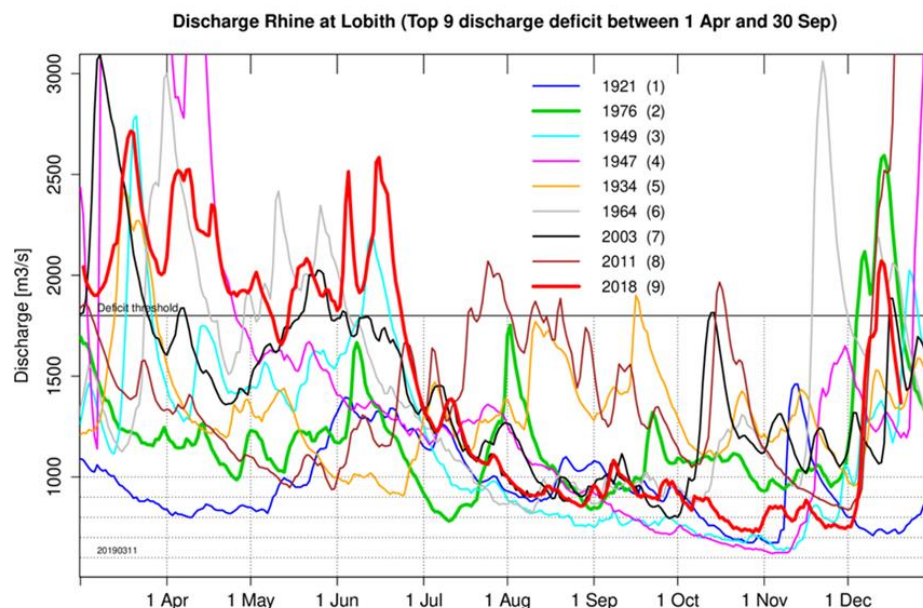


Figure 13: Discharge of the river Rhine at Lobith (the Netherlands) for the nine driest years on record. Data from Rijkswaterstaat

Z500 and SST (1921)

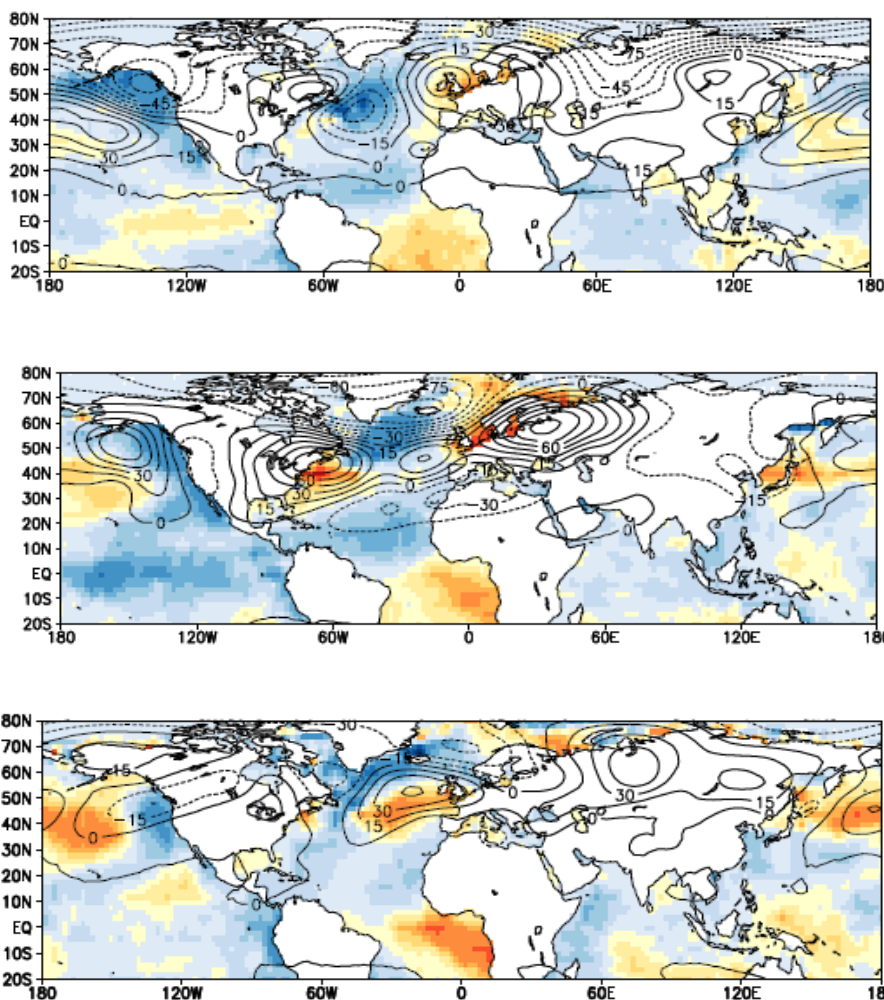


Figure 14: The Z500 level (contours) and SST (colour) as anomalies from the long-term mean for winter 1920/1921 (top), spring 1921 (middle) and summer 1921 (bottom), based on the 20th Century Reanalysis.

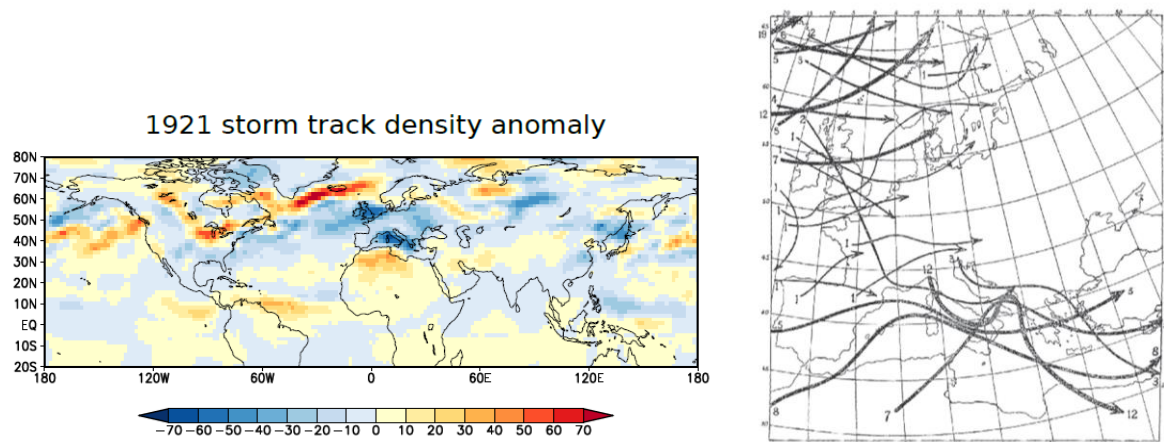


Figure 15: The 1921 storm track density anomaly for the northern hemisphere based on the 20th Century Reanalysis (left) and a reconstruction of individual storms based on synoptic charts from Erida (1922)

The impacts over Europe in relation to the drought were quantified by using the approach pioneered by Stahl et al. (2016). Drought impacts were assessed by collecting text-based reports on the drought of 1921. The reported drought impacts were classified into major impact categories, each of which had a number of subtypes. The distribution of these categories and types was then analyzed over time and for five countries in Europe. The text-based reports were collected from digitized newspapers. For the United Kingdom, the *Birmingham Gazette*, for the Netherlands the *Algemeen Handelsblad*; for Belgium, the *Standaard*; for Germany the *Berliner Tageszeitung*, and for the Czech Republic, the *Lidové Noviny*. All these newspapers are accessible through their digital archives and searchable. The search term ‘drought’ (in each of the native languages) was used. The resulting newspaper clippings were then categorized, following Table A2 of Stahl et al. (2016) and labelled by area or place and date.

ASIDE ON MEDITERRANEAN PERSPECTIVE OF THE 1921 DROUGHT

The drought and heat wave that have been central in this storyline affected most of western – central and eastern Europe, but did not affect the Mediterranean. This is interesting as we see a drying trend and a tendency toward more frequent, hotter and earlier heat waves in the Mediterranean over the last decades as a result of global warming. In the Figure below, the drought of 1921, captured in the SPEI6 index (Vicente-Serrano et al. 2010). The figure nicely shows the evolution of the drought and shows that, for western Europe, the first signs of a drought started to appear in late autumn of 1920. It also shows that the northwestern Mediterranean experienced a pluvial with rather wet conditions in 1921 throughout the year. This picture is consistent with the blocking feature over the British Isles, diverting cyclones to either the north or the south (into the Mediterranean region).

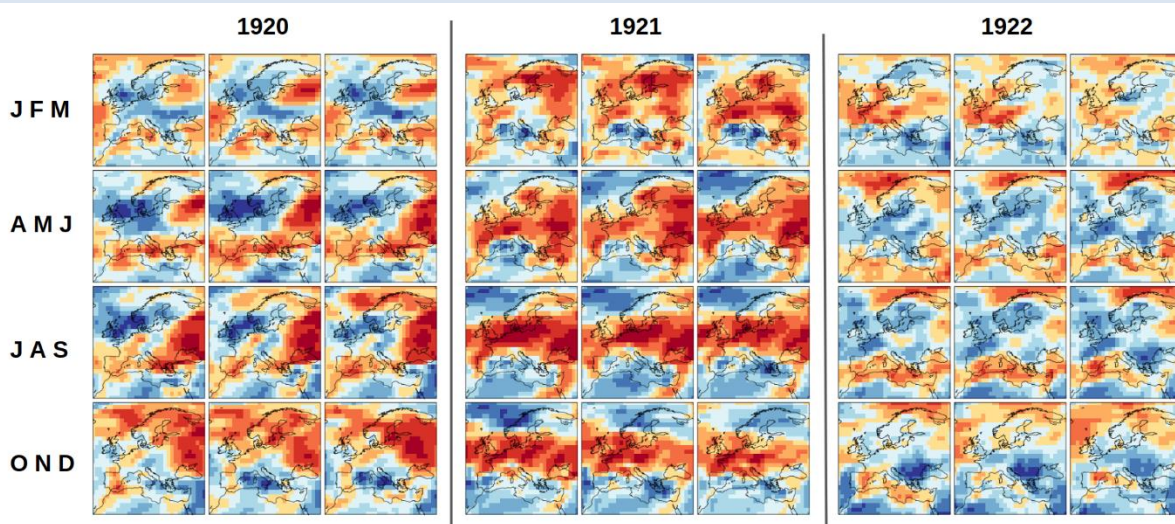
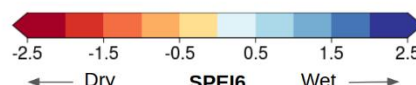


Figure presents the SPEI6 for all the months (first row - JFM; second row - AMJ; and so on) for the years 1920 to 1922. This figure helps to visualize the evolution of the drought



SPEI6 is able to capture the spatial distribution of the drought in 1921

Figure 16 shows the impacts versus time for each of these five countries. From these diagrams it is clear that most reports are found in summer and the dominant category is 'Agriculture and Livestock Farming'. A dominant impact, more so in the United Kingdom and the Czech republic than in the other three countries, is 'Wildfires', although this category is often reported in all countries as one of the first impacts of the drought. Interesting is that up to late in the year, the impacts on 'water supply' appear while all countries already report water supply problems in late spring or early summer. In addition to the water supply, which includes the availability of water for consumption and sanitation, a separate category 'Human health' is included. This category includes heat stress problems (as a drought and heat wave often go hand-in-hand), an increase in respiratory ailments (because of e.g. dust) and excess mortality during heat waves. The number of reports for this category is

not high – absent even for Germany – but the reports that are made, coincide mostly with the summer season and a few in the latter half of the year.

Figure 17 shows the specification of the categories ‘Water supply’ and ‘Agriculture and livestock farming’ for the five countries. Limitations to water supply in rural and urban areas is strong in all five countries, but mostly so in England, Belgium, Czech Republic and Germany where this category takes up about half or more of the reports. Regional water supply shortage is most frequently reported on in the Netherlands.

In agriculture, the most common impact for all countries is ‘Reduced productivity of annual crop cultivation’. While all countries have reports on farmers reducing their stock, this is by far the most reported on in the Czech Republic. All countries report about evenly on the impact on ‘Regional shortage of feedwater of livestock’.

3.1.7 Conclusion

The chain of events described in this storyline lead from a reduction in the Atlantic Meridional Overturning Circulation to a response on the pressure distribution in the North Atlantic sector that fosters stable conditions, clear skies with much radiation and a reduction in precipitation. The mechanism described nudges the background situation to a situation that is more likely to develop a drought if the high-pressure over the British Isles persists sufficiently long and is sufficiently strong. Based on analysis of global climate models, the overturning in a future climate is likely to slow down. This process is already observed in direct measurements over the last two decades and using indirect measurements over the last five decades. However, an assessment of the speed of the future slow down varies with the model configuration. Low-resolution models, similar to the CMIP5 models, show a less steep decline than the same models in their high-resolution configuration. With this variation in decline of the overturning, the effects on the atmospheric circulation will vary likewise and the impacts of the ensuing drought and heat waves will vary between these two perspectives.

Concluding, the perspective of the high-resolution models is likely to give a more persistent and stronger anti-cyclone over the British Isles than the perspective of the low-resolution models. The impacts of a circulation like the one set-up in this storyline occurred prior and during the 1921 drought.

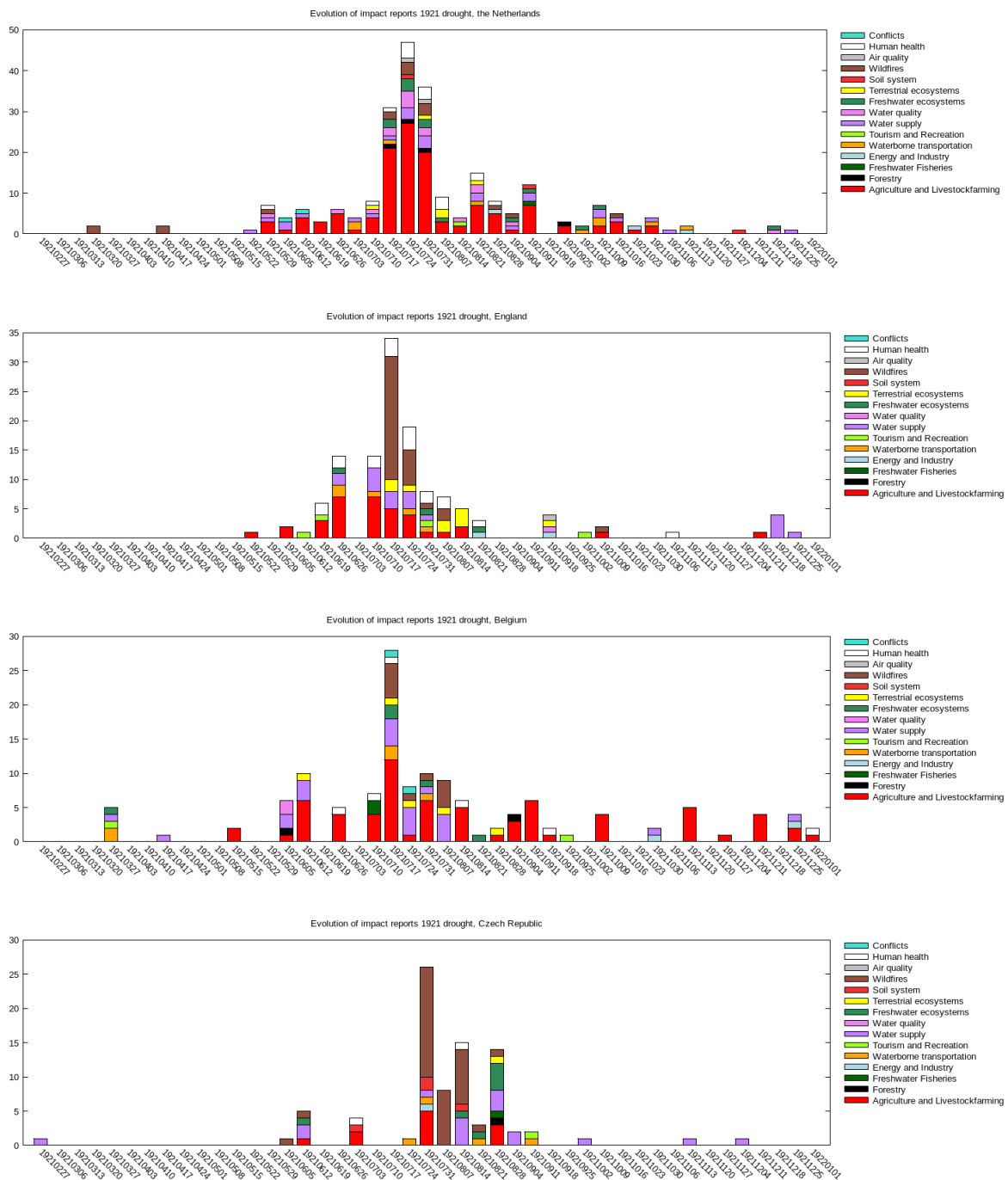
As climate change makes evaporation stronger due to higher temperatures, one needs to expect impacts like wild fires to occur earlier. The growing season will advance because of climate change, but in a 1921-like situation poorly developing crops in early spring will be seen. In summer, damage to annual crops will be strong, livestock needs to be reduced and fodder supply problems are likely. These effects will be stronger in the high-resolution perspective than in the low-resolution perspective. Note that the analogy with 1921 requires an adjustment because of the

change in vulnerability to such problems in a more modern society. An example is that international trade is more easily accessible, although the increase in prices for fodder is similar in 1921 as in a future drought (and the possibility that farmers are not in the position to access funds).

Similar to 1921, water reservoirs and drinking water supplies will be affected both in rural and in urban areas. These effects appear in early summer and linger-on until well into autumn. These effects will be stronger in the high-resolution perspective than in the low-resolution perspective. Note that the analogy with 1921 here needs additional attention as well. Many cities which are supplied by rain-fed rivers for their water supply are now much larger than in 1921, making their vulnerability larger.

3.1.8 Key Points

- Observations and reconstructions show that the Atlantic Meridional Overturning Circulation (AMOC), a key-component in transporting heat from the equator to the poles, has been slowing down since the 1950s
- The cooling of the northern North Atlantic caused by the slow-down, is instrumental in setting-up a high-pressure system located somewhat downstream of the cooling, over the British Isles.
- This persistent anti-cyclone favours dry and stable weather over Europe and fosters the development of droughts.
- The AMOC is observed to slow-down more rapidly in a future climate when simulated by the latest generation of climate models than with models with a resolution similar to the current CMIP5 generation.
- Depending on the strength of the slow down, the severity of droughts that may hit west and central Europe may vary.



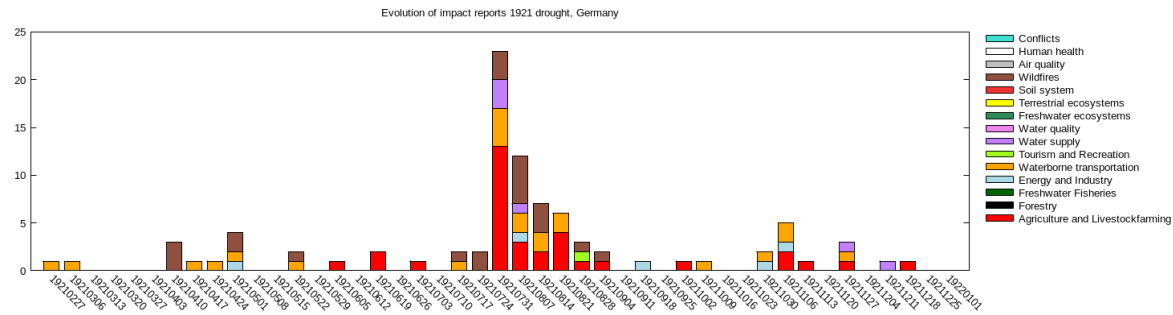


Figure 16: Impact analysis following the categories defined by Stahl et al. (2016) for the 1921 drought vs. time, for (from top to bottom) the Netherlands, United Kingdom, Belgium, Czech Republic, Germany.

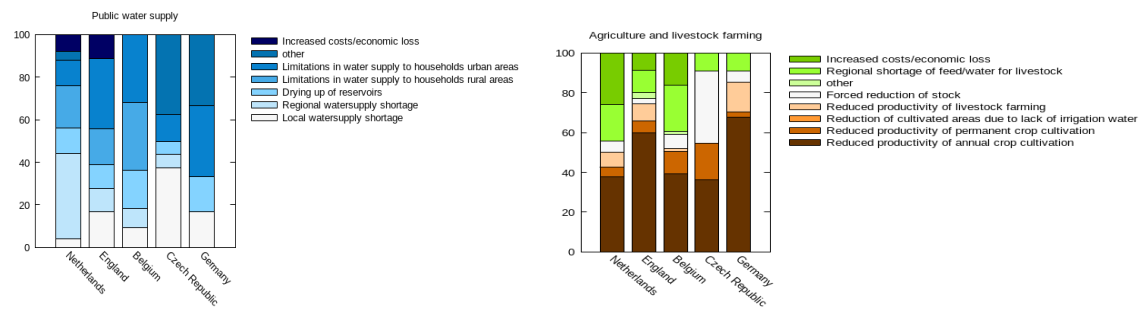


Figure 17: Specific impacts for 'water supply' (left panel) and 'Agriculture and livestock farming' (right panel) for each of the five analysed countries.

3.2 Impacts on the insurance sector from tropical cyclones, post-tropical cyclones and extratropical cyclones

Erika Palin, Julia Lockwood, Galina Guentchev and Malcolm Roberts, Met Office; Alexander J. Baker, Kevin Hodges, Reinhard Schiemann, Benoît Vannière and Pier Luigi Vidale, UREAD; Rein Haarsma and Dimitris Kapetanakis, KNMI; Louis-Philippe Caron and Phillip Kreussler, BSC

3.2.1 Introduction

3.2.1.1 The importance of tropical (TC), post-tropical (PTC), and extratropical (ETC) cyclones for the insurance sector

Tropical cyclones (TCs) typically originate equatorward of 30 degrees and are radially symmetrical storms with high wind speeds occurring just above the boundary layer. A tropical cyclone has a warm-core temperature structure and its horizontal size is typically 100-1000 km. Maximum pressure gradients and surface winds of strong tropical cyclones – which in the Atlantic basin are known as hurricanes – exceed 33m/s and are stronger than those typical of extratropical storms. As tropical cyclones propagate poleward, they may undergo extratropical transition, engendering an extratropical cyclone (ETC) or a hybrid storm. In the North Atlantic, approximately 50-60% of tropical cyclones transition and have a distinct post-tropical cyclone (PTC) phase. Not all ETCs form from TCs, however. Extratropical cyclones are essentially any cyclonic-scale storm without a tropical, axisymmetric structure—largely, frontal cyclones occurring in the mid- and high-latitudes. Their horizontal sizes are typically greater than 1000 km.

The use cases in D10.1 focused on ETCs alone; this has been expanded for this deliverable to include PTCs and TCs. ETCs and PTCs affect Europe directly; major windstorms that have directly impacted Europe (RMS, 2000; 2007; Roberts et al. 2014; Met Office, 2017; Laurila et al. 2019) include:

- *Ex-Hurricane Debby, 1982
- "87J" ("Great Storm"), 1987
- Daria ("Burns' Day Storm"), 1990
- Lothar and Martin, 1999
- Kyrill, 2007
- Xynthia, 2010
- *Ex-Hurricane Katia, 2011

- St Jude's Storm, 2013
- *Ex-Hurricane Ophelia, 2017

where asterisks denote PTCs. Additionally, TCs affect European Overseas Countries and Territories (e.g. Bermuda, the Cayman Islands, Guadeloupe, Madeira, and Martinique), and European Outermost regions (e.g. the Azores, and Madeira).

All three types of storm are responsible for insurance losses in Europe, whether due to damage in Europe itself or indirectly via damage elsewhere. Figure 18 illustrates that insurance loss events are distributed globally and highlights that several of the catastrophes that occurred in 2017 were TCs (labelled as “hurricanes” and “typhoons” on the figure). Figure 19 suggests that there has been an upward trend in both the overall losses and insured losses from natural hazards with time (though some of this trend is due to societal factors/economic growth, as well as to the increase in the number of meteorological loss events), and demonstrates that meteorological hazards make up a large fraction of loss events from year to year.

NatCatSERVICE

Loss events worldwide 2017

Munich RE

Geographical overview

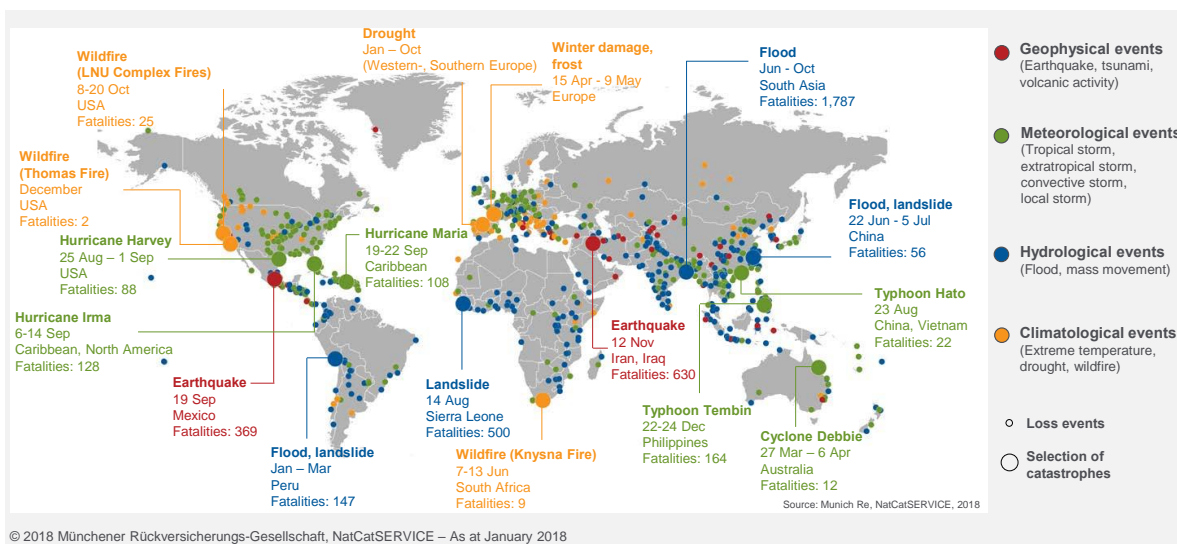
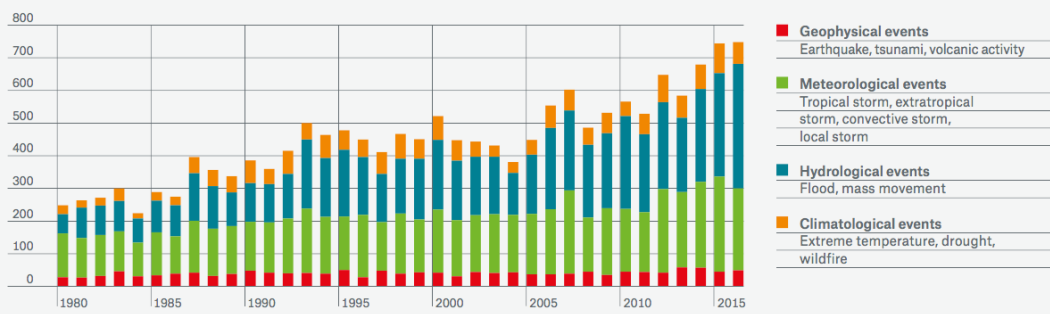
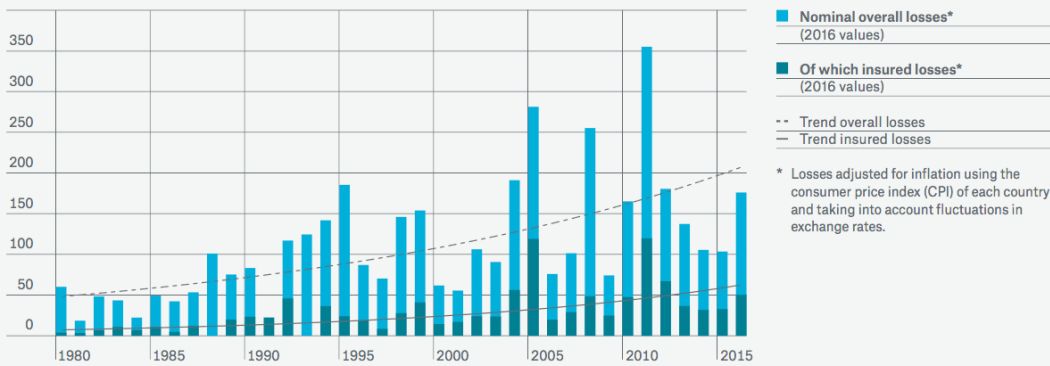


Figure 18 Insurance loss events during 2017. Source: Munich Re NatCatSERVICE.

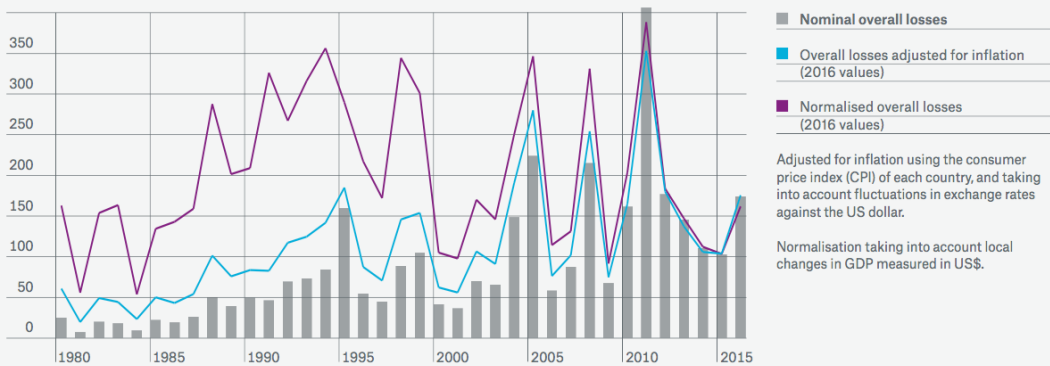
Number of loss events 1980–2016



Overall losses and insured losses 1980–2016 (in US\$ bn)



Loss events worldwide 1980–2016



Source: Munich Re NatCatSERVICE

Figure 19 Timeseries of various metrics of insurance loss arising from natural hazards: top panel – number of loss events; middle panel – overall losses and insured losses; bottom panel – loss events worldwide, comparing the nominal overall losses (losses recorded at the time) with inflation-adjusted (blue line) and normalised (GDP-adjusted; purple line) losses. Source: Munich Re NatCatSERVICE.

3.2.1.2 Structure of this section

This section discusses four aspects of user-focused PRIMAVERA model analysis relevant for insurance.

The impact of model resolution on the **integrated kinetic energy of TCs** is explored in Section 3.2.2. As a large portion of the costs caused by TCs is insured (Munich Re 2018), insurance companies are highly interested in predicting storm activity and the associated potential damages and losses. Traditionally, the destructive potential of TCs is estimated using the maximum 1-minute sustained wind speed and their corresponding classification on the Saffir-Simpson scale, or the Accumulated Cyclone Energy index and the Power Dissipation Index. However, all these metrics neglect a key storm component when it comes to estimating damages: the storm size. It is possible that by focusing on such metrics when estimating the probable impact of climate change on TC activity and neglecting a key factor driving losses, our projected changes in TC activity will not be representative of the associated losses. Here, the intensity metric Integrated Kinetic Energy (IKE), which takes into account storm size and correlates more closely with damages than other commonly used metrics, is evaluated in PRIMAVERA models and the effect of resolution is investigated. By using a metric which tracks more closely with insured losses, we aim to make analyses of TC activity in climate models more relevant to the insurance sector.

In Section 3.2.3, the representation of **TCs' precipitation and moisture budget** is explored. Simulating tropical cyclone precipitation in GCMs with parameterised convection remains a challenge as TC precipitation relies on a tight coupling between model dynamics and physics. Improving tropical cyclone precipitation in GCMs would benefit TC flood forecasting and allow to issue more reliable projections of the future evolution of tropical cyclone precipitation. Our analysis focused on two metrics: the precipitation per tropical cyclone averaged in a 5 degree cap (TCP5), as a measure of the total cyclone precipitation, and in a 2 degree cap (TCP2), to estimate the largest precipitation rates in the core region. We found that TCP5 has little dependence on GCMs resolution and is more sensitive to model formulation. We explained this result by the large-scale balance between precipitation and the moisture flux convergence, which low and high resolution models represent equally well. From this analysis, we conclude on the additional value of high-resolution in simulating the intense precipitation in the core region of TCs, which would benefit TC flood forecasting. In addition, we found a large inter-model spread of the response of TC precipitation to future conditions: some models simulate an increase of precipitation in the inner core region, but others project a decrease at the core and an increase in the outer region. The response of precipitation in the frame of reference of the storm, relates well to the difference of the distribution of TCP5 between models. A better understanding of the response of precipitation in the frame of reference of the storm to environmental drivers will help issue better projections of tropical cyclone extreme precipitation.

Section 3.2.4 discusses the creation and evaluation of **ETC event sets created from high-resolution models** and their potential value in understanding insurance losses. Event sets are used to provide input to catastrophe modelling in the insurance sector, so the interest here is in understanding whether PRIMAVERA models are better than existing sources of climate information at simulating these events. In particular, there are two broad approaches to constructing event sets: a statistical approach, and an approach which combines statistical and dynamical information. The former is computationally cheap, but is based on a short observational period (~50 years or less), which means that thousands of windstorm footprints can be generated, but their frequency is difficult to estimate. The latter is computationally expensive, but allows the windstorm frequency to be taken directly from the model. However, low-resolution global climate models suffer from biases in the North Atlantic storm track (Zappa et al. 2013), meaning that there could be biases in storm frequency and location that are difficult to correct for. Some of these biases are reduced in PRIMAVERA models, and they may therefore be a better option for use in the dynamical-statistical method.

Finally, in Section 3.2.5 the nature of the **tropical-to-extratropical transition in PTCs** in different high-resolution models is analysed. Although rare, landfalling PTCs are an important natural hazard for Europe. Historical high-impact European events, such as Debby (1982), Floyd (1999) and Ophelia (2017), brought the potential risks associated with PTCs to the attention of policy-makers, the insurance sector, and the public. Many storms originating in the tropics undergo a complex structural evolution, including extratropical transition, and the simulation of these processes is expected to benefit from increased horizontal resolution. PRIMAVERA offered an opportunity to move beyond case studies to examine PTC risk systematically across models using objective identification and classification methods.

3.2.2 Impact of resolution on integrated kinetic energy of tropical cyclones in present and future climate

Louis-Philippe Caron and Phillip Kreussler, BSC

3.2.2.1 Motivation

Commonly used indices to estimate the damage potential of tropical cyclones are the Accumulated Cyclone Energy index (ACE, Bell et al. 2000) and the Power Dissipation Index (PDI, Emanuel 2005) which are integrated measures of number, intensity and duration of cyclones. They are typically used to represent the level of activity of a hurricane season. However, ACE and PDI neglect a key factor relating to damages: the actual storm size. Studies by Mahendran (1998), Kantha (2006) and

Zhai and Jiang (2014) show that including the storm size and structure is beneficial to damage estimates and the explained variance in associated losses.

To address this issue, a measure called Integrated Kinetic Energy (IKE, Powell and Reinhold 2007), was developed. This metric, unlike other integrated measures such as ACE and PDI, includes the size of the storm by integrating the energy of the entire wind field. Storms from the past two decades have shown the importance of introducing storm size to damage estimates: hurricanes that caused extensive damage in the US like Ivan (2004) and Katrina (2005) were rated as relatively weak on the Saffir-Simpson scale at landfall. However, in terms of IKE, these storms would be rated as significantly dangerous owing to the large extent of their wind fields, more in line with the large devastation they brought (Kantha 2006, Powell and Reinhold 2007, Kozar & Misra 2019). Storm surge and waves generated by tropical cyclones, too, have been found to be closely connected to IKE as the shear stress of the wind on the ocean surface also scales with kinetic energy (Powell et al. 2003, Donelan et al. 2004)

3.2.2.2 Process

IKE is the volume integral of the kinetic energy per volume unit (KE) of the horizontal wind field of a storm and is calculated as the area over which the wind field exceeds a certain wind speed threshold, vertically integrated over a 1-metre layer centred around 10 metres height for which the conditions are considered representative for the entire 1-metre layer:

$$\text{IKE} = \int [V] \text{ KE } dV = \int [V] 0.5 * \rho * \sqrt{(u^2 + v^2)^2} * dV$$

In this study, only grid points with wind speeds larger than 18 ms^{-1} , which is the threshold required for a storm to be classified as a tropical cyclone, contributes to the IKE. Figure 20 below shows an example of a surface wind speed field associated with a tropical storm. The green dot represents the centre of the storm as identified by the tracker. The yellow isolines display the 18 ms^{-1} isotachs. Thus, all the grid points within the isolachs are considered for the IKE computation.

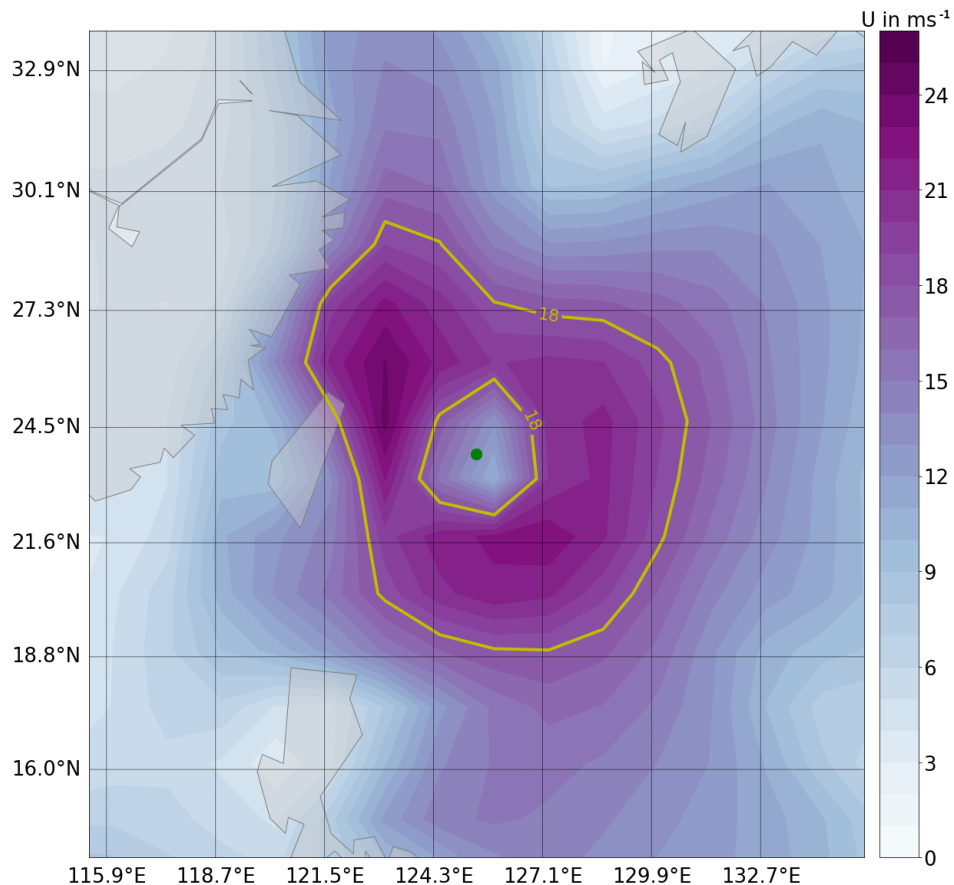


Figure 20: Example of a wind speed field selected by the tracker. The storm centre as detected by the tracker is represented by the green dot. The 18 ms⁻¹ isolachs are highlighted in yellow. All the grid points located within the isolachs are taken into consideration when calculating IKE.

The model used to assess the effect of horizontal resolution and climate change on tropical cyclone IKE is the CNRM model, specifically the CNRM-CM6-1 model ([Volodire et al. 2019](#)). The CNRM-CM6-1 model has been found to produce TC wind speeds and frequencies close to observations, as discussed in [Roberts et al. 2020](#) which makes it the ideal choice for this study. The model horizontal resolution is about $1.4^\circ \times 1.4^\circ$ and $0.5^\circ \times 0.5^\circ$ at the equator for LR and HR, respectively. This study only makes use of the atmosphere-only experiment (highresSST and highresSST-future). However, we are currently extending this study to coupled simulations and other GCMs as well.

The tracker used to detect the formation and propagation of tropical cyclones within the model output data is the GFDL Vortex Tracker V3.5b ([Bao et al. 2013](#)) used through the ESMValTool infrastructure. We consider the entire 1950-2050 period, but only tracked systems located in the Northern Hemisphere between 1 June and 30 November.

3.2.2.3 Results

Roberts et al. (2020) have shown that an increase in resolution leads to an increase in the maximum surface winds of tropical cyclones in PRIMAVERA simulations. Thus, the question arises whether this increase in maximum winds translates into higher IKE values. Figure 21 shows a scatter plot of wind speed and the storm area with surface winds above the 18 ms^{-1} threshold, i.e. the area of the storm that contributes to the IKE (“IKE area”), at the time of maximum lifetime IKE for all storms in the entire NH from 1950 through 2050 and for both resolutions. The colour in the figure shows the IKE values for these storms.

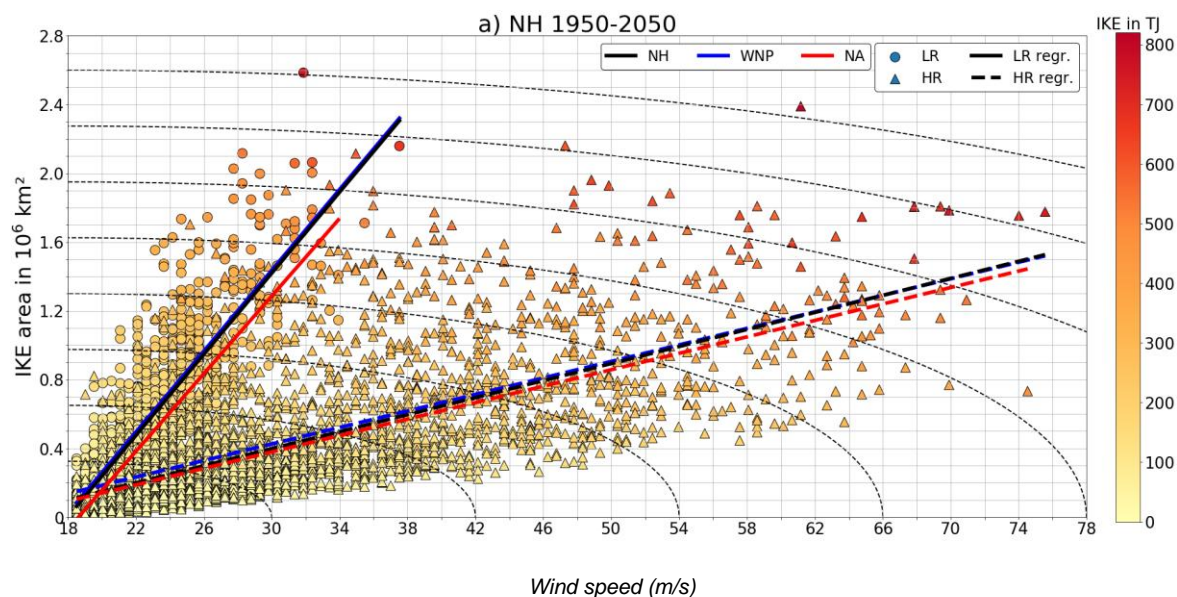


Figure 21: Scatter plot of storm area above 18 ms^{-1} wind speed threshold (“IKE area”) against wind speed associated with maximum lifetime IKE of all the storms in the entire northern hemisphere from 1950-2050. IKE values are colour-coded for both resolutions, LR (circles) and HR (triangles). Regression lines are drawn in solid for LR and in dashed for HR. The regressions for the storms attributed to the WNP and NA are shown in blue and red, respectively. The dashed ellipses show an approximation of constant IKE values across the scatter plot.

The figure shows that there is a higher number of storms in the HR simulation (triangles) and that these are more intense storms (as measured by the maximum surface wind speed) than the storms in the LR simulations (circles): the maximum wind speed associated with maximum lifetime IKE almost doubles from roughly 38 ms^{-1} to about 76 ms^{-1} . It also shows that the largest storms are similar between both experiments, with about $2.6 * 10^6 \text{ km}^2$ for LR and approximately $2.4 * 10^6 \text{ km}^2$ for HR. Surprisingly, both configurations also manage to produce storms of comparable maximum IKE. However, a clear difference between LR and HR is the distribution of the data points with storms in HR being shifted toward higher wind speeds and smaller size whereas LR tends to produce larger but weaker storms. The linear regressions (solid and dashed black lines) confirm this difference and reveal that TCs in HR are characterised by a smaller IKE area relative to TCs in LR (at constant

wind speed). The blue and red lines, depicting the regressions for storms in the WNP and NA, show a similar behaviour.

To determine whether storm intensity or size is the main factor determining maximum IKE, the correlations are computed and displayed in Table 1. Additionally, the correlation between IKE and the minimum MSLP of the storm associated with the lifetime maximum IKE is shown. As expected, the correlations show that there is a strong relationship between the quantities and show that storm size is the dominant factor in driving IKE, at both resolutions. Correlations are lower for the wind speed and minimum MSLP, but both still provide an excellent predictor for maximum IKE. Interestingly, MSLP seems to be more correlated to IKE than maximum wind speed at HR, but this is not the case in LR. Although the differences are small, they are consistent across basins. The reason for this is not clear at this stage.

	LR	HR
maximum surface wind speed	0.87	0.82
IKE area	0.99	0.96
minimum MSLP	-0.78	-0.85

Table 1: Correlations of maximum lifetime IKE (for the period from 1950-2050) with associated maximum wind speed, IKE area and minimum MSLP for the northern hemisphere.

3.2.2.4 Benefits of PRIMAVERA

It is clear from previous PRIMAVERA studies (Roberts al. 2020) that increasing the resolution improves the representation of tropical cyclones in climate models. The number of storms, their intensity and their geographical distribution generally tend to improve with resolution. However, it is less clear that resolution has a similar impact on their integrated kinetic energy. Because of the dominant role played by the storm size in calculating IKE and the compensating effect between size and intensity between LR and HR, both configurations tend to produce storms with IKE of similar magnitude (although for different reasons).

However, when computing the total IKE produced over an entire season, large differences between LR and HR emerge, with HR producing much larger values (not shown). In this case, the differences are driven, not by the differences in the IKE of

individual cyclones, but by the differences in the number of cyclones in the two configurations.

3.2.2.5 Caveats

The main caveat to highlight comes from the fact that these results are derived from only one climate model. In particular, the CNRM model is known to produce unusually strong cyclones in both of these configurations. This is the reason that motivated us to use this model first, as we were expecting to detect cyclones that were closer in intensity to the ones that are observed. However, it is possible that these results are not representative of other climate models. Furthermore, this study only made use of simulation performed in atmosphere-only mode. It is possible that the coupling might impact our findings. We are currently extending our analysis to additional PRIMAVERA models (both in AMIP and in coupled mode), so the impact of the model itself and the coupling will be addressed.

3.2.2.6 Implications for the insurance sector

As mentioned in the introduction, IKE is more correlated to cyclone-related damage than maximum surface wind speed. Because insurers are ultimately interested in the impact of cyclones, the former is a more relevant quantity to that sector than the latter. The fact that IKE, unlike maximum wind intensity, shows little sensitivity, at least in the CNRM model, suggest that damage analysis based on this quantity should show little sensitivity as well. However, if the IKE of the individual cyclones doesn't show statistically significant differences, because the resolution also impacts the number of storms, the total IKE produced over a given cyclone season will be very different between LR and HR. Thus IKE derived from higher resolutions tends to be more realistic.

Furthermore, the fact that the maximum surface wind speed correlates well with IKE suggests that the current practice of using this quantity in evaluating change in hurricane activity is a reasonable proxy for estimating change in related impact. It is interesting to note that IKE correlates better with maximum wind speed at low resolution and better with minimum in SLP at higher resolution. While the differences are small, they are constant across basins. The reason for this isn't entirely clear at the moment, but it might be in part due to the constraints on how momentum is transferred from the atmosphere to the surface at very high wind speed. It will be interesting to see if this is only a feature of the CNRM model or whether it is also shared by other GCMs as well.

3.2.2.7 Key points

- IKE is a useful metric for cyclone-related damage, and hence of interest to insurers
- Other metrics such as ACE and PDI neglect the storm size, which is a key factor relating to damage
- In the HR simulation, there are more storms, and they are more intense than those in the LR simulations. They also tend to be smaller in size
- Storm size is the dominant factor in driving IKE at both LR and HR
- The number, intensity and geographical distribution of tropical cyclones tend to improve at higher resolution, but it is less clear that resolution has a similar impact on IKE
- This study was undertaken using only one GCM, the CNRM model, in both LR and HR configurations, and in simulations performed in atmosphere-only mode; it is possible that other GCMs, and coupled models, could impact the results

3.2.3 Tropical cyclone precipitation and moisture budget in HighResMIP models

Benoît Vannière UREAD, Malcolm Roberts Met Office, Pier Luigi Vidale UREAD, Kevin Hodges UREAD, Marie-Estelle Demory UREAD, Louis-Philippe Caron BSC, Enrico Scoccimarro CMCC, Laurent Terray CERFACS and Retish Senan ECMWF

3.2.3.1 Motivation

- 1) When they make landfall, tropical cyclones represent a major hazard, potentially causing torrential rain and freshwater floods. In the total number of fatalities in the US caused by tropical cyclones originating from the North Atlantic over the period 1963-2012, fresh water floods are responsible for a substantial fraction (27 %), which is to be compared with surge (49 %) and wind (8 %) (Rappoport, 2014). Those numbers may vary a lot from one period (see previous estimates by Rappoport, 2000, which reached different conclusions), one region or one event to another (compare Harvey and Irma for instance, which occurred two weeks apart in 2017, but Harvey hit more densely populated regions and generated larger rain rates). An important difference of freshwater floods compared to surge is that they can occur far away from coastal areas. For instance, in 2017, Harvey damaged 204,000 homes. Three-fourths of those homes were outside of the 100-year flood plain, where owners did not have flood insurance.

- 2) The EU and countries of PRIMAVERA partners have several territories potentially affected by tropical cyclones. Out of the 9 Outermost Regions (OMRs) of the European Union, 7 are in the tropical band and 5 on major tropical storm tracks. Just to name one example, Saint-Martin was devastated by TC Irma in 2017, where 95% of structures were destroyed and the cost of damaged was evaluated to 3.5 billion dollars. The website of the European Parliament does emphasise the need for synergies between “the Structural Funds’ support for ORs and EU-level programmes such as **Horizon 2020**, LIFE+ and COSME.” Most of the OMRs are islands with relatively high-orography, which represent an additional complexity in terms of modelling tropical cyclone precipitation and impacts.

- 3) Climate models are used both to estimate the risk of such events and to forecast them. Low resolution GCMs can be used to provide mean state conditions which can be used to drive statistical models (see following point 4). High-resolution GCMs, together with a data assimilation system providing initial conditions, can model TC dynamics with enough accuracy to be used for probabilistic forecast (see following point 5).

- 4) How do insurances estimate the risk? Catastrophe modelling typically use hybrid models, i.e. a combination of statistical and physically-based modules trained by the outputs of GCMs (e.g. Columbia Hazard Model, CHAZ; Lee et al. 2018). Low-resolution models, even if they simulate unrealistic TCs, can be used to evaluate the large-scale environmental conditions favourable to cyclogenesis. Some natural questions arising from this are: Is there additional information that could be gained from high-resolution or are drivers captured well enough by low-resolution models? Can we trust the precipitation predicted by low-resolution models, so that it can be used directly to train statistical models, or shall we rely on high-resolution models and observations?

- 5) How are climate models used to predict TC floods? As part of the Global Flood Awareness system (GloFAS), ECMWF issues TC flood forecasts which are based on the precipitation of the ECMWF ensemble forecasts system (ENS). Note that GloFAS is part of the EU-funded Copernicus Emergency Management Service (CEMS). GloFAS forecasts were used in the aftermath of tropical cyclones Kenneth and Idai in Mozambique in 2019, to predict where, and for how long, flooding may occur, which proved to be a valuable information to develop humanitarian aid. Some challenges remain, in particular, to reduce biases in TC tracks, and in the location and amount of precipitation simulated by IFS. Note that the resolution of ENS is close to that of PRIMAVERA ECMWF-IFS-HR, so our results might prove relevant for TC flood prediction at ECMWF.

- 6) Future projections:

- a. Tropical cyclone precipitation is expected to increase at a rate close to that predicted by the Clausius-Clapeyron relation (7%/K). This is larger than the rate of increase of global mean precipitation (~3%/K) which is limited by energetic constraints. Some studies (e.g., Knutson et al 2015; Liu et al 2019) have projected “super Clausius-Clapeyron rates” for tropical cyclone precipitation, arguing that there could be a mutual enhancement of latent heat release and vertical velocity.
 - b. If one wants to use GCMs to address how the return period of TC rainfall events of a given amplitude will change in future, a question which was addressed in Emanuel (2017), Risser and Wehner (2017) and Van Oldenborgh et al. (2017) in the case of the Hurricane Harvey, a prerequisite is to determine how GCMs project changes in the number of tropical cyclones, the amount of precipitation per tropical cyclone and the source inter-model uncertainty arises.
- 7) Note that the primary intention of this work was not to provide relevant information to the insurance sector, but rather to understand the physics of tropical cyclones in GCMs. The following questions are reflections based on the findings published in Vanniere et al. (2020):
- a. What is the impact of resolution on the representation of tropical cyclone precipitation? Do models with a resolution of ~25km represent tropical cyclone precipitation with enough fidelity to issue TC flood forecasts? Can we expect some additional improvement when resolution is increased even further?
 - b. Is the relation between physical parameters and precipitation well simulated by climate models so that it can be used directly to train statistical models? What could be gained by using higher resolution models for the training?
 - c. How will tropical cyclone precipitation change in a future climate? Where does uncertainty arise (model formulation and/or resolution)?

3.2.3.2 Method

- 1) We have used the following sets of observations: IBTrACS, TRMM-3B42 and CMORPH-v0x.
- 2) Observations are complemented with the reanalyses: ERA-Interim, ERA5, JRA-55.

- 3) The PRIMAVERA models ensemble is composed of EC-Earth3P, ECMWF-IFS, CMCC-CM2, CNRM-CM6-1, HadGEM3-GC31.
- 4) The PRIMAVERA simulations and the reanalysis have been tracked with the TRACK algorithm (Hodges et al, 2017).
- 5) Tropical cyclone precipitation (TCP) is averaged in a polar cap defined by its radius in degrees from the centre of the storm following the technique described in Scoccimarro et al (2014).

See Vanniere et al. 2020 for further information about the method.

3.2.3.3 Results

- 1) At high resolution, TCs have a more compact structure, leading to more intense precipitation in the inner region (i.e. for radii less than 2 degrees). However, IFS-derived models show a lesser increase of TC precipitation with increasing resolution. This latter result can be extended to the reanalysis ERA5 when it is compared to ERA-Interim.
- 2) We first considered precipitation averaged in the entire TC (5-degree cap, TCP5) (Figure 22). Interestingly, the frequency of high intensity TCP5 is not sensitive to resolution but the frequency of low intensity TCP5 is. We have explained this result by the fact that (i) TCP5 is the result of a large-scale balance and the distribution has little sensitivity to resolution (hence the overall lack of sensitivity of the distribution); while (ii) the threshold of the tracking algorithm makes TCs of low intensity in LR models under-detected (hence the lower frequency of low intensity TCP5 in LR models).
- 3) We then considered the distribution of precipitation in a 1-degree cap (TCP1, not shown), which is a better measure of how models simulate the inner core precipitation. HR models do represent very large precipitation rates, several times larger than in LR models. This is consistent with more concentrated precipitation in the inner region at HR as mentioned in point (1). IFS-based models show a lesser sensitivity than CNRM-CM6-1 for instance. In addition, CMCC-CM2, CNRM-CM6-1 and HadGEM3-GC31 can simulate precipitation rates larger than in the observations. This raises the question of whether the observations underestimate the inner core precipitation or models generate overly strong convection in the inner region.
- 4) The fact that TCP5 has a low sensitivity to resolution might be surprising, considering that moist processes play a crucial role in the intensification of tropical cyclones and that HR models do predict that TCs can reach higher intensity than LR. However, we should make sure not to distinguish two

different views. On the one hand, the moisture budget of tropical cyclones is the result of a large-scale balance, with the source radius of surface evaporation extending as far as 15 degrees from the centre of the storm. LR and HR models capture equally well this large-scale balance and this is why TCP5 has a low sensitivity to resolution. On the other hand, tropical cyclones intensification is sensitive to the amount of evaporation in the region close to the core of the tropical cyclone, where the specific humidity of an air parcel can be changed more effectively. Since HR models simulate stronger winds and extract more moisture from the ocean in the inner core region, they do generate warmer core anomalies and larger TC intensities.

- 5) Another important finding of our study is the sensitivity of TCP distribution to the tracking algorithm itself. The underprediction of the low intensity TCP5 in LR models is even larger when the tracking is performed with Tempest Extreme. This is because Tempest Extreme tracks grid-point features (minimum SLP anomalies), whereas TRACK tracks vorticity anomalies after spectral truncation of T63. We believe that tracking large-scale features on the T63 grid represents a fairer comparison between LR and HR.
- 6) Regarding future projections, our findings are as follows:
 - a. The main uncertainty for the total precipitation associated with TC comes from the evolution of the number of TCs. The annual count of TCs is projected to decrease in the PRIMAVERA atmosphere-only simulations, in the range 5 to 7%/K, which cancels out the increase of 5 to 7%/K of TCP5 (Clausius-Clapeyron), so that the total amount of precipitation associated with TCs is not predicted to change globally. However, different results emerge from coupled experiments, in which the annual count of TC is projected to decrease by 15 to 20%/K, while the amount of precipitation per TC continues to increase at a Clausius-Clapeyron rate.
 - b. The difference of composite of tropical cyclone precipitation between future and present conditions depend both on resolution and model formulation (Figure 23 and Figure 24). Some models represent an increase of precipitation in the inner core, whereas other represent an increase in the outer region. We expect models showing a future increase of precipitation at the core (HadGEM3-GC31 and CMCC-CM2) to generate more extreme precipitation than the other models. Conversely, models with an increase of precipitation in the outer region and a decrease of precipitation in the inner core should have a lesser increase of extreme precipitation (CNRM-CM6-1 and MPI-ESM1-2).
 - c. We finally considered the change in cumulative frequency of precipitation associated with all tropical vortices (Figure 25). The

intensity of extreme events increases more than the intensity of less extreme events: for weak vortices the energetic constraint on global precipitation is “felt” and the increase is around 3%/K (Fig. 4c). Larger intensity extremes (which correspond to tropical cyclone precipitation), however, are “free” of the energetic constraint, they generally distribute around 7%/K. Those larger intensity extremes exhibit a larger diversity of rate of increase, with both resolution and model formulation playing a role. This diversity of responses among models can be tracked back to changes described in Figure 23 and Figure 24, and are in agreement with the hypothesis formulated in our point (b) above.

Results mentioned in point 6 will be published in an upcoming manuscript.

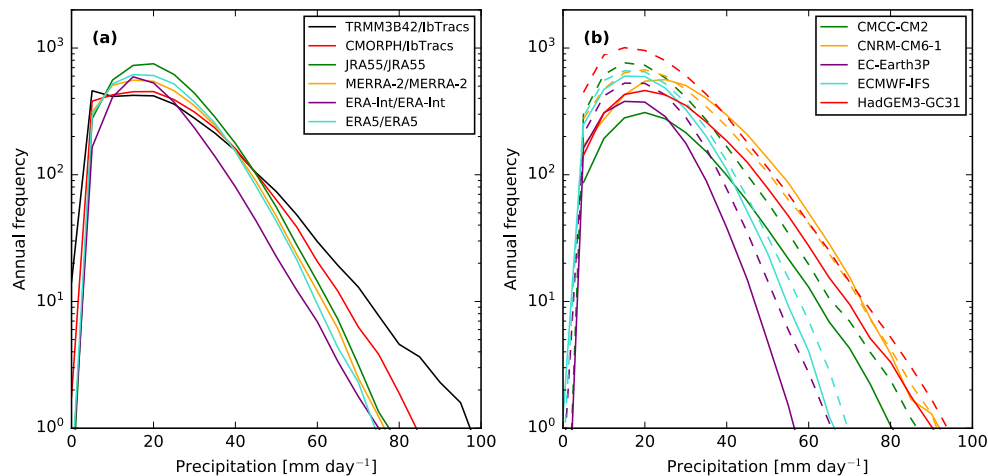


Figure 22: Distribution of TCP5 in (a) observations and (b) in PRIMAVERA models. Solid curves stand for LR and dashed curve stands for HR.

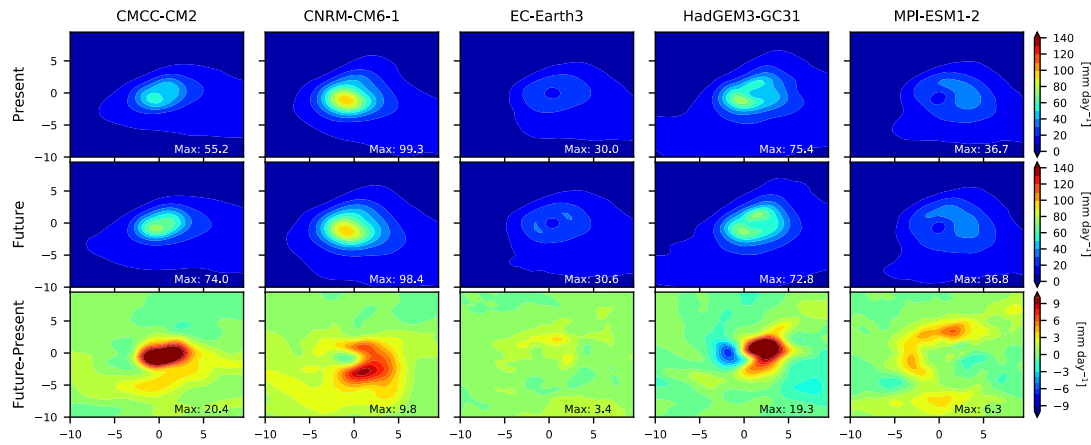


Figure 23: Composite of the 200 strongest tropical cyclones in the low-resolution AMIP configuration of each PRIMAVERA model over the period 1950-1965 [first row] and 2035-2050 [second row] and their difference.

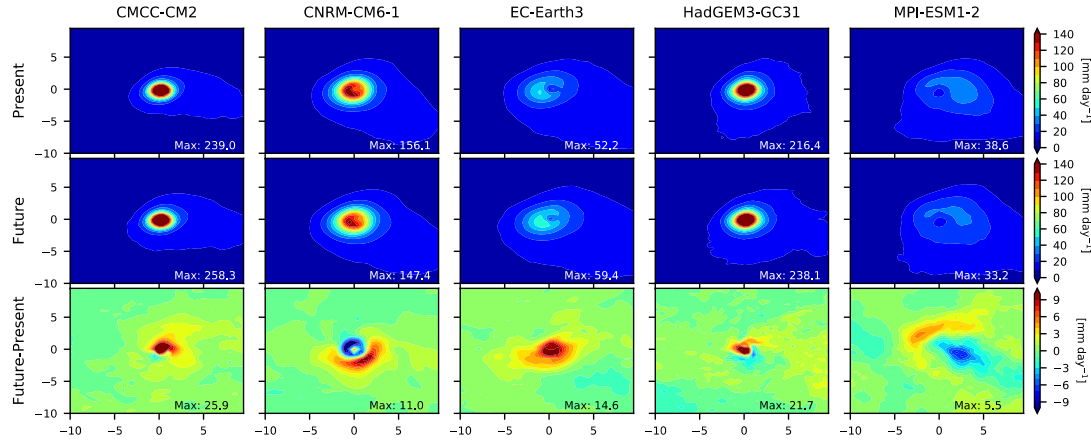


Figure 24: Same as Figure 23 but for high-resolution AMIP simulations

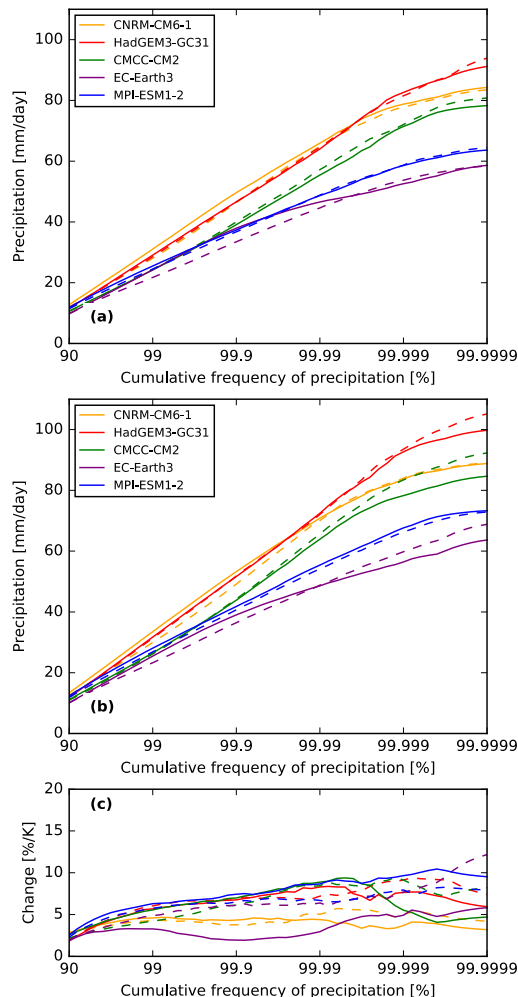


Figure 25: Distribution in cumulative frequency of precipitation associated with all tropical vortices and averaged in a 5-degree radial cap for (a) 1950-1965, (b) 2035-2050 and (c) their difference normalised by the global mean surface temperature change. Plain curves stand for low-resolution and dashed curves for high-resolution.

3.2.3.4 Implications for the insurance sector and future questions to answer

- 1) Our study allowed a better understanding of the drivers of tropical cyclone precipitation in observations and models. While TCP5 appears to be a metric that models can simulate robustly, TCP1 is strongly sensitive to resolution. Several models predict larger TCP1 than in the observations. It is difficult to say if models simulate overly strong inner core precipitation or if satellite observations and reanalyses underestimate the largest precipitation rates. It is crucial to understand where the “truth” is to make future projections with more confidence. One way forward to solve this issue is to assess more case studies of TC floods, in forecast mode, for TCs which were well monitored (with both satellite and rain gauge observations).

- 2) We believe models capture TCP5 with enough reliability so that they are used to estimate return periods of extreme TCP5 events. However, TCP1, which is conducive to flash floods, suffers too strong biases/uncertainty to estimate return values with high confidence. Reducing this uncertainty is crucial if one wants to estimate trustworthy return values of intense TC rainfall events.
- 3) Statistical models of TC precipitation can be based on low-resolution models if they try to predict TCP5: there is possibly more to gain by having longer simulation than better resolved ones. However statistical models should use the highest resolution possible if they try to predict inner core precipitation rates.
- 4) ECMWF-IFS underestimates the intensity of TCs, the amount and location of TCP, with potential bias in forecasting systems such as GloFAS.

3.2.4 Exploring event sets created from high-resolution climate models for European windstorm risk assessment

Julia Lockwood, Galina Guentchev, Erika Palin; Met Office

3.2.4.1 Motivation

One of the use cases described in PRIMAVERA deliverable 10.1 was the construction of a European winter windstorm ‘event set’ for use in catastrophe modelling for insurance and risk analysis (D10.1 section 4.3.4.1). An event set is a large number of windstorm ‘footprints’ (where a footprint is a map of maximum gust for each storm), preferably containing enough footprints to understand variability of windstorm impacts over hundreds to thousands of years.

Windstorm event sets produced by the insurance industry are often proprietary so there is limited information on the methods used to generate them. However, methods published in scientific literature are broadly divided into statistical methods or a combination of dynamical and statistical modelling. In the former, the statistical properties of historical windstorms can be analysed to create a statistical model to simulate new windstorms with similar properties (eg Youngman and Stephenson 2016), or historical footprints can be ‘perturbed’ to generate a number of new events that differ slightly from past ones, so are deemed to be physically plausible (eg Welker et al 2020). In the dynamical-statistical method, due to the high computational costs of running dynamical (climate) models, a long run of a climate model is performed at a low spatial resolution and then downscaled statistically over the region of interest (eg Pinto et al 2013).

Advantages of the statistical methods include low computational costs, but they are ultimately models based on a short observational time period (typically less than 50 years for re-analysis and observational datasets), and although they can be used to generate thousands of footprints, the *frequency* of each of those footprints is difficult to estimate. The dynamical-statistical methods are computationally expensive but the frequency of the windstorms can easily be taken directly from the model. However, it is known that low resolution global climate models suffer from biases in the North Atlantic storm track (Zappa et al 2013), meaning that there could be biases in storm frequency and location in the region of interest which are difficult to correct for.

As shown in previous PRIMAVERA deliverables (D10.2, D10.3), there is a reduced bias in storm frequency and intensity in PRIMAVERA models compared to the older generation of CMIP5 models. The thousands of years of high resolution PRIMAVERA climate model data is therefore ideal for generating a new dynamical-statistical windstorm event set. In this section we outline the method used to construct the event set, and present initial analysis and implications for the insurance industry risk assessment. We also look into future windstorm activity using simple measures of storm risk (number of ‘storm days’ and total area affected by storms in a season).

3.2.4.2 Method

For this event set we only attempt to model storms in the extended winter season (October-March). These storms tend to be associated with extra-tropical cyclones and are on a large scale compared to smaller, convective storms that occur in summer.

To be consistent with the previous event set project WISC (Steptoe 2017), the European domain is defined as 25°E to 40.5°W in longitude, and 34.4°N to 71.5°N in latitude. To comply with industry standards, a windstorm footprint is defined as the maximum gust associated with the storm over a 72 hour period. However, only two PRIMAVERA models outputted maximum gusts, so instead the footprints are made from daily maximum surface windspeed (sfcWindmax) and converted to gusts during the bias correction (described below).

The footprints analysed in this section are made from the highresSST-present PRIMAVERA experiment, covering the time period 1950-2015. This experiment has prescribed sea surface temperatures and was chosen because the models are less likely to have storm track biases than coupled models, although in the future it would be worth repeating a coupled model event set to verify if this is the case. Footprints are also being made for the highresSST-future experiment (2015-2050), although at the time of writing these footprints are not yet complete. Instead, in Section 3.2.4.3.3

we look at changes in daily maximum winds and storm counts to infer future storm activity.

The models used (with atmospheric grid spacing at 50°N given in brackets) were MPI-ESM1-2-HR (67km), MPI-ESM1-2-XR (34km), CNRM-CM6-1 (142km), CNRM-CM6-1-HR (50km), HadGEM3-GC31-LM (135km), HadGEM3-GC31-HM (25km), EC-Earth3P (71km), EC-Earth3P-HR (36km), CMCC-CM2-HR4 (64km) and CMCC-CM2-VHR4 (18km). All models had one ensemble member, apart from HadGEM3-GC31-LM with 5 members, HadGEM3-GC31-HM with 3 members, and EC-Earth3P and EC-Earth3P-HR with 2 members each. Footprints were not made from the ECMWF IFS model because *maximum* surface winds were not output, and use of mean or instantaneous winds may cause an underestimation of storm intensity from this model.

Storm tracks were identified from each model run using the TRACK algorithm (Hodges 1995). TRACK is actually designed to identify extra-tropical cyclones, defined by maxima in the vorticity field at 850hPa, and not all extra-tropical cyclones are associated with strong enough winds to be considered windstorms. Nevertheless, footprints are made for every cyclone track, as filtering can be performed to reject footprints not associated with high winds at a later stage.

Since footprints are defined as maximum gusts over a 72 hour period and storm tracks are often longer than this, the day to centre the 72 hour period is identified by finding the day of the maximum 10m wind speed over land within 3° of the track centre. This is consistent with other windstorm catalogues such as XWS (Roberts et al 2014).

3.2.4.2.1 Footprint contamination

Often two or more cyclones will have the same or overlapping 72 hour periods identified for their footprints. Simply taking the maximum gusts over the whole domain for the specified 72 hour period for each storm would result in several cyclones being present in a single footprint, and mean that many cyclones would be double counted in the resulting event set. To overcome this footprint contamination issue, for each day in the model run, each grid point in the daily maximum wind field is assigned to a storm track, by identifying the closest cyclone track point during that day. Grid points more than 1500km from any track point are not assigned to a cyclone track. To generate the footprint for each cyclone track, the daily maximum winds for the 72 hour period (specified as above) are extracted, with the grid points assigned to other cyclones masked out, and the maximum is taken. This method was tested with footprints generated from the ERA5 re-analysis (Copernicus Climate Change Service 2017), and it was found to separate the gust fields of famous storms such as Lothar and Martin, which occurred on 26th-27th December 1999 within 24

hours of each other. The ERA5 footprints are used as the observations for the analysis presented in Section 3.2.4.3.

3.2.4.2.2 Statistical downscaling/bias correction and conversion from winds to gusts

In section 3.1.2 of D10.3 it was shown that there are large biases in the tail of daily maximum wind speed distribution in some of the PRIMAVERA models, especially over high altitudes. The cause of this bias is under investigation although it is perhaps related to the surface drag scheme in the models (Williams et al., 2020). Since the estimated insured loss of an event is strongly dependent on extreme windspeeds, it is necessary to perform bias correction so that the event set will give reasonable loss estimations. In addition, although PRIMAVERA models are considered ‘high-resolution’ in terms of global climate models, typical insurers’ windstorm event sets have spatial resolutions less than 25km. To encourage uptake of the data set by the insurance industry statistical downscaling is necessary. Lastly, insurers’ vulnerability models use maximum gust rather than maximum wind as inputs, so the footprints must be converted from wind to gust speeds.

The above issues are overcome with a quantile mapping correction method. For this, before generating the footprints, the model daily maximum wind speeds are regridded to the ERA5 grid (approximately 18km grid spacing at 50°N) using linear interpolation. At each grid point, the empirical cumulative distribution function (CDF) is calculated at probability intervals of 0.5% up the 98th percentile. Above the 98th percentile, the CDF is fitted using a generalised Pareto distribution (GPD). This is repeated on the ERA5 gust distribution, which is used as the reference. The model CDFs are estimated on wind speeds only in the time period which overlaps with the ERA5 dataset, 1979/80-2014/15 (October-March only), to take into account any non-stationarity in the wind/gust speed distribution due to climate change and/or low frequency climate variability.

Wind speeds are then converted to gust speeds by estimating the percentile at each grid point from the model CDF, and taking the corresponding gust for that percentile from the ERA5 CDF at that grid point, ie. $g_i = f_{\text{ERA5},i}^{-1}[f_{\text{mod},i}(w_i)]$, where g_i is the estimated gust at grid point i , w_i is the model wind speed at grid point i , and $f_{\text{ERA5},i}(x)$ and $f_{\text{mod},i}(x)$ are the estimated CDFs of the ERA5 gusts and model windspeeds at grid point i respectively.

It was necessary to estimate $f_{\text{ERA5},i}(x)$ and $f_{\text{mod},i}(x)$ separately at each grid point because the conversion varies dramatically from grid point to grid point, depending on factors such as altitude and surface roughness. This does, however, mean that there are a limited number of data points available for fitting the GPD so extreme gust values in the corrected footprints should be considered highly uncertain. Also note that the data points used for the GPD fits are not all independent: the GPD fits

are performed on daily maximum gusts but during a storm extreme gusts may be present at a particular location for more than 24 hours. This should have little effect on the values of the fitted parameters but the theoretical uncertainty will be underestimated.

3.2.4.2.3 Loss estimation

In order to estimate the damage resulting from each storm in the event set, the loss index derived by Klawa and Ulbrich (2003) is used, with insured loss $\sim \sum_i area_i \times popdens_i \times \left(\frac{v_{max,i}}{v_{98,i}} - 1 \right)^3$, where $area_i$ and $popdens_i$ are the area and population density of grid point i , $v_{max,i}$ is the maximum gust speed in the footprint at grid point i , and $v_{98,i}$ is the 98th percentile gust speed at that same location. Following the WISC project, the summation is over land grid points for the following countries: Luxembourg, United Kingdom, Ireland, France, Spain, Portugal, Belgium, Netherlands, Germany, and Denmark.

3.2.4.3 Results

3.2.4.3.1 Loss distributions

Figure 26 compares the distribution of loss index between low and high resolution models and those in ERA5 (for footprints with a non-zero loss only). The vertical axis is normalised by number of winters (approximately 64 years for each model, 35 years for ERA5). Note that the horizontal axis uses a log scale so bin sizes are much smaller for low intensity storms. The numbers of storms with moderate loss indices (10^7 - 10^{10}) are underestimated in the lower resolution models, and there is significant improvement for the high resolution models. There are fewer loss causing storms in the low resolution models overall, which is consistent with the track density analysis presented in D10.2 and D10.3.

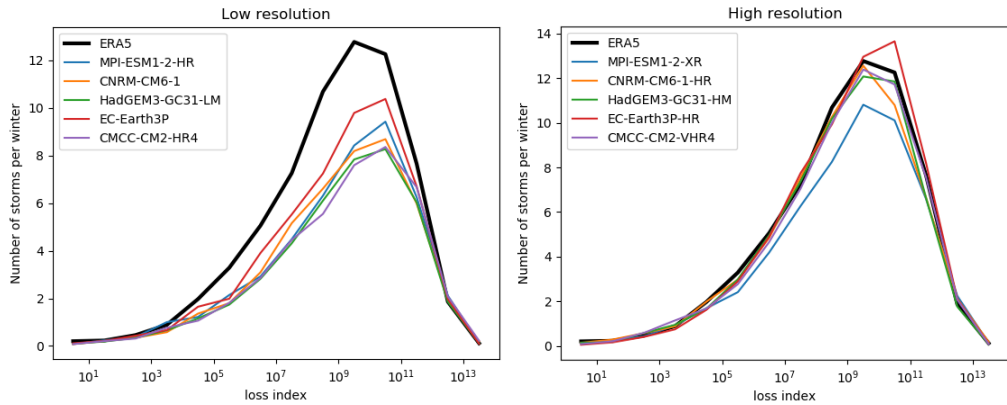


Figure 26: Distribution of loss index from storms in low resolution (left) and high resolution (right) models. The observed distribution (ERA5) is shown with the thick black line. Note that the vertical axis is normalised by number of winters (approximately 64 years for each model, 35 years for ERA5) and the horizontal axis uses a log scale

It should be noted that the range of loss index values is considerable – 13 orders of magnitude -- so the underestimation of moderate loss storms by the lower resolution models may not adversely affect seasonal aggregate losses. This is investigated in Figure 27, which shows the CDF of seasonal aggregate loss index for the low and high resolution models. Despite the underestimation in the number of storms in the low resolution models, the maximum loss seasons have higher losses than the high resolution models. A closer inspection of these high loss seasons reveals that the losses tend to be dominated by one storm for the low resolution models (for example, one storm made up 90% of the losses in the highest loss season from HadGEM3-GC31-LM). This is in contrast to ERA5 and the high resolution models, where the highest loss seasons are dominated by 2 or more storms. The huge loss storms in the low resolution models are probably a result of uncertainty in the maximum gust speeds due to the bias correction method explained above – the conversion to the ERA5 grid may be more unstable for the lower resolution models owing to the larger difference between model and observations. There is perhaps an indication that the models overestimate the frequency of high loss seasons (those with aggregate loss index values $> 10^{13}$), but in general the CDFs compare well to ERA5 for both the low and high resolutions models, given the uncertainty in the ERA5 probabilities.

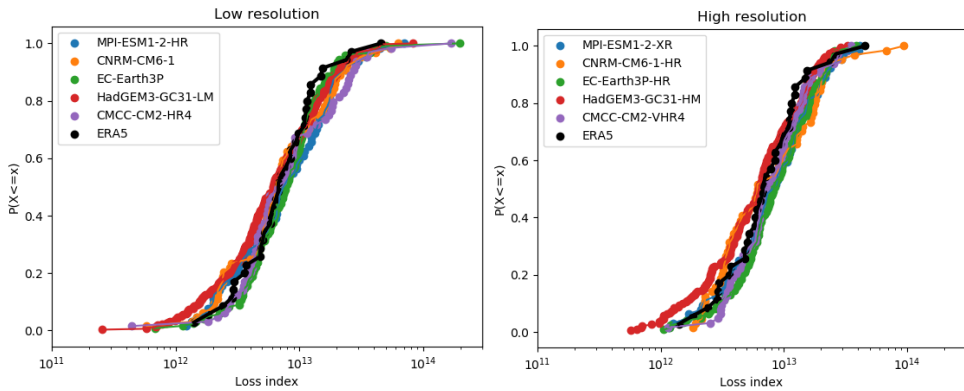


Figure 27: CDFs of seasonal aggregate loss index from storms in low resolution (left) and high resolution (right) models. The observed distribution (ERA5) is shown in black. The points represent each season in the dataset.

3.2.4.3.2 Storm area

It has been suggested by members of the insurance industry that low resolution climate models may have difficulty simulating narrow, intense storms such as the Great Storm of 1987 (15th October 1987). The footprints enable evaluation of storm area, which was not possible with only the storm track information. Figure 28 shows scatter plots of *storm severity index* against storm area for the low and high resolution models, where the storm severity index is calculated in the same way as the loss index but without the population density weighting. The summation is performed over the whole domain rather than the selected countries given above to better represent the intrinsic properties of the storms. Storm area is defined as the total area of the footprint with gusts greater than the local 98th percentile.

The plots show that, as expected, there is a positive correlation between storm severity and storm area, and the models show a similar relationship as seen in ERA5. The black line (estimated by eye) in the plots roughly defines ‘high intensity, low area’ storms, with these storms lying to the left of the line, away from the main cloud of points. These storms have a smaller than expected area, given their intensity. Both the low and high resolution models can simulate such storms, and the proportion of ‘high intensity, low area’ storms (for storms with a storm severity index $> 10^{10}$) is very similar between both sets of models (13% and 15% for the low and high resolution models respectively, compared to 9% for ERA5). These initial results therefore do not reveal an obvious difference in ability to simulate ‘high intensity, low area’ storms, although further investigation is needed.

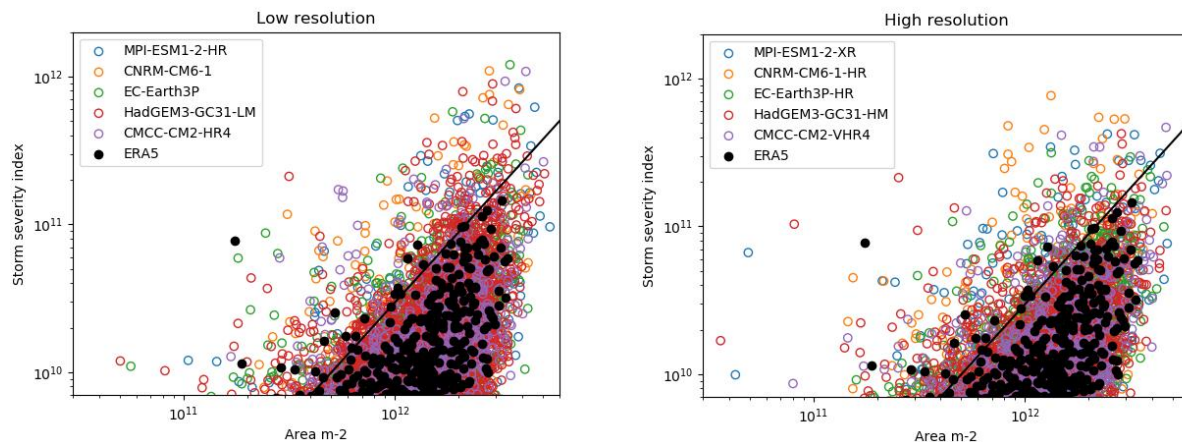


Figure 28: Scatter plots of storm severity index against storm area for the low resolution (left) and high resolution (right) models. ERA5 footprints are shown with black filled circles. The black line is used to define ‘high intensity, low area’ storms (see text).

3.2.4.3.3 Future changes in windstorm activity

At the time of writing, the footprints for the highresSST-future experiments are still being generated. Therefore future windstorm activity is instead assessed by time series of number of ‘storm days’ and total storm area per season. A ‘storm day’ is defined as a day for which the area of land with daily maximum windspeed greater than the local 98th percentile (in the countries listed above) is greater than 5000km². The total area is the sum of the daily areas exceeding the 98th percentile (in the same countries) over each season. These measures are chosen as they may better quantify the change in storm risk compared to extra-tropical cyclone counts from the TRACK analysis, which picks up events that may have little impact over Europe.

Figure 29 shows there is no obvious trend in future storm activity by either measure. It may be that a longer time period is needed to see the effects of climate change emerge above natural variability.

The interannual variability appears to be well captured by the models, although the low resolution models underestimate the number of storm days compared to observations.

Figure 29 also reveals moderate agreement in storm area between the low resolution models (Figure 29b) for the periods 1960-1965 and 2010-2014. For the 1960-65 period, all models but one show reduced storm area compared to the rest of the period. The reduced storm activity is consistent with the unusually negative North Atlantic Oscillation (NAO) observed at that time (Ostermeier and Wallace 2003). For the 2010-2014 period, the models appear to follow the interannual variability seen in observations. These findings need to be assessed for statistical significance, but they reveal the role of sea surface temperature forcing in storm

activity. Such agreement between models is not obvious in the high resolution models.

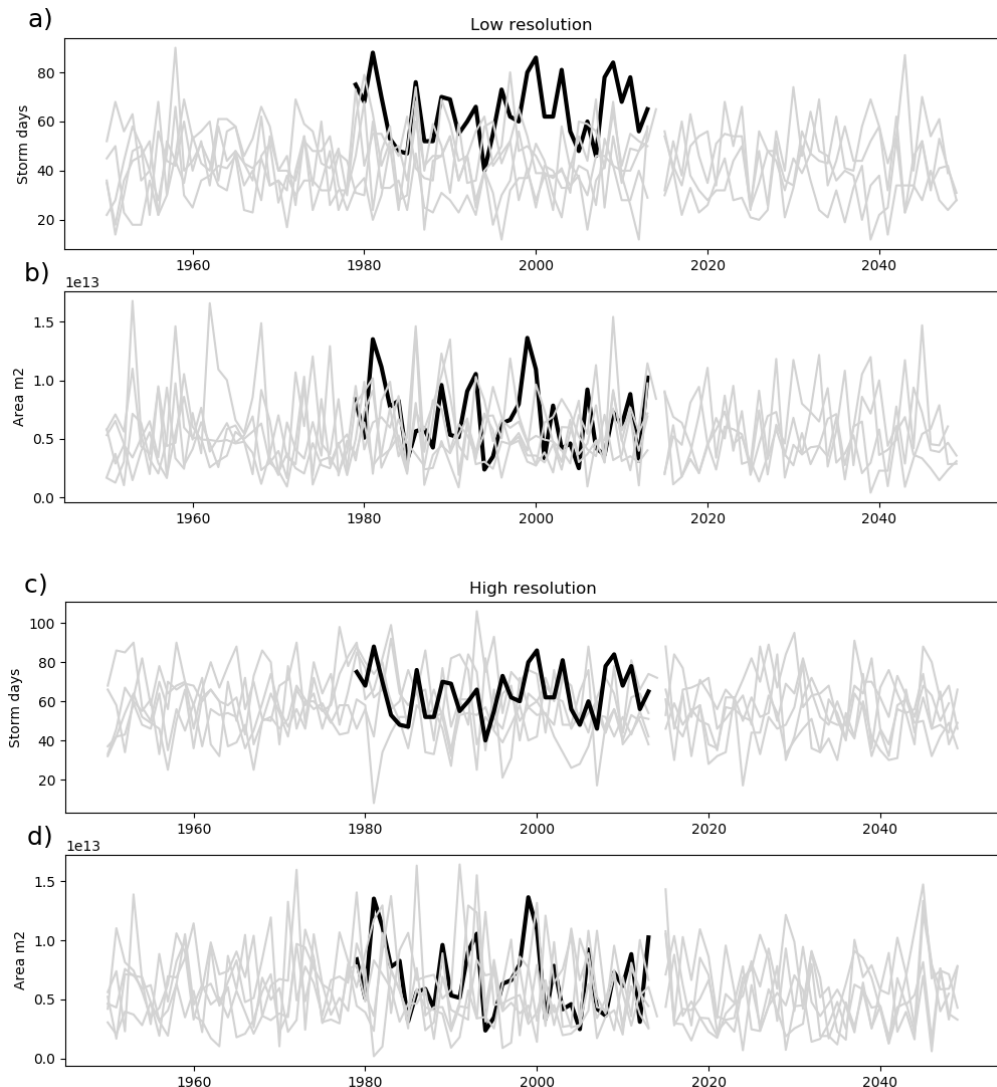


Figure 29: Time series of number of storm days (a) and total storm area (b) per season, for the low resolution models (grey) and ERA5 (black). c) and d) as above, but for the high resolution models. Note that for the models were more than one ensemble member was available, only the first member has been analysed. Also the MPI-ESM1-2-HR model for the future period has been omitted from (a) and (b) due to an issue with the time coordinate in the sfcWindmax data (currently under investigation)

3.2.4.4 Conclusion and discussion

In this section we have outlined the method used to generate a windstorm event set from PRIMAVERA highresSST-present models. The higher resolution set of models show an improvement in distribution of storm losses compared to the low resolution

models, but this does not have much effect on the distribution of seasonal aggregate loss. The low resolution models, however, tend to produce storms with extremely high losses which dominate a season. These losses are highly uncertain due to the bias correction method. We have not found evidence that the high resolution models have a greater ability to simulate high-intensity, low-area storms. Overall, however, both sets of models compare reasonably well to observations and therefore may be useful for insurers to understand long term windstorm risk.

The (re)insurance broker Aon has been testing the footprint data and have found the results are in line with industry catastrophe models. In particular they believe that the event set will be useful in studying windstorm clustering (when multiple strong events occur in a single season), and for studying the effect of large-scale climate modes of variability such as the NAO on windstorm risk (monthly NAO indices were provided with the sample data sent to Aon, and other climate indices will be added). These are topics which we plan to study in the near future. Several other (re)insurance companies have also been in contact to enquire about the event set.

Assessment of future storm risk shows no obvious trend, although a more thorough analysis will be performed when the future footprints have been generated.

3.2.4.5 Caveats

The main issue to highlight is the uncertainty of extreme gust speeds in the footprints (and consequently uncertainty in storm severity and loss indices), especially those from the lower resolution models. This uncertainty arises from the bias correction method which was necessary to convert from wind to gust speeds on a uniform grid, and to correct for model biases in surface winds over high land. We would therefore recommend caution in studying the most extreme events in the models, and urge users to avoid over-interpretation. Instead the event set should be useful for understanding the frequency of storms similar to those in the observational period (1979-2014), temporal storm clustering and the variation of storm risk under different large scale climate modes.

3.2.4.6 Key points

- A windstorm event set has been generated from the PRIMAVERA highresSST-present experiments, providing more than 1000 years of windstorm data.

- The higher resolution models compare better to observations in terms of distribution of loss indices, although both sets of models compare well to observations when considering seasonal aggregate losses.
- The event set allows insurers to directly compare windstorm risk as estimated by the PRIMAVERA climate models with those from industry catastrophe models, and it is anticipated that it will be a valuable resource for insurers in terms of providing an independent view on windstorm risk.

3.2.5 Historical and future extratropical transition of tropical cyclones in a multi-resolution ensemble of atmosphere-land-only and fully coupled global climate models

Alexander J. Baker UREAD, Kevin Hodges UREAD, Malcolm Roberts Met Office, Rein Haarsma KNMI, Dimitris Kapetanakis KNMI, Pier Luigi Vidale UREAD, Reinhard Schiemann UREAD

3.2.5.1 Introduction

Tropical and post-tropical cyclones are an important natural hazard across the midlatitude North Atlantic (Bieli et al. 2019; Evans et al. 2017; Jones et al. 2003; Keller et al. 2019). The poleward propagation of tropical cyclones and the occurrence of extratropical transition exposes populous midlatitude regions, such as Europe, where risks to life and infrastructure are high, to hurricane-force wind speeds and extreme precipitation. For instance, Ex-hurricane Ophelia (9th–15th October, 2017) caused severe wind damage across Ireland, the United Kingdom, and Scandinavia (Stewart 2018). Both systems possessed tropical-cyclone-like structural characteristics and intensities at landfall, engendering significant human and economic impacts during their post-tropical stages. Moreover, five tropical-origin systems threatened Western Europe in 2019 alone, heightening the urgency with which studies of post-tropical cyclone frequency, lifecycles and landfall characteristics are needed. Much of the existing literature on post-tropical systems concerns case studies (e.g., Laurila et al. 2019) or climatological assessments based on limited datasets (e.g., Bieli et al. 2019; Dekker et al. 2018). Cyclone-associated hazards are primarily related to cyclone structure and its temporal evolution, which is expected to be better simulated when horizontal resolution is increased. In PRIMAVERA, we have exploited the available model ensemble as well as recent developments in global reanalysis data to study extratropical transition and post-tropical cyclone risk systematically.

Globally, approximately half of all tropical cyclones undergo extratropical transition (Hart and Evans 2001; Studholme et al. 2015; Zarzycki et al. 2017), but pronounced interannual variability (Baker et al. 2020) and basin-to-basin differences (Bieli et al. 2019) exist. Over the period 1979–2018, statistically significant, positive secular trends in the frequency of North Atlantic extratropical transition events exist in some, but not all, reanalyses (Baker et al. 2020). Projections of future changes in extratropical transition must account for natural variability and observational uncertainties, but a nascent consensus points to more frequent transition events in many ocean basins, particularly the North Atlantic (Baatsen et al. 2015; Haarsma et al. 2013; Liu et al. 2017; Michaelis and Lackmann 2019; Semmler et al. 2008). However, no systematic multi-model studies are yet published, nor has the impact of increasing models' atmosphere or ocean resolution on simulated extratropical transition and post-tropical cyclone statistics been quantified. Both insufficiencies are addressed in PRIMAVERA.

3.2.5.2 Data and methodology

3.2.5.2.1 Reanalysis data

We evaluated model simulations against seven global reanalyses: the European Centre for Medium-Range Weather Forecasts' Interim Reanalysis (ERA1; Dee et al. 2011) and 5th Reanalysis (ERA5; Copernicus Climate Change Service 2017); the Japanese 25-year Reanalysis (JRA25; Onogi et al. 2007) and 55-year Reanalysis (JRA55; Kobayashi et al. 2015); the National Aeronautics and Space Administration's Modern-Era Retrospective Analysis for Research and Applications (MERRA; Rienecker et al. 2011) and subsequent version 2 (MERRA2; Molod et al. 2015); and the combined National Centers for Environmental Prediction Climate Forecast System Reanalysis and Climate Forecast System version 2 dataset (NCEP; Saha et al. 2010; Saha et al. 2014)—the sole fully coupled (atmosphere, ocean, land surface, and sea ice) reanalysis used here.

3.2.5.2.2 Lagrangian tropical-cyclone tracking

To identify and track the evolution of tropical cyclones, we used the objective feature-tracking algorithm—*TRACK*—of Hodges (1995), a tool now well established in identifying cyclones in reanalyses (Hodges et al. 2017) and model simulations (Roberts et al. 2020). The *TRACK* algorithm was applied to six-hourly, spectrally filtered and vertically averaged vorticity at the 850, 700 and 600 hPa isobaric levels, computed from zonal and meridional wind fields. Spectral filtering to T63 resolution

removes large-scale, planetary motion (total wavenumbers 0–5) and small-scale noise (total wavenumbers >63). Vorticity maxima exceeding $5 \times 10^{-6} \text{ s}^{-1}$ (in the Northern Hemisphere; scaled by –1 in the Southern Hemisphere) were identified and formed into tracks using a nearest-neighbour approach and subsequently refined by minimising a cost function for track smoothness, subject to adaptive constraints on track displacement and smoothness (Hodges 1995, 1999). The use of the vertically averaged vorticity is found to improve temporal coherence in instances where vorticity maxima shift between levels. Following Hodges et al. (2017), tropical cyclones were considered to be the identified vorticity features (i) whose genesis occurred equatorward of 30 °N; (ii) exhibits a warm core, which is inferred from a vorticity decrease with increasing height between 850 and 250 hPa exceeding $5 \times 10^{-6} \text{ s}^{-1}$ for at least 1 day over ocean contiguously; and (iii) whose total lifetime exceeded 2 days. These criteria minimise inclusion of spurious short-lived or relatively weak vorticity features.

Crucial to our analyses, vorticity-based tracking determines longer cyclone lifetimes (compared with central-pressure-based algorithms), allowing for objective analyses of the evolution of the post-tropical storm stages (Hodges et al. 2017). Cyclone-centred sampling of meteorological fields along cyclone tracks was performed to detect warm-core structures and measure cyclone intensities, following Hodges et al. (2017). For further details, see Baker et al. (2020).

3.2.5.2.3 Cyclone phase-space analysis

The temporal evolution of cyclone structure, including identifying extratropical transition, is quantifiable by analysis of a cyclone's thermal wind field (Hart 2003; Hart and Evans 2001). Cyclone phase-space analysis involves three parameters: the thermal symmetry of the cyclone (B) and the lower- (T_L) and upper-tropospheric cyclone thermal wind (T_U). B is defined as:

$$B = h \left(\overline{Z_{600} - Z_{900}}|_R - \overline{Z_{600} - Z_{900}}|_L \right)$$

where $h = 1$ for the Northern Hemisphere and –1 for the Southern Hemisphere, Z_p is geopotential height (m) at isobaric level p (hPa), and R and L denote the right- and left-hand semicircles relative to the cyclone's displacement direction, respectively. Following previous research (Dekker et al. 2018; Hart 2003), we defined thermal axisymmetry (i.e., non-frontal) as near-zero B values and asymmetry (i.e., frontal) as $B \geq 10 \text{ m}$. The lower- (900–600 hPa) and upper-tropospheric (600–300 hPa) thermal

wind, T_L and T_U , respectively, are defined as vertical derivatives of the horizontal geopotential height gradient:

$$T_L \equiv -|V_T^L| = \frac{\partial(\Delta Z)}{\partial \ln p} \Bigg|_{P_l}^{P_u}$$

$$T_U \equiv -|V_T^U| = \frac{\partial(\Delta Z)}{\partial \ln p} \Bigg|_{P_l}^{P_u}$$

where p is pressure and $\Delta Z = Z_{max} - Z_{min}$, where Z_{max} and Z_{min} are the maximum and minimum geopotential height, respectively, at a given isobaric level within a 5° radius of the cyclone centre. The slope of the regression between ΔZ and $\ln p$ is used as the derivative of ΔZ relative to $\ln p$ to determine the mean ΔZ over the pressure range P_l to P_u —the lower and upper isobaric levels, respectively. The levels 925, 600 and 250 hPa were used. Positive (negative) T_L or T_U indicate the presence of a warm- (cold-) core in the upper or lower troposphere. A deep warm- or cold-core structure is defined as occurring at both the lower and upper levels. Extratropical transition (ET) is defined by the occurrence of $B \geq 10$ m and $T_L < 0$ for at least four consecutive timesteps (i.e., 1 day). As such, cyclone phase-space analysis is a crucial tool for the evolution of cyclone structure.

3.2.5.2.4 Cyclone lifecycle analysis

Cyclone structures were classified using the cyclone phase-space parameters at the point of landfall. To construct composite lifecycles, storms for each phase-space category were aligned by their landfall point (i.e., $t = 0$) and a composite cyclone-associated maximum 10-metre wind speed, v_{max} , and minimum mean sea-level pressure, p_{min} , timeseries computed. Averaging was performed for every landfall-centred timestep where the number of cyclones exceeded five, a criterion employed to homogenise sampling of pre- and post-landfall intensity evolution.

3.2.5.3 Results

3.2.5.3.1 Spatial statistics

We first examine spatial patterns of cyclone track density, computed following Hodges et al. (2017), simulated across the PRIMAVERA ensemble. Reanalyses demonstrate that tropical cyclones undergo ET in all ocean basins; although relatively few transitioning systems are identified over the Northern Indian Ocean (Figure 30a), where landfall disrupts potential ET events (Bieli et al. 2019). The highest ET frequencies are identified in both the Western North Pacific and South Pacific basins, with climatological-mean values of ~ 12 cyclones year $^{-1}$. The North Atlantic is the second-most active basin in terms of ET, with less activity occurring across the South Atlantic and South Indian basins (Figure 30a).

The frequency of ET events simulated by PRIMAVERA models increases when resolution is increased from ~ 100 km to ~ 25 km in all basins, both in highresSST-present (Figure 30b) and hist-1950 (Figure 30c). The North Atlantic and Western North Pacific basins are regions of relatively widespread inter-model agreement on the sign of resolution sensitivity in track density, regardless of whether sea-surface temperature is prescribed. If prescribed, inter-model agreement is also identified in the South Pacific and South Indian basins. This result is consistent with a similar analysis of all tropical cyclones (Roberts et al. 2020), finding increased tropical-cyclone frequencies simulated across all ocean basins at higher model resolution, for which one explanation is increased conversion of pre-tropical-cyclone precursors that seed cyclogenesis (Roberts et al. 2020; Vecchi et al. 2019). At low resolutions (typically ~ 100 km), PRIMAVERA models simulate too few ET systems compared with reanalyses, but increasing resolution improves the representation of ET, as measured by track density, particularly across the North Atlantic and Western North Pacific (Figure 30d,e). These reductions in ensemble-mean absolute biases are identified in both highresSST-present and hist-1950 simulations. Areas of inter-model agreement in bias reduction are identified over the western boundary currents in both basins. That these regions of resolution-dependence and bias reduction are coterminous and occur in both atmosphere-land-only and fully coupled simulations implicates the importance of capturing the sharpness of sea-surface temperature fronts and associated baroclinicity in simulating ET. In the Southern Hemisphere, little change in ensemble-mean biases are found, with a caveat that observational or reanalysis-based climatologies are themselves more uncertain across the Southern Ocean.

The climate change response of track density for transitioning tropical cyclones in the high-resolution model configurations is basin-dependent, with differences between atmosphere-land-only and fully coupled simulations apparent. In highresSST-future, increased track density is simulated across the North and South Atlantic (but decreased over the eastern United States) and over the Maritime Continent; decreases are simulated over the West and East Pacific and South Indian basins; an unclear response characterises the North Indian Ocean is (Figure 31a). Model agreement about the sign of these changes is confined to genesis regions (e.g. equatorial West Africa) and over western boundary currents. In highres-future

simulations, positive responses are confined to the central and East Pacific basins. The spatial response pattern over the North Atlantic—increased over central and eastern North Atlantic and decreased along United States east coast—is similar between highresSST-future and highres-future, but the magnitude of the response is reduced by ocean-atmosphere coupling (Figure 31c). Overall, horizontal resolution increase has little impact on the climate change response of track density (Figure 31b,d).

In highresSST-future, resolution-sensitive responses to climate change that are common across models are seen only over the central North Atlantic and parts of the Southern Ocean. In highres-future, spatially coherent and resolution-sensitive climate change responses are seen over the South Atlantic and East Pacific basins, where track density is shifted equatorward at high resolution.

Genesis density increases over equatorial Africa and immediately west of Africa, indicating increased genesis from African easterly waves (supplementary information). Low- and high-resolution models simulate AEW frequencies within the range of reanalyses (Roberts et al. 2020) and the frequency of historical TCs generated by AEWs is generally well-captured by the models.

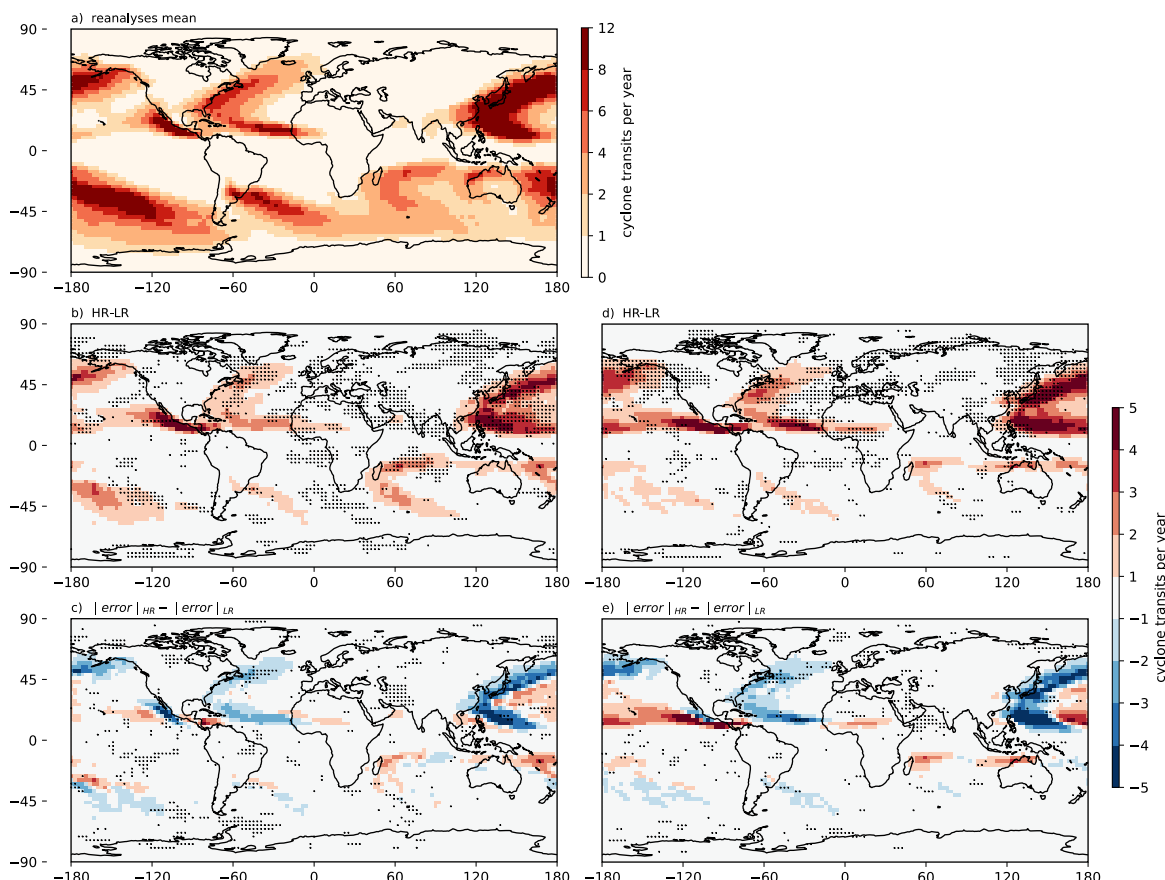


Figure 30: Track density—historical biases and model agreement. (a) multi-reanalysis mean, (b,c) highresSST-present and (d,e) hist-1950. Unit is cyclone transits per year per unit area (within a 5° geodesic radius of storm centres).

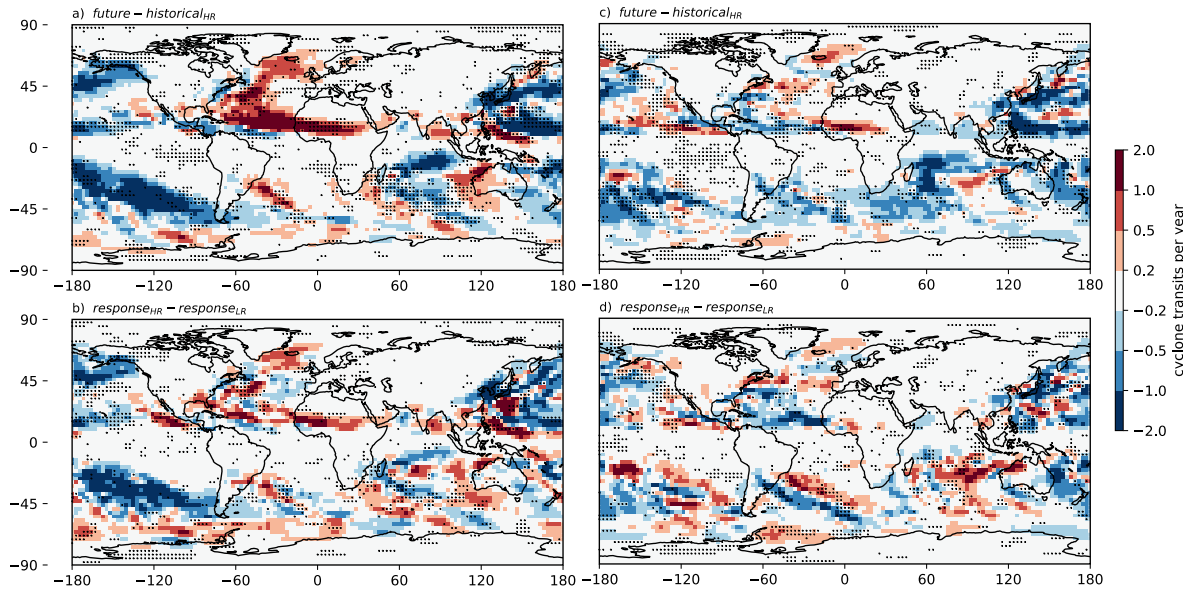


Figure 31: Track density—climate change response and model agreement. (a,b) highresSST-future minus highresSST-present and (c,d) highres-future minus hist-1950. Unit is cyclone transits per year per unit area (within a 5° geodesic radius of storm centres).

3.2.5.3.2 Interannual variability

Models do not show secular trends in ET count or ET % in either highresSST or fully coupled simulations (Figure 32). The small differences between highresSST and coupled suggests that environmental baroclinicity is important. Ensemble-mean climatological mean is underestimated at low resolution and matched quite well, if slightly over-estimated, at high resolution. However, if compared against only the four latest reanalyses from each centre, then match is better still (Figure 32). Generally, there is little skill in highresSST-present simulations for interannual variability (Figure 32). Future work will exploit Stream 2 simulation (namely, additional ensemble members) to establish whether skill improves. Interannual variability in the fully coupled simulations is similar in magnitude to that of highresSST. Overall, there is no change in mean frequency per year or in interannual variability between highresSST and fully coupled simulations (Figure 33).

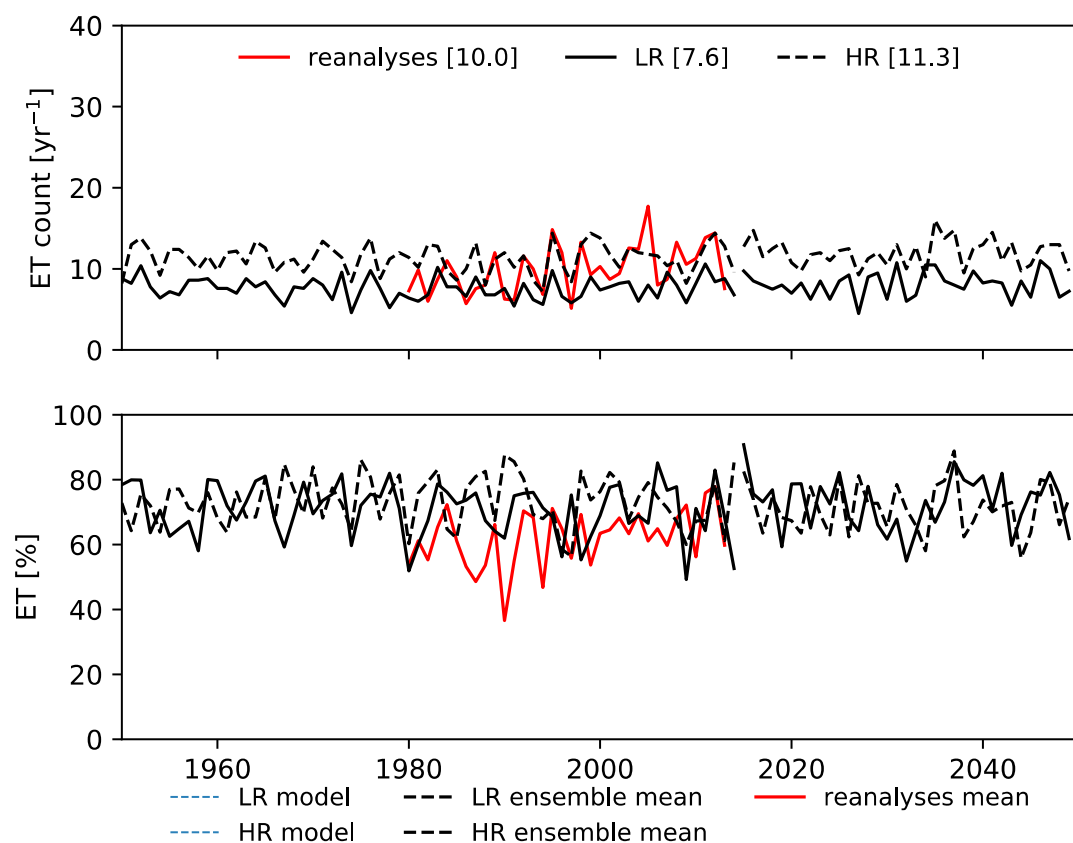


Figure 32: Interannual variability in (left) the number of extratropical transition events and (right) the percentage of tropical cyclones undergoing extratropical transition in the North Atlantic simulated by atmosphere-land-only simulations, compared with reanalyses. Legends show climatological mean values over the reanalysis period for (red) the multi-reanalysis mean, (solid black) low- and (dashed black) high-resolution ensemble means.

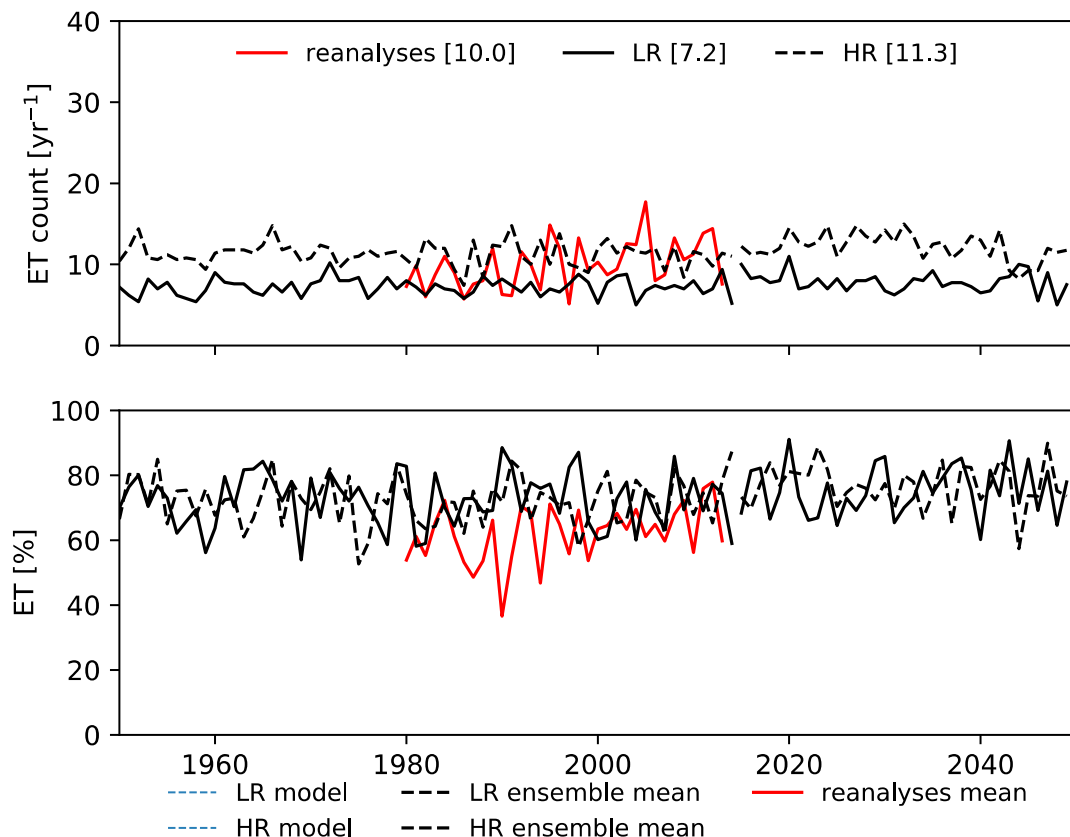


Figure 33: As Figure 32 for the fully coupled simulations.

3.2.5.3.3 Cyclone landfall structures

Cyclones originating in the tropics make landfall over Europe with both warm- and cold-core characteristics (Baker et al. 2020). It is important that models are able to capture the observed occurrences of cyclones structures at landfall, primarily because this is related to wind-speed hazards. Considering tropical cyclones that undergo ET, models overall simulate more cold-core than warm-core landfalls, matching reanalyses (Figure 34). However, there are large inter-model differences and little systematic sensitivity to resolution (Figure 34). CNRM and MOHC overestimate the proportion of cyclones making landfall with a warm-core structure. There are no significant changes in the proportions of each structural type simulated in future; again, inter-model differences dominate (Figure 35). This analysis will be extended to Stream 2 simulations (additional ensemble members) to increase the sample size of landfalling systems.

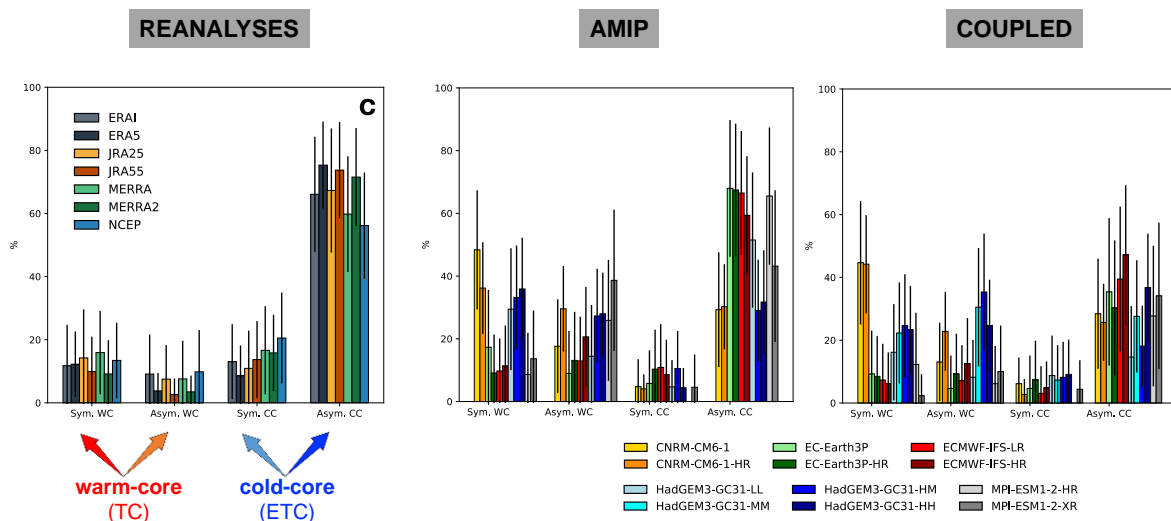


Figure 34: Historical climate relative proportions of cyclone structures at time of landfall over Europe. Symmetrical (Sym.) / asymmetrical (Asym.) warm-core (WC) / cold-core (CC).

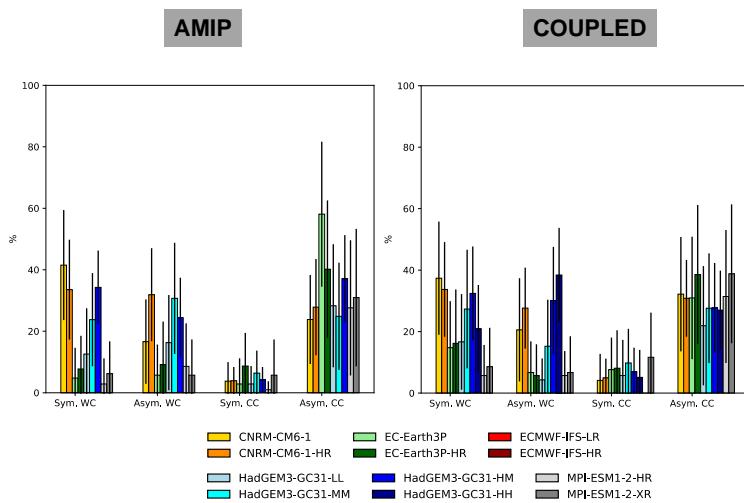


Figure 35: Future climate relative proportions of cyclone structures at time of landfall over Europe. Symmetrical (Sym.) / asymmetrical (Asym.) warm-core (WC) / cold-core (CC).

3.2.5.4 Conclusion

Increased horizontal resolution leads to improvements in spatial track statistics and mean intensities with respect to multi-reanalysis-mean fields. Also improved at high resolution are the historical climatological mean frequencies in both highresSST and full coupled simulations. For Europe, the proportions of landfalling post-tropical cyclones with either warm- or cold-core structures is generally well-reproduced (compared with reanalyses) across the PRIMAVERA ensemble, but there are substantial inter-model differences, the magnitudes of which exceed inter-resolution differences and differences between highresSST-future/highres-future and

highresSST-present/hist-1950 experiments. Analysis of Stream 2 ensemble members is ongoing to determine whether skill in reproducing interannual variability is improved and whether robust climate change signals are discernible in post-tropical cyclone landfall characteristics.

3.3 Blocking, jets and consequences for wind power

Paula Gonzalez, David Brayshaw and Reinhard Schiemann, UREAD; Gerard van der Schrier KNMI

With higher penetration of renewable energies and the effort to decarbonise power production, there is a strong interest in the objective characterization of the wind power resource. Over Europe, wind power accounts for around 17% of total power capacity and almost 30% of renewable capacity and is the overall second largest form of generation capacity after gas.

With increases in renewable shares, the climate sensitivity of the energy systems has also increased significantly. A case study for the Great Britain (Bloomfield et al. 2018) has shown that the current power system is more sensitive to interannual variability in wind power generation than to variations in temperature – which largely control variability in electricity demand. Therefore, an extremely calm winter over the UK is now more impactful than a particularly cold one. As a result, in addition to the description of mean wind power capacity, there is an increasing need to characterise its variability and extremes.

The enhanced horizontal resolution of the PRIMAVERA GCMs has led to a better representation of global climate as well as to improvements in the structure of weather systems such as blocking (e.g., Schiemann et al 2020) and storms (e.g., Gao et al 2020, Baker et al 2019), which have significant influences on European climate. This makes the PRIMAVERA dataset particularly relevant for impact studies over Europe such as those related to wind power variability and change.

This section focuses on three dynamical processes that play a fundamental role in conditioning wind speeds –and therefore wind power- over Europe. In subsection 3.3.1 we introduce some results from the climate projections of the winter North Atlantic jet stream (NA jet), which strongly influences the mean wind speed conditions over Europe, and its impact on near-surface wind speeds. In subsection 3.3.2 we summarize the outcomes from a study exploring the role of the North Atlantic Oscillation (NAO), the leading climate mode of seasonal-to-interannual variability over Europe, on the future vulnerability of renewable energy sources over Europe. On subsection 3.3.3 we present some results from the impact of winter atmospheric blocking, which are closely linked to the occurrence of energy sector-relevant extreme events, and their future projections on the occurrence of low wind and low temperature events over Europe. Finally, on subsection 3.3.4 we discuss more generally the implications of these findings for European wind power and the energy sector.

3.3.1 Impact of North Atlantic jet changes on winter near-surface wind over Europe

Paula Gonzalez, David Brayshaw; UREAD

With the motivation of achieving a carbon free energy system in the coming decades (e.g., Paris Agreement (UNFCCC 2015), EU Green Deal (EU Commission 2019)), having reliable projections for future potential of renewable energy generation sources becomes extremely relevant (e.g., Craig et al. 2019). Future projections for near-surface wind speeds and wind power, however, have received relatively little attention compared with other impact-relevant variables such as temperature, precipitation and even streamflows. The assessment of the impact of climate change on wind power resource is still identified as a research need, particularly at the regional scale (Archer et al. 2014, Karnauskas et al. 2018, Veers et al. 2019).

Overall, a general pattern of wind speed change can be identified, associated with increases in Central and Northern Europe and decreases in Southern Europe. But large differences between models (both GCMs and RCMs) are observed (e.g., Tobin et al. 2015, Carvalho et al. 2017, Karnauskas et al. 2018).

This general pattern of projected changes is somewhat consistent with the projected northward shift and eastward extension of the North Atlantic jet and storm track into Europe (e.g., Ulbrich et al. 2009; Simpson et al. 2014; Zappa et al. 2015), but GCM projections of the large-scale atmospheric circulation changes remain themselves uncertain (e.g., Shepherd et al. 2014). Moreover, the pattern of surface speed changes does not directly match the one expected by these large-scale changes (e.g., Gonzalez et al. 2019).

On an initial study using 25 CMIP5 runs from the historical and RCP8.5 simulations (Gonzalez et al. 2019) we proposed to isolate the component of wind change associated with the large-scale atmospheric circulation changes to achieve – at least partially – a process-based understanding of European wind speed changes, along the lines of what it is considered a ‘storyline’ approach (Shepherd 2019). This work showed that the approach was helpful to understand cold season wind speed changes over Western Europe: projected changes are the result of two distinct processes. The first is associated with changes in the large-scale atmospheric circulation (i.e., poleward shift of the NA jet), while the second appears related to the near-surface boundary layer (not very consistent amongst models).

Using the PRIMAVERA GCMs, with the benefit of their increase resolution resulting in a better representation of physical processes that directly impact European climate (e.g., Baker et al. 2019, Gao et al. 2020, Fabiano et al. 2020), this study extends the aforementioned results. The main goals can be described as:

- to conduct an initial assessment of near-surface wind speed projections from next-generation GCMs;

- to evaluate if it yields the same results as in the case of CMIP5 regarding the role of large-scale vs. boundary layer processes;
- to assess how does the increase in horizontal resolution impact the above.

3.3.1.1 Data and methods

We present here results from the use of 3 PRIMAVERA GCMs: HadGEM3-GC3.1, at MM and HM resolutions; CMCC-CM2 at HR4 and VHR4 resolutions; and MPI-ESM1.2 at HR and XR resolutions, using one ensemble member in each case. We used 1979-2014 (highresSST-present) and 2015-2050 (highresSST-future) to represent the historical and future periods. In each case, 850hPa 10-day low-pass filtered zonal wind over the North Atlantic domain and 10m, 850hPa and 500hPa wind speeds over a European domain were considered, following the CMIP5 study.

Following Gonzalez et al. (2019), the methodology can be described by the following steps:

- the North Atlantic large-scale variability is assessed as that represented by the first two EOFs of 10-day low-pass filtered 850hPa zonal wind. This accounts for most of the jet variability and have been found to be strongly linked to the NAO and the East Atlantic pattern.
- The variability of wind speed linked to the large-scale is reconstructed through a multiple linear regression model between historical PCs (timeseries) and the variable at each gridpoint and is labelled the EOF-MLR reconstruction.
- To reconstruct the future projections, the EOF-MLR model is fixed and projected principal components are used as input. A different EOF-MLR model is trained for each model independently.
- The EOF-MLR reconstructed wind speed change patterns are created for the three levels and compared to the raw GCM-based projected changes for each model.

3.3.1.2 Results

The initial step involves the computation of the EOF analysis of filtered 850hPa zonal wind. Figure 36 presents the two leading EOF patterns obtained for each model, in the historical and future simulations; and compared with the ones corresponding to the ERA-Interim reanalysis (Dee et al. 2011).

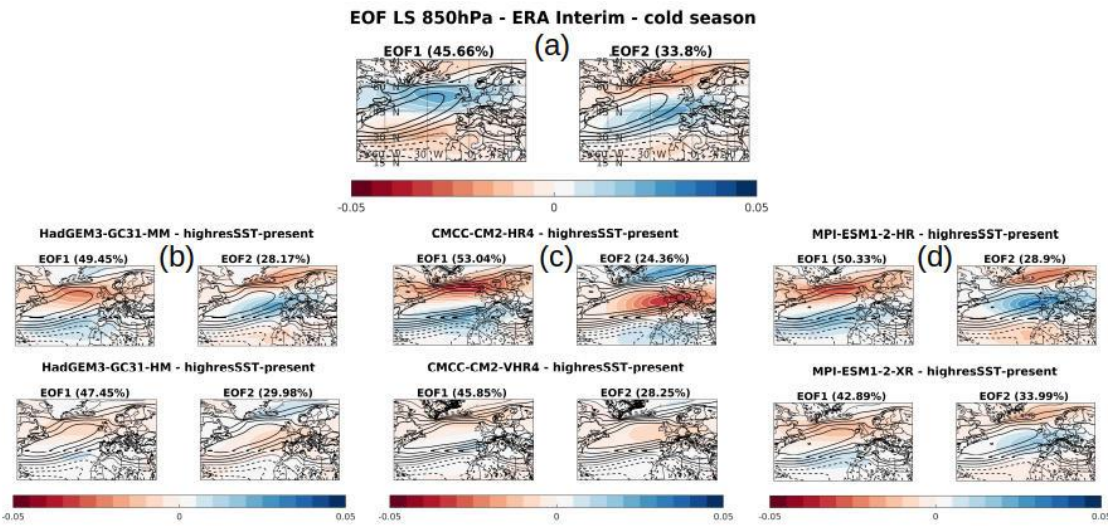


Figure 36: EOF1 and 2 patterns corresponding to the EOF decomposition of cold season filtered 850hPa zonal wind. Corresponding explained variances are indicated on top, in between parenthesis. Black contours are 850 hPa zonal wind historical mean for a qualitative comparison and are plotted every 2 m/s. Panels correspond to: a) ERA interim analysis (from Gonzalez et al. 2019), b) HadGEM3-GC3.1 model at MM (top) and HM (bottom) resolutions; c) CMCC-CM2 model at HR4 (top) and VHR4 (bottom) resolutions; and d) MPI-ESM1.2 model at HR (top) and XR (bottom) resolutions.

Regarding the historical period (top panels in b), c) and d)), it can be seen that there is good agreement between models and ERA-I (panel a)) and between models. The largest differences are obtained for CMCC-CM2, where all the structures are more zonally oriented and the gradients are steeper. These and other biases in the NA jet of this model have been previously identified in the literature (e.g. Shepherd 2014, Cherchi et al. 2018). For the future period, the models do not project significant changes in the leading EOFs, but they do present differences in the explained variances.

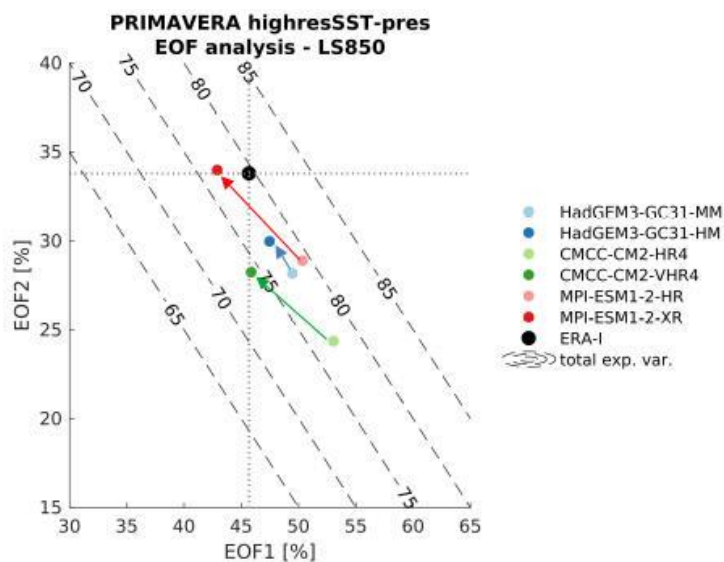


Figure 37: Summary plot of the EOF analysis applied to filtered 850hPa zonal wind. The x axis presents the variance explained by EOF1 and the y axis for EOF2. Diagonal dashed lines correspond to different amounts of

variance accumulated by the two. The black dot represents the values obtained for ERA-I and individual GCMs are included as different coloured dots: HadGEM3-GC3.1 in blue, CMCC-CM2 in green and MPI-ESM1.2 in red.

Figure 37 summarizes the results for the explained variances over the historical period and shows three robust results:

- the models underestimate the variance explained jointly by both EOFs;
- the high-resolution of the models has less variance linked to EOF1 and more to EOF2 than the low-resolution version;
- the high-resolution version of the models has less variance explained jointly by the EOFs (2 out of 3 models).

3.3.1.2.1 Skill of the EOF-MLR reconstruction

Next, we evaluate the skill of the winds reconstructed by the EOF-MLR model to capture winter variability. Figure 38 presents the determination coefficients (R^2) between raw and reconstructed filtered 850hPa zonal wind over the Atlantic domain. For comparison, the plots corresponding to ERA-I (panel a) and the CMIP5 multi-model mean (MMM, panel b) are included. It can be seen that the results from the PRIMAVERA models are comparable to the CMIP5 MMM, with the reconstruction being slightly less skilful in the central NA than in ERA-I, but extending further inland in western Europe, in particular for CMCC-CM2 (panels d, g) and MPI-ESM1.2 (panels e, h). The change from high-resolution to low-resolution versions of the model seems to derive in a slight eastward shift in the skills of the reconstruction, consistently across models. The skill is additionally degraded in HadGEM3-GC3.1-HM (panel f).

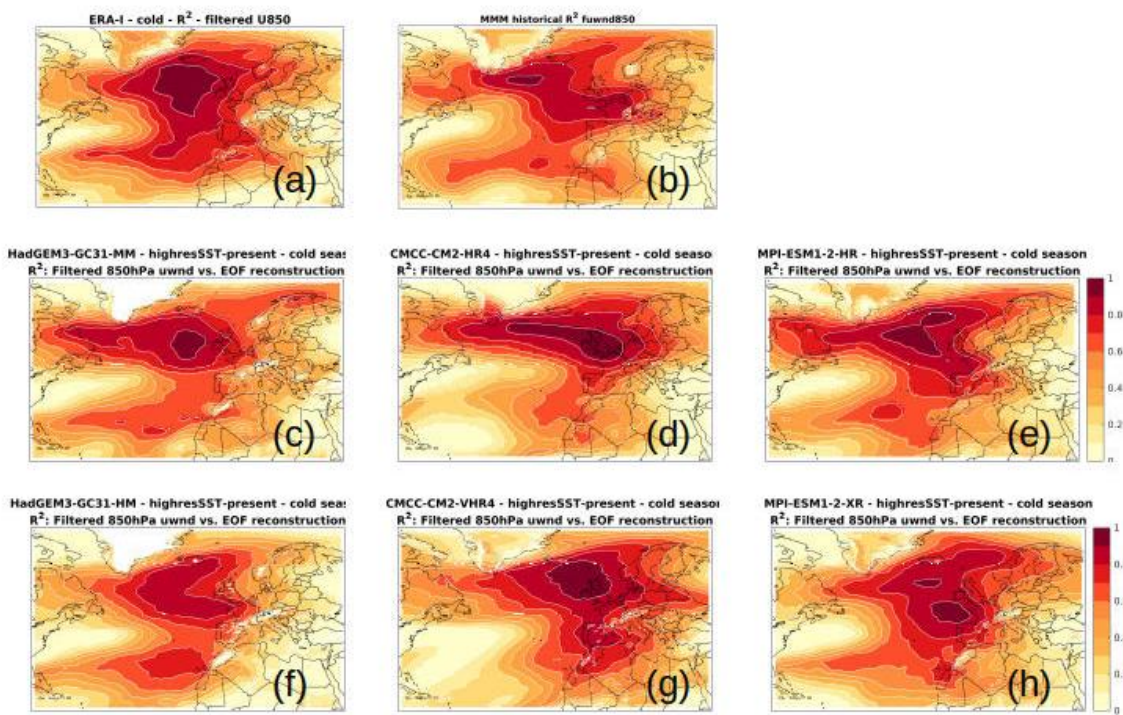


Figure 38: Cold season coefficients of determination (R^2) between 10-day filtered 850 hPa zonal wind over the North Atlantic sector and the EOF-MLR estimated fields. a) Corresponds to ERA-I and b) to the CMIP5 multi-model mean (MMM), both adapted from Gonzalez et al. 2019. Individual PRIMAVERA GCMs are included as follows, with low and high resolutions respectively: c) and f) HadGEM3-GC3.1, d) and g) CMCC-CM2 and e) and h) MPI-ESM1.2.

Figure 39 presents analogous R^2 results but for 10m wind speeds over the European domain. The observed levels of skill are unsurprisingly lower than for filtered 850hPa zonal wind, since the EOF decomposition was meant to retain variability in this field. Nonetheless, all the plots show explained variances of at least 50% in diverse sectors of western Europe.

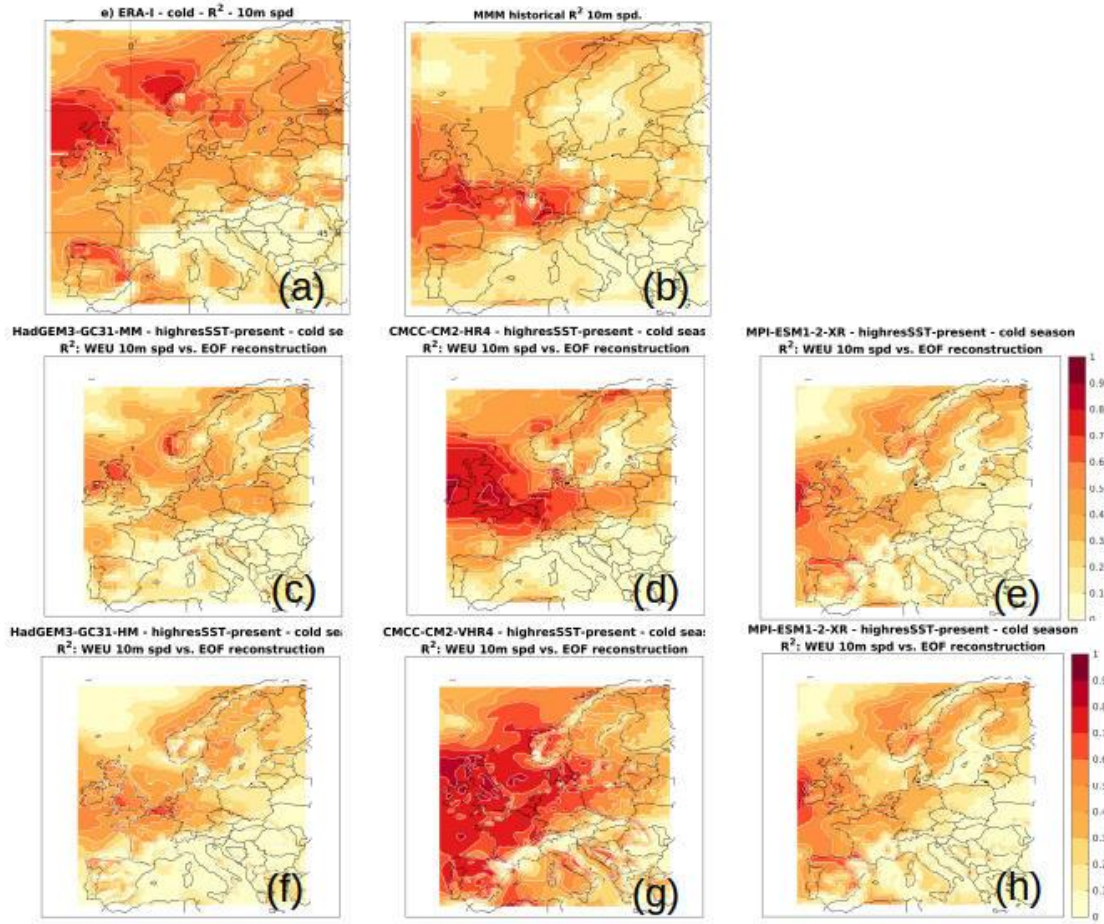


Figure 39: As Figure 38 but for European sector 10m wind speeds.

There is large spread in the skill of the reconstruction amongst models, both in pattern and in magnitude. Most extreme being HadGEM3-GC3.1 (panels c and f), for which the skill is the lowest, indicating a weaker connection between NA variability and European surface winds than in ERA-I; and CMCC-CM2 (panels d and g) for which the values are much higher than in ERA-I, suggesting an overestimation of the connection to the large scale.

3.3.1.2.2 EOF-MLR reconstructed vs. GCM-based projected changes

Considering the reconstructed levels of variance shown above, the next step is to analyse the EOF-MLR reconstructed projected wind speed changes, and to compare them with the raw GCM-based ones. Figure 40 presents such a comparison for the future projections in the NA filtered 850hPa zonal wind. The CMIP5 MMM results are present in panel a) for reference and show a large level of agreement between raw (left) and reconstructed (right) changes over the ocean, suggesting a projected poleward shift in the NA jet. The main difference takes the form of anticyclonic circulations centred over the Mediterranean (Zappa et al. 2015), and a weaker centre

on the western Atlantic basin. It is important to point out that due to the reduced length of the PRIMAVERA future projections (only reaching 2050), the magnitudes of the projected changes are much smaller than in the CMIP5 study, which targeted the future period 2070-2099. Furthermore, this might introduce additional challenges for the decomposition, in the context a signal-to-noise framework between the induced trends and interannual-to-decadal variability.

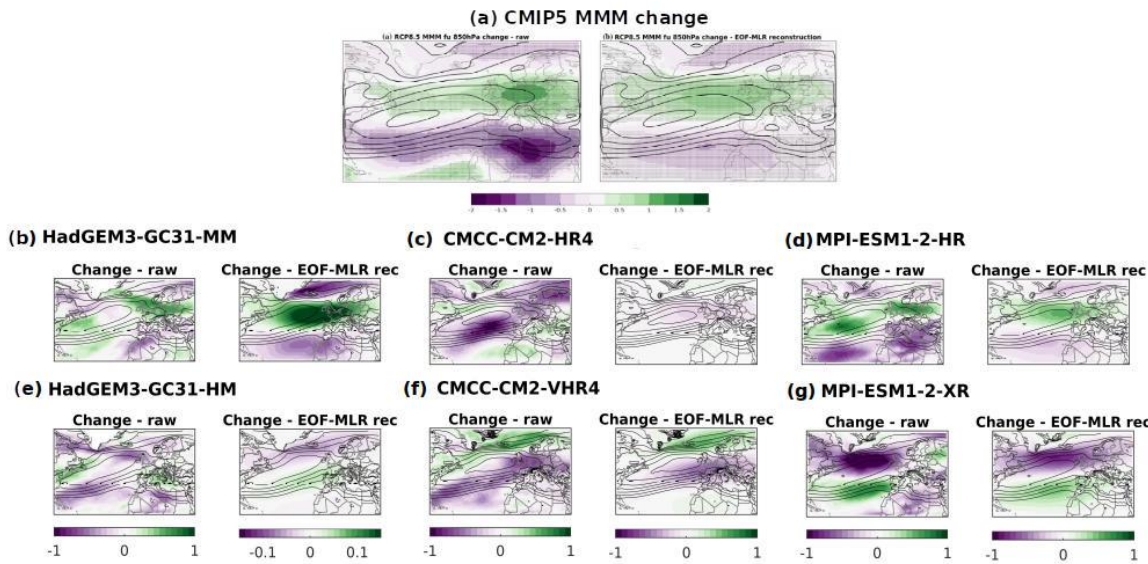


Figure 40: (a) Multi-model mean (MMM) GCM-based change for the 10-day filtered 850 hPa zonal wind field (left) and the EOF-MLR estimated fields (right) in m/s. The black contours represent the historical MMM mean field plotted every 2 m/s. (Adapted from Gonzalez et al. 2019). Similar plot for individual PRIMAVERA GCMs are presented as: b) and e) HadGEM3-GC3.1; c) and f) CMCC-CM2; d) and g) MPI-ESM1.2. Colour scales vary with each dataset.

The raw changes projected by the PRIMAVERA GCMs (left plots on panels b to g) show strong differences between both models and resolutions of the same model, and also very little agreement with the CMIP5 MMM. The differences in period can at least partially explain the latter. In the case of the reconstructed changes, two results stand out:

- HadGEM3-GC3.1 and MPI-ESM1.2 show similar reconstructed projected changes in their low-res versions, though consistent with an eastward extension of the NA jet rather than the poleward shift observed in CMIP5 MMM.
- In the case of their high-res versions, these two models both project an equatorward shift in the jet, though the change is much weaker in HadGEM3-GC3.1.
- the results for CMCC-CM2 are very different and in many places of opposite signs.

Very large differences in between different resolutions of CMIP6 models were also very recently reported by Hahmann et al. (2020), though no hypothesis were presented for the causes of such differences.

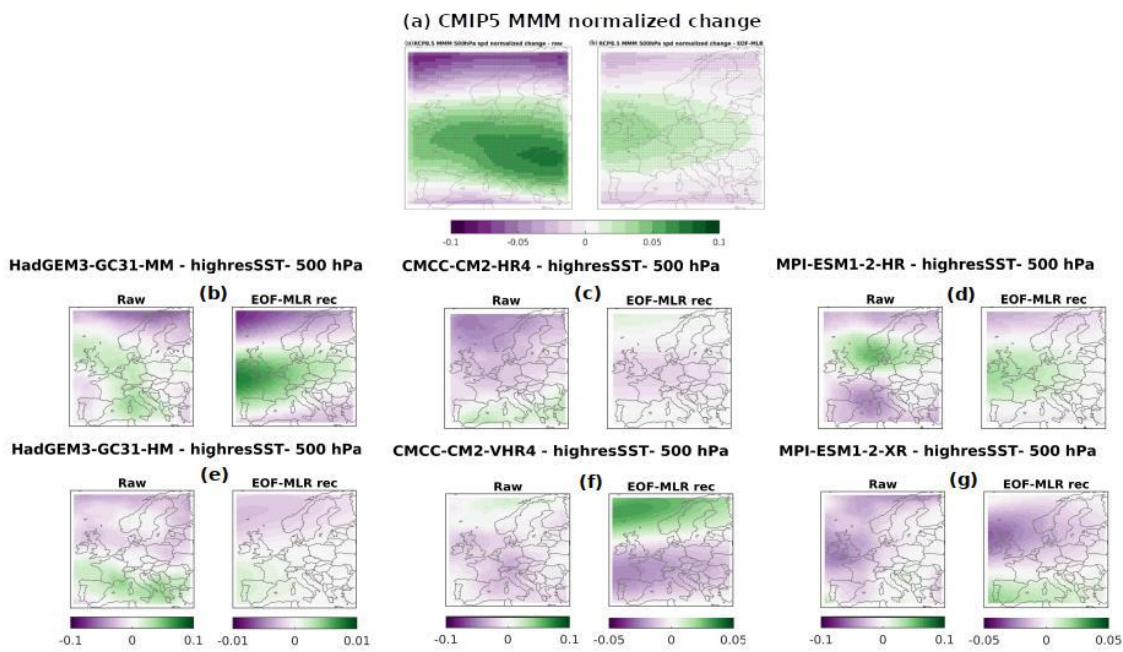


Figure 41: As in Figure 40 but for European sector 500hPa wind speeds.

Figure 41 presents the equivalent results but for 500 hPa wind speed changes over the European domain. At this higher level of the troposphere, it can be assumed that the influence of the surface and local processes is minimal and therefore more of the variability can be explained by the large scale. The results are very similar to the mentioned above for Figure 40, showing a relative agreement between HadGEM3-GC3.1 and MPI-ESM1.2, and a change to a poleward shift in the speeds in the high-res versions. Another interesting result from these models is the fact that there is a close agreement between the high-res raw and reconstructed changes (panels in e and in g). This implies that according to these models, more of the projected speed changes at high levels are explained by changes in the NA large scale. Results projected by CMCC-CM2 are very different and suggest speed weakening in central and southern Europe.

Finally, Figure 42 shows the same analysis but for 10m wind speed changes. Some agreement is again found between HadGEM3-GC3.1 and MPI-ESM1.2, in the reconstructed changes even more so than in the raw ones (panels b, d, e and g). The low-res versions of the models show more of an agreement between the raw and the reconstructed changes than that observed in CMIP5 MMM which might suggest that the negative residuals observed in the Gonzalez et al. (2019) analysis and likely linked to boundary layer processes are not that relevant in these models.

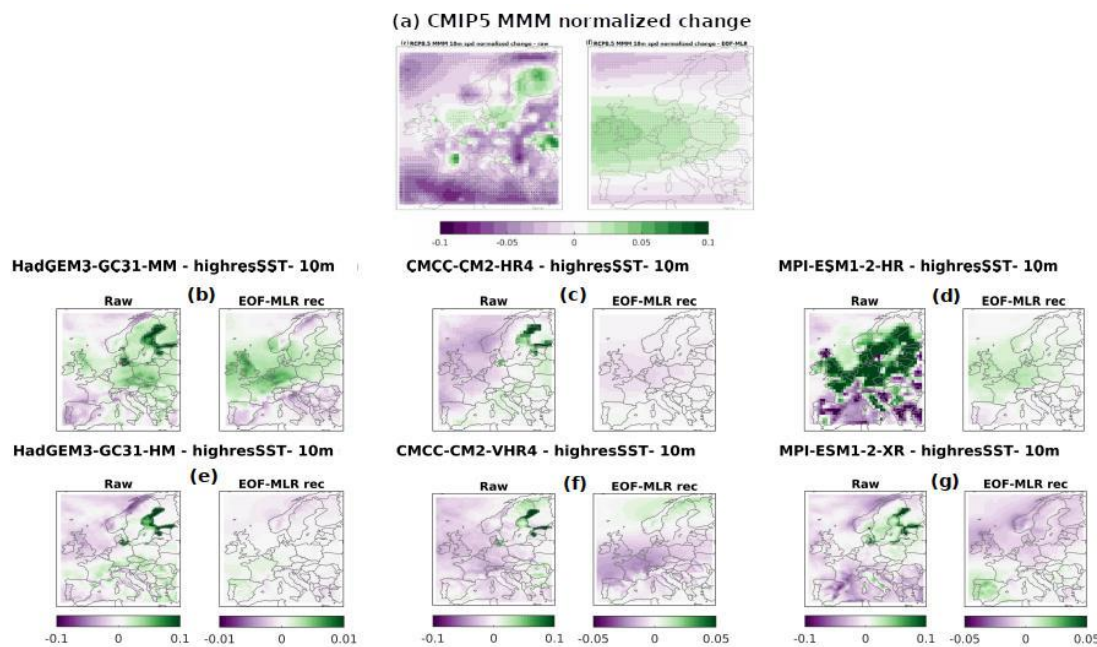


Figure 42: As in Figure 40 but for European sector 10m wind speeds.

3.3.1.3 Preliminary discussion

This analysis has revealed that large uncertainty is still present in the next generation of wind speeds future projections. Disagreements are observed between different models, but also between different resolutions, even after the EOF-MLR reconstruction., though the ensemble considered here is still very limited. Another limitation of the present study is given by the near-future nature of the PRIMAVERA projections. A study using an earlier future period when analysing the CMIP ensemble could suggest if there is a temporal emergence sensitivity in the influence of NA variability on projected wind changes. It derives that it is of utmost relevance to expand the ensemble used in the analysis, as well as to extend it to longer CMIP6 projections.

A very significant result is the suggestion that at higher resolutions, the models project an equatorward shift of the NA jet. More exploration is required to understand the physics behind this process, and an initial point might be to link it to the fact that there is a consistent change of the relevance between EOF1 and EOF2 when resolution increases, but also to explore a potential relationship to the representation of the tri-modal structure of the NA jet latitude. The Stream 2 PRIMAVERA simulations should be included in this further exploration.

Given the current results, the proposed methodology to isolate the influence of the changes in NA large-scale variability on near-surface wind speed changes over Europe hasn't shed more light into what these changes might look like or their implications for the wind power sector.

3.3.2 The role of the NAO in future vulnerability of European renewable energy sources

Gerard van der Schrier; KNMI

What will a future climate look like? There is a large uncertainty surrounding this question. This uncertainty relates to uncertainty in the future emissions of greenhouse gasses and our ability to curb the impacts of our economy on climate. But there is also an uncertainty related to the atmospheric circulation. While the atmospheric circulation responds on the planetary scale to the spatial variations in solar radiation, and redistributes heat from the equator to the poles, on smaller scales it may be seen as a chaotic system. However, there is now growing consensus that global warming nudges the atmospheric circulation toward e.g. a poleward shift of the mid-latitude westerlies associated with a poleward expansion of the Hadley circulation (Zappa, 2019).

This perspective suggests that the atmospheric response to climate change can be usefully understood as a combination of what might be called a thermodynamic component (surface warming, moistening, melting of ice) and a dynamic component (changes in atmospheric circulation). The distinction between these two aspects might be useful. There is a sharp contrast between the degree of confidence we have in the two components. There is a large body of evidence indicating that the thermodynamic aspects of climate change are robust in theory, observations and models. However, the degree of trust we have in the dynamic aspects associated with global warming is low (Shepherd, 2019).

The main reason is that changes in the atmospheric circulation related to climate change are fairly small compared with natural variability (Trenberth et al. 2015). Although large changes in atmospheric circulation can be readily apparent in a single climate model run, they are not robust and can change considerably in the next run or model. Hence, forced circulation changes are not well established, and it is difficult to detect changes in circulation-related extremes in observations because of small signal-to-noise ratios.

The distinction between thermodynamic and dynamic aspects of climate change provides an alternative to the usual approach of considering ensembles of model simulations, which mix together uncertainties in the two aspects, and may help to provide information on where the largest uncertainties lie (e.g. Pfahl et al. 2017). In particular, storylines can be considered for each aspect (Shepherd, 2019).

The distinction between thermodynamic and dynamic aspects of climate change is also useful when it comes to representing the uncertainty in projections of future change. A practical example of this is the KNMI Climate Change Scenarios, which provide four discrete sets of weather and sea-level variables, assuming a given global temperature increase and a regional amplification due to circulation responses

(Van den Hurk et al. 2014). In essence, these provide storylines of regional climate given large-scale changes in physical climate.

The framework of the KNMI Climate Change Scenarios has been used to provide storylines on the generation of intermittent renewable energy sources (I-RES), such as wind and solar power. The dependency of I-RES on local weather conditions renders power output from I-RES vulnerable to climate change and natural climate variability. The basis of these storylines is the study by Ravestein et al. (2018).

With the climate model, EC-Earth four scenarios of future weather data were created to span the spectra of climate change and climate variability. The results of these four scenarios were combined with estimates of future spatial distributions of I-RES to calculate the I-RES generation across for each of these four scenarios. Finally, the resulting generation profiles were compared with generation profiles based on observational weather data to assess the impact of the variations captured in the four climate scenarios on the generation of I-RES.

3.3.2.1 Climate scenarios and data

The climate model used is the EC-Earth model which is a state-of-the-art global coupled earth system model, consisting of the Integrated Forecast System (IFS) of the European Centre for Medium Range Weather Forecasts (ECMWF) as the atmosphere component and the Nucleus for European Modelling of the Ocean (NEMO) developed by Institute Pierre Simon Laplace (IPSL) as the ocean component.

With EC-Earth an ensemble of 16 simulations for the period 1950-2100 is made assuming a RCP 8.5 emission pathway. Each simulation is initialized differently, aiming to span the full spectrum of internal climate variability and provides an equally probable and realistic estimate of day-to-day weather consistent with the emission pathway.

The ensemble was divided into four scenarios based on two parameters: global temperature, and atmospheric circulation. Since the relation between global temperature and greenhouse gas is well-understood and linear, data from the 2051-2065 period are taken to represent climatic conditions with a strong global warming while data from the 2036-2050 period represent climatic conditions with a moderate warming.

The impact of atmospheric variability is captured by labelling each winter and summer season by the phase of the North Atlantic Oscillation (NAO). The NAO is the most important mode of atmospheric variability over the North Atlantic sector in the winter and plays a major role in weather and climate variation over eastern North America, the North Atlantic, and the Eurasian continent. The NAO can be in a

positive or a negative phase, relating to the sign of the NAO index, which is the normalized atmospheric pressure differences between the Azores and Iceland. When the pressure difference in the NAO is higher or lower than average, it is in its positive or negative phase, respectively. In the winter, a positive NAO generally leads to windy conditions in northern Europe, with a south-westerly wind bringing mild, cloudy and rainy weather, while southern Europe enjoys relatively sunny and dry conditions. With a negative NAO, the storm track over the North Atlantic Ocean is located much more to the south, bringing cloudy and windy conditions to the southern part of Europe while northern Europe generally has calm, cool and dry weather. The equivalent of NAO in the summer season, the so-called summer North Atlantic Oscillation (sNAO), is characterized by a more northerly location of the high- and low-pressure areas over the North Atlantic and a smaller spatial scale than its winter counterpart. While the sNAO is the dominant mode of atmospheric variability in the summer, it explains less the prevailing weather patterns than the NAO (Ravestein et al. 2018).

This division in moderate (M) and high (H) warming and positive ($>=0$) and negative (<0) (s)NAO index resulted in the four scenarios: M+, M-, H+ and H-, where e.g. M+ represents a moderate global warming with a dominantly positive (s)NAO index.

The capacity distributions for both PV and wind turbines are shown in Figure 43. For the wind turbine distribution, information on the locations and hub height of installed capacity in 2013 was retrieved from a public database. The spatial distribution of PV installations considers already installed capacity of PV and new capacity to the regions to comply with the ECF 80% renewable pathway has been added. A similar approach was used in the case of wind power. It was assumed that all new turbines have a hub height of 100 m onshore, and 150 m offshore.

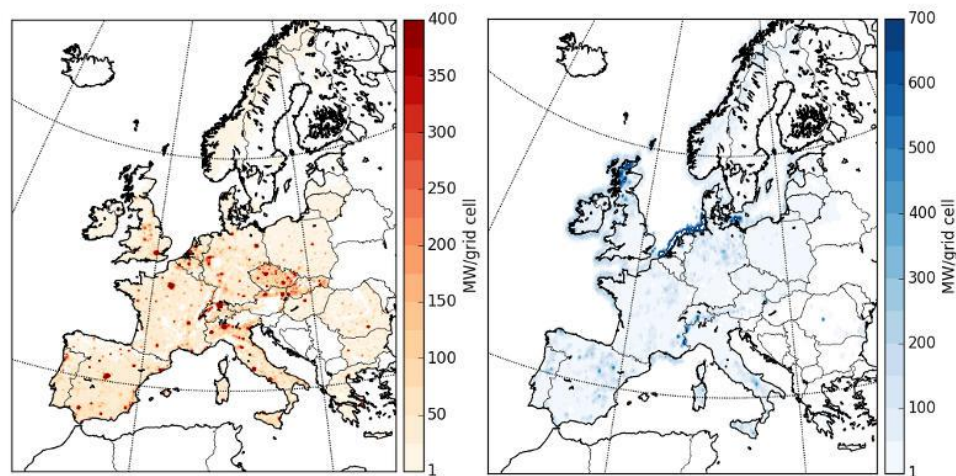


Figure 43: Distribution of 880 GW PV (left) and 440 GW wind turbines (right) over Europe in 2050, produced with the CLIMIX model with a spatial resolution of 0.11° latitude-longitude (figure from Ravestein et al. 2018).

3.3.2.2 Effects in summer

Figure 44 shows that in the positive sNAO phase, PVpot increases moderately by 0.4 to 1.6 percentage point (pp) on average in the whole of Europe compared to the observations, except for Norway and southern Iberia where it decreases. The decrease in Iberia is the result of a strong increase in temperature, caused by drier conditions, this temperature increase reduces the efficiency of solar panels.

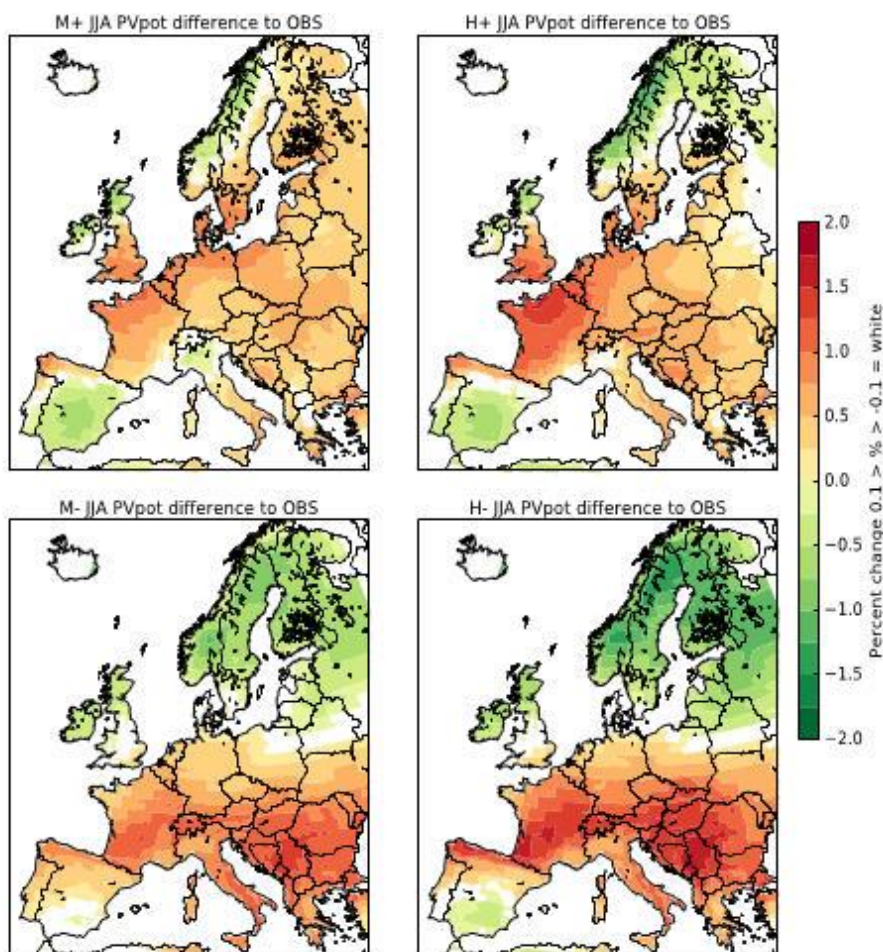


Figure 44: Difference (in pp) between the average PVpot in the summer (JJA) under 2050 weather conditions in each scenario and those under observed weather conditions (in 1981-2010). The upper two represent the sNAO positive phase, the lower two the negative sNAO phase. The moderate and high global warming scenarios are shown on the left and right, respectively.

While in the positive sNAO phase the storm track heads north from northern Scotland over the Atlantic resulting in cloudy conditions along the Norwegian coast, it heads south eastwards in the negative sNAO phase resulting in more cloudy conditions in whole northern Europe and consequently 0.8 – 2 pp lower PVpot. Continental Europe sees a significant increase of 1 – 2 pp in the negative sNAO phase, especially in central and southern regions.

Unlike PVpot, Wpot decreases significantly in the positive sNAO phase in Europe: by 4 - 8 pp from the west of southern England across the channel to the southern North

Sea region, and in the rest of Europe by 2 - 4 pp (Figure 45). This relates to the position of the storm track, which brings the most windy conditions to the north-eastern Atlantic and calm conditions over most of Europe. In the negative phase of the sNAO, an increase in wind power is observed in Scotland, the North Sea, southern Scandinavia and the Baltic.

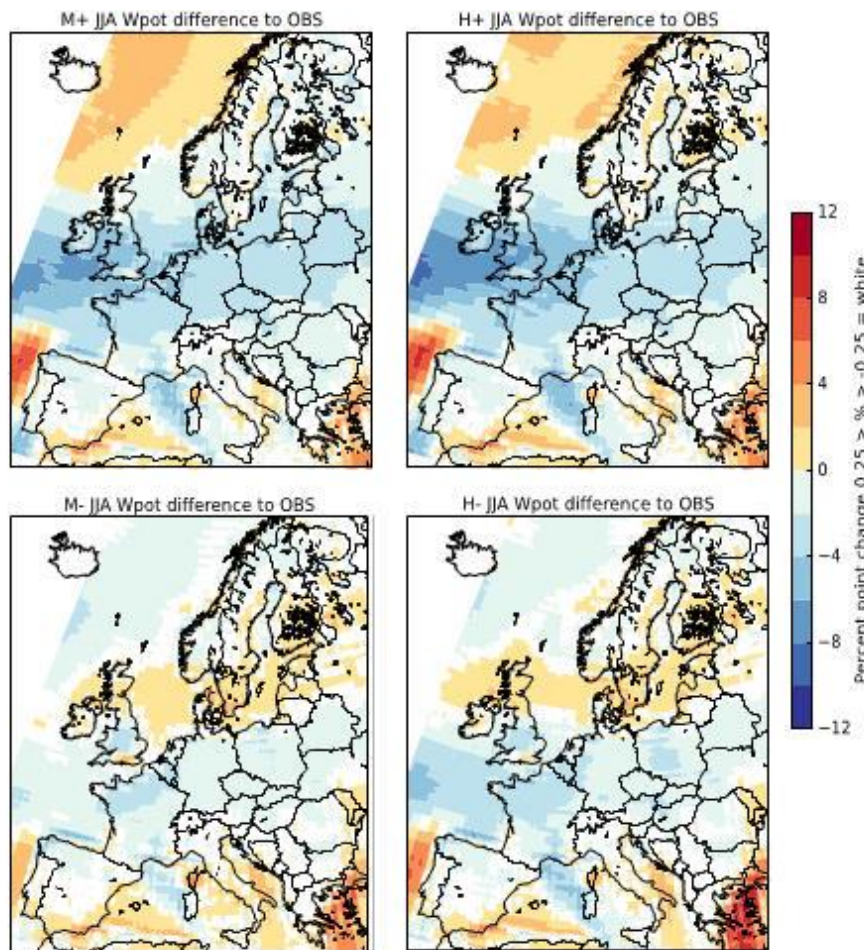


Figure 45: Difference (in pp) the average Wpot at 80 m in the summer (JJA) under 2050 weather conditions in each scenario with those under observed weather conditions (in 1981-2010). The upper two represent the sNAO positive phase, the lower two the negative sNAO phase. The moderate and high global warming scenarios are shown on the left and right, respectively.

3.3.2.3 Effects in winter

The positive NAO phase has a limited impact on PVpot over Europe. In most of Europe it causes a low to moderate decrease: 0.2- 0.4 pp in western Europe, and 0.4 – 1.6 pp in central and eastern Europe. Only along the Mediterranean coast, it results in an increase which is highest on the Iberian Peninsula (up to 2 pp). In the positive phase of the NAO, the storm track – which brings cloudy conditions - is well-developed and wide and its position is over the British Isles and southern Scandinavia. This is shown in Figure 46.

The negative phase of the NAO leads to a strong decrease in PVpot for the whole of continental Europe, including the largest part of the Iberian Peninsula, ranging from 0 – 1.6 pp. Only the coasts of Norway and Scotland see a slight increase in PVpot.

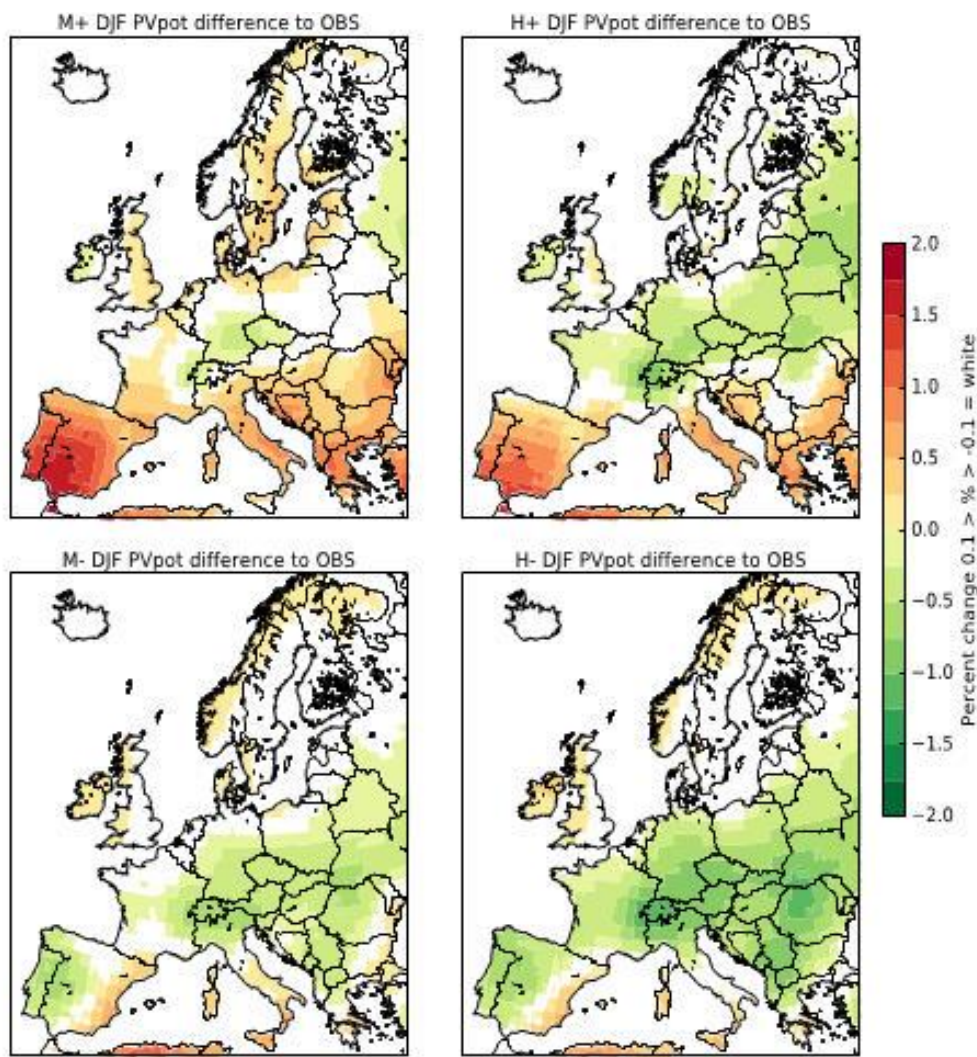


Figure 46: Difference (in pp) between the average PVpot in the winter (DJF) under 2050 weather conditions in each scenario and those under observed weather conditions (in 1981-2010). The upper two represent the sNAO positive phase, the lower two the negative NAO phase. The moderate and high global warming scenarios are shown on the left and right, respectively weather conditions in each scenario and those under observed weather conditions (in 1981-2010). The upper two represent the NAO positive phase, the lower two the negative sNAO phase. The moderate and high global warming scenarios are shown on the left and right, respectively.

In contrast to PVpot, Wpot is strongly influenced by the positive NAO phase (Figure 47). In countries around the North Sea and the Baltic Sea it increases by 6-12 pp, while in southern Europe and around the Mediterranean Sea it decreases by 2 – 8 pp. For the Wpot the negative phase of the NAO leads to a decrease ranging to 10 pp in northern regions. In the south there is an increase of 0-4 pp, however, many white spots indicating an irregular spatial pattern of change.

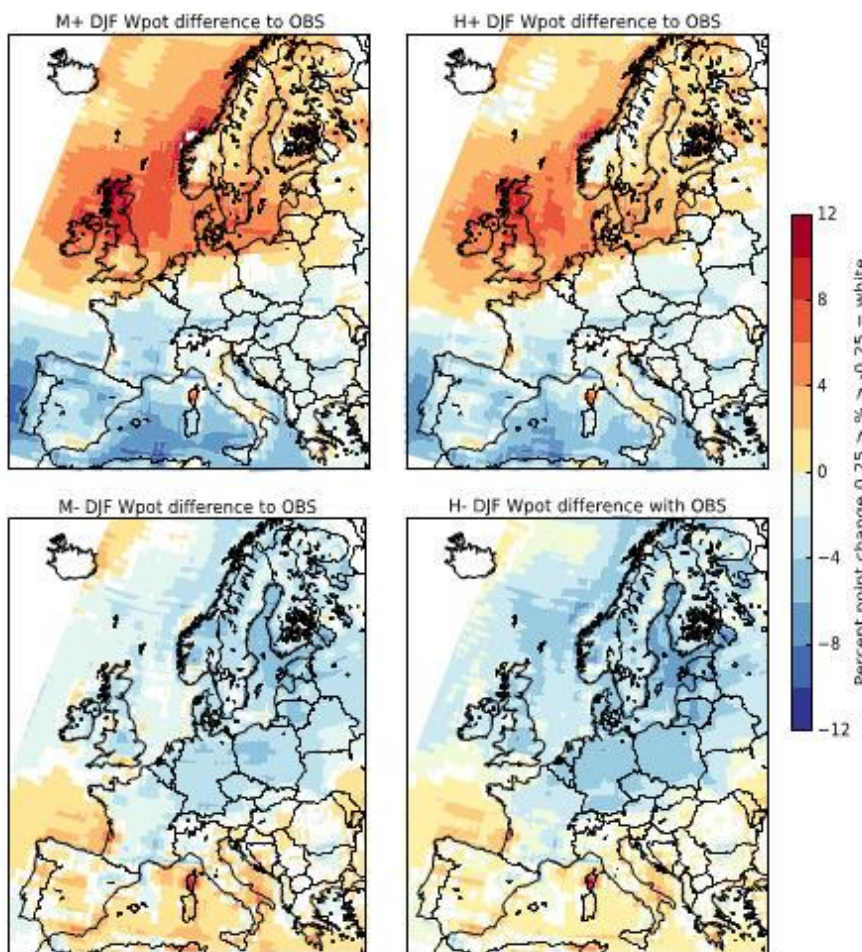


Figure 47: Difference (in pp) the average Wpot at 80 m in the winter (DJF) under 2050 weather conditions in each scenario with those under observed weather conditions (in 1981-2010). The upper two represent the NAO positive phase, the lower two the negative NAO phase. The moderate and high global warming scenarios are shown on the left and right, respectively.

3.3.2.4 Impact of climate change versus NAO/sNAO phase

Overall the impact of climate change on the energy yield is low compared to the changes observed due to the opposing phases of both the NAO in winter and the sNAO in summer. Figure 45 and Figure 47 clearly show little difference in average PVpot and Wpot between the M and H scenarios, and clear differences between the NAO/sNAO phases. In some scenarios climate change affects the intensity of the projected output changes, but the directions of change are determined by the NAO/sNAO phases. Both for Wpot and PVpot, we observed that the changes in energy yield are much larger between the two phases of the NAO/sNAO than between the moderate and warm scenarios.

3.3.2.5 Identification of winters with very low energy yields

To analyse the impact of the NAO phase on the security of renewable energy supply, winter months with extremely low renewable energy yield are identified. The three winters in the climate simulations with the lowest absolute yield of around 75 TWh instead of the average 116 TWh in the Benelux-Germany area are all characterised by a negative NAO. The yields in these winters are 34 %, 37 %, and 36 % lower than the average for sample 003, 080, and 101 respectively. The difference for single months is significantly larger: December of sample 003 is the lowest producing month of these winters, with a wind yield that is 66 % lower than the long-term December average.

The maps in Figure 48 shows the relative change in Wpot and PVpot of the months with the lowest I-RES yield in these three winters compared to the average of the H scenarios. In these months the Wpot decreases significantly in nearly all of Europe, in some regions with more than 75% of their average potential. In one of the minimum yield months (model year 101), very low Wpot is combined with lower PVpot due to a stagnant high-pressure area over Europe which brings the dull weather with calm and cloudy conditions. The other two months show classic negative phase patterns: Wpot decreases and the PVpot increases as dry eastern winds result in less cloud cover and therefore an increase in the PVpot. However, this increase is negligible compared to the loss of wind power yield due to the low irradiation in the winter.

Figure 48 also shows the Heating Degree Days (HDD) (based on 18 °C reference temperature) which represent the demand for energy used for heating. With a need to switch away from conventional fuels and save energy, heat pumps will likely supply a large proportion of the future domestic heat demand resulting in a higher electricity demand. The frigid continental winds carry cold air from the north and east to Europe cause a very strong increase in the amount of HDDs, up to 30% more for western Europe and in sample 080 even up to 50% for South-East Europe. Apparently, a reduction of up to 75% in the electricity supply from wind turbines in high wind-dependent regions can coincide with a strong increase in energy demand.

Based on the EC-Earth climate model it is estimated that these ‘worst-case’ winters, based on taking the numbers of samples observed (3) divided by the number of winters in the M or H scenarios (~240) can occur once every 80 years. However, single months with a very low production are likely to occur much more often.

3.3.2.6 Conclusions

Four storylines are developed which describe the impact of changes in global warming and atmospheric circulation over Europe on the generation of renewable energy. What these storylines show is that particularly the uncertainty in the atmospheric circulation impacts on the generation of renewable energy – both in winter and in summer.

The variability in the atmospheric circulation (which we captured in this study by the NAO in winter and the sNAO in summer) is such that periods were identified with persistently calm conditions over Europe linked to the inflow of frigid arctic air. These conditions result in a decrease in wind power accompanied with extreme cold which increases the heating degree days with 30%. The example provided in this study of such extreme situation within one scenario illustrates the breath of situations a power system set-up needs to be able to cope with.

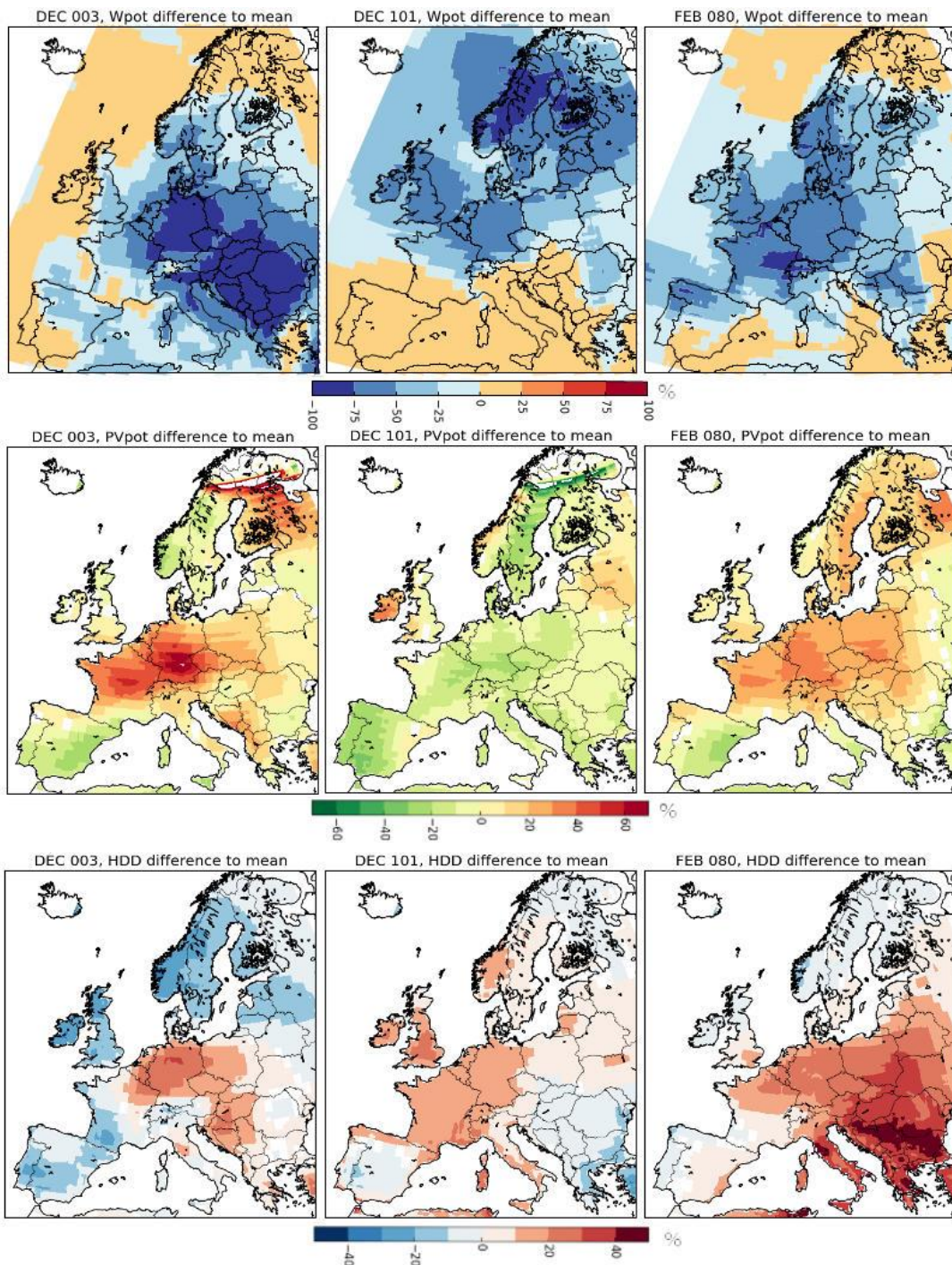


Figure 48: Presenting the Wpot, PVpot, and HDD percentage differences between the three lowest production months in winter and the average of the respective months over both NAO phases.

3.3.3 The impact of blocking on future winter low wind and low temperature events

Paula Gonzalez, David Brayshaw, Reinhard Schiemann; UREAD

Low wind events and persistent low wind events are of particular interest in energy meteorology because, during these events, the energy system needs to rely on

‘backup’ sources, such as gas, coal and nuclear. Over the United Kingdom and other parts of Europe, these events are often linked to the occurrence of blocking (e.g., Cannon et al. 2015, Grams et al. 2017, Thornton et al. 2017), which is the initial focus of this study. Additionally, blocking events have an impact on near-surface temperatures over Europe, which implies an effect in weather-dependent energy demand.

The reliability of the representation of blocking in the PRIMAVERA models has been explored by WP2 (see for instance, PRIMAVERA Deliverable D2.2, Section 3.3.4, Deliverable D5.2 and Schiemann et al. 2020). This study focuses on the impacts of blocking conditions on low wind (LWE) and low temperature events (CE) events on the European winter, and how this impact is projected to change according to the PRIMAVERA models. Preliminary results from this study were included in PRIMAVERA Deliverable 10.3 (D10.3), section 3.2.2. It was shown that blocking events over Europe have a significant impact on the occurrence and duration of low wind speeds at the country level. In addition to becoming more frequent, LWE are also more persistent under blocking conditions over large areas of Europe. In general, both effects are captured by most of the PRIMAVERA GCMs, revealing that models which simulate blocking conditions reasonably under highresSST-present forcing also capture the basic dynamical connection with wind anomalies. Nonetheless, the fact that the simulated weather conditions have deficiencies introduces biases in the properties of the events and their joint occurrence. The errors in the models depend on the statistic, the country and the resolution. No robust improvements in the representation of these effects were observed in the high-resolution versions of the PRIMAVERA models, nor where the highest resolution runs consistently outperforming coarser simulations.

Using the improvements in the methodology proposed in D10.3, the current results further explored this connection, adding the influence on low temperature events and exploring some initial future projections.

3.3.3.1 Data and methodology

As in D10.3, we use here the blocking index defined by Schiemann et al. (2017), calculated for ERA-Interim reanalysis as well as for a subset of PRIMAVERA GCMs, in their forced highresSST-present (1950-2014) and highresSST-coupled (2015-2050) simulations.

An improvement introduced in the analysis was the incorporation of regional blocking indices. Following Schiemann et al. (2017), we consider here the two indices that have a significant impact on winter climate over Europe:

- ATL: Atlantic blocking (centred in 0E,56.25N)

- GRL: Greenland blocking (centred in 43.125W, 67.5N)

All the indices were calculated for the season covering December to January (DJF).

As in the previously discussed D10.3 analysis, the definitions of low wind and low temperature days are determined according to the monthly climatological 20th percentile for each grid point. Country-level LWE and CE are then identified when at least 50% of the gridpoints classify as an event.

The future projections presented here were defined as the difference between the statistics corresponding to the 2015-2050 future period and those of the 1950-2015 historical baseline.

3.3.3.2 Historical results

We present here results from the comparison between the Met Office/Hadley Centre (MOHC) HadGEM3-GC3.1 model at its MM (low resolution, LR) and HM (high resolution, HR) versions and ERA-Interim. It was seen that the overall effect of blocking on low wind events was captured by all the PRIMAVERA models analysed, but the biases present in the simulations depend on the model and resolution.

3.3.3.2.1 Impact of blocking on low wind events

First, we present in Figure 49 the probability of observing a low wind day given the occurrence of winter blocking (ATL and GRL) in ERA-I and the MOHC models. It can be seen that ATL blocking results in an increased probability of observing LWE with respect to climatology in central Europe and the UK, and a decrease in Scandinavia and the Mediterranean countries. In the case of GRL blocking, the increase is smaller and covers central and northern Europe, whereas the decrease remains in Southern Europe.

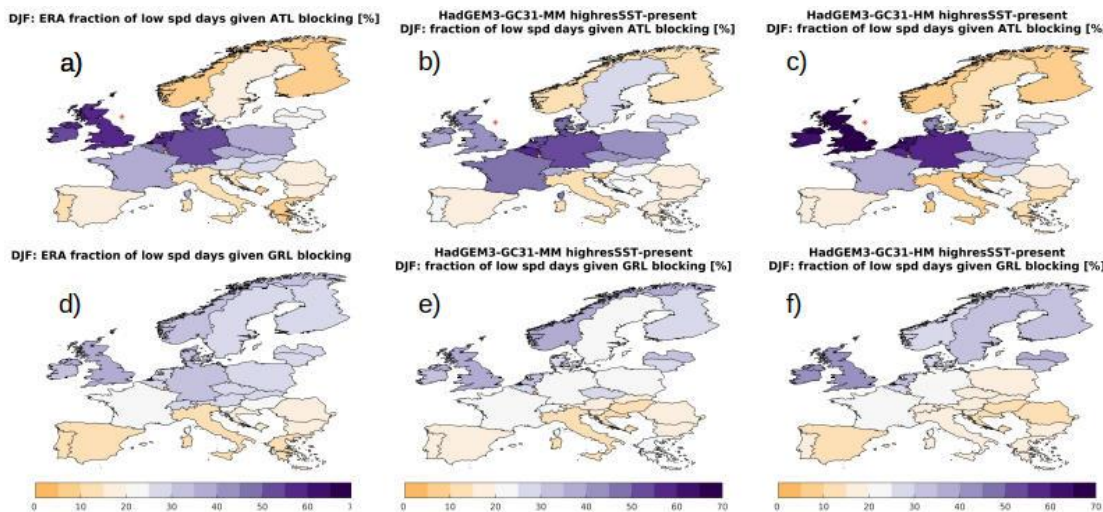


Figure 49: Probability of observing low wind days given the occurrence of winter blocking. Top panels correspond to ATL blocking and bottom panels to GRL blocking. a) and d) present the probabilities corresponding to ERA-I, b) and e) those for the LR version of HadGEM3-GC3.1, and c) and f) to the HR version of the same model. Purple shades indicate an exceedance with respect to the climatological probability, which is 20% by definition.

The HadGEM3-GC3.1 model captures the effect at both resolutions but with some biases. Most notably, the increase in probability associated with GRL blocking over central Europe is underestimated.

3.3.3.2.2 Impact of blocking on low temperature events

Figure 50 shows the probability of observing a low temperature day given the occurrence of winter blocking (ATL and GRL). Cold days during winter are associated with an increase in energy demand. During the occurrence of DJF ATL blocking, ERA-I detects an increase in the probability of observing cold days over central and southern Europe, and a decrease over Scandinavia and the Baltic countries. The pattern is well captured by the HadGEM3-GC3.1 models, but the increase is overestimated. In the case of winter GRL blocking ERA-I shows increases in the occurrence of CE over most of Europe but almost no change over Iberia, Italy and Greece. The models capture the effect with some biases in the magnitudes. The increases are overestimated in the HR version.

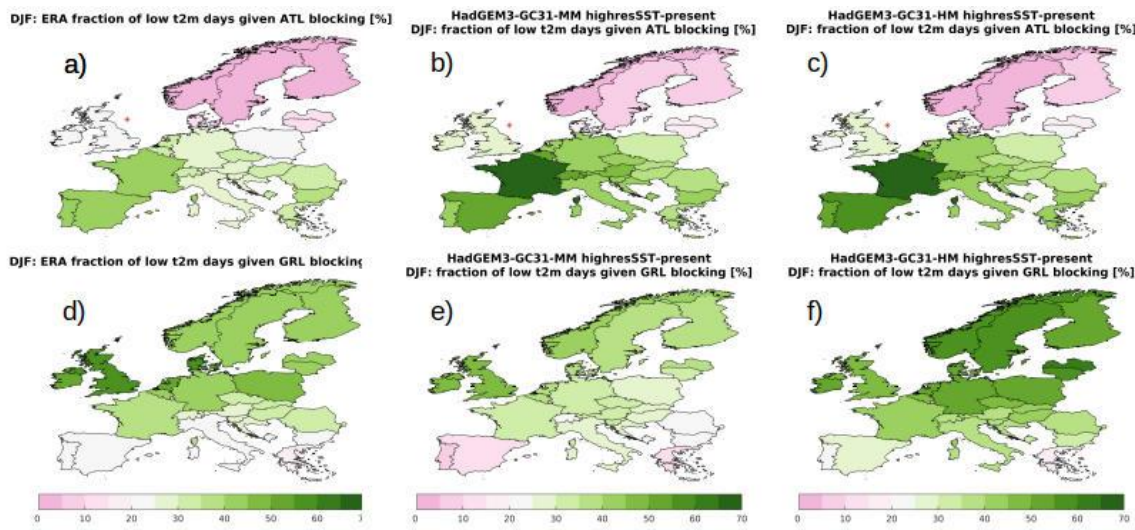


Figure 50: Probability of observing low temperature days given the occurrence of winter blocking. Top panels correspond to ATL blocking and bottom panels to GRL blocking. a) and d) present the probabilities corresponding to ERA-I, b) and e) those for the LR version of HadGEM3-GC3.1, and c) and f) to the HR version of the same model. Green shades indicate an exceedance with respect to the climatological probability, which is 20% by definition.

3.3.3.2.3 Impact of blocking on joint low wind and low temperature events

The occurrence of joint low wind and low temperature days is of particular interest for the energy sector because they pose an additional stress in energy systems with significant penetrations of wind power, for being associated with high demand but decreased wind power generation. Figure 51 presents the probability of observing such joint events under winter blocking conditions.

Given the occurrence of DJF ATL blocking, ERA-I registers an increase in joint LW-CE days over most of Europe, with the exception of Scandinavia and the Baltic countries, and some Adriatic countries. The pattern is well capture by the models, but they overestimate the increases in France and Germany quite notoriously. In the case of DJF GRL blocking, the increases cover central and northern Europe and there is almost no change in the Mediterranean region. The models get the sign of the change correctly in most countries, but have unstructured biases in the magnitudes.

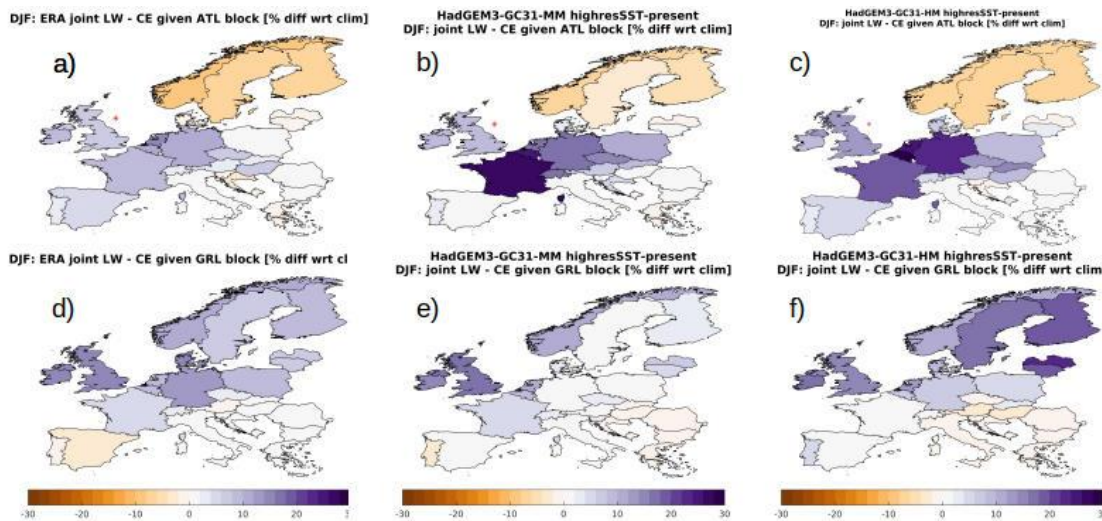


Figure 51: Probability of the joint occurrence of low wind and low temperature days given the presence of winter blocking. Top panels correspond to ATL blocking and bottom panels to GRL blocking. a) and d) present the probabilities corresponding to ERA-I, b) and e) those for the LR version of HadGEM3-GC3.1, and c) and f) to the HR version of the same model. Probabilities are expressed as differences with respect to the climatological value, which varies for each country. Purple shades indicate an exceedance with respect to the climatological probability.

We have observed here that under winter blocking conditions, both ATL and GRL blocking, there is a number of large central European countries such as the UK, Germany and France that observe an increase in the occurrence of low wind, low temperature and joint conditions which are linked to stress in the energy system. The HadGEM3-GC3.1 models capture the sign of the connection but not without biases. No significant improvement can be observed in the HR version versus its LR counterpart.

We haven't included here results on the impact of winter blocking on the persistence of these extreme conditions for length limitations. Nonetheless, the increases in the persistence of the LW and CE described in deliverable D10.3 hold true here and some were presented at the PRIMAVERA GA5 (Gonzalez et al. Impact of blocking).

3.3.3.3 Future projections

We now present some results from the analysis of the PRIMAVERA future projections, starting from the changes in the blocking indices themselves. Figure 52 presents the projected changes in the statistics of winter blocking for the HadGEM3-GC3.1 models. It can be seen that these models project decreases in both the duration and frequency of ATL and GRL blocking events. In the case of ATL blocking duration, the model goes from almost no change at LR to a 10% decrease at HR. Frequency of ATL blocking events is projected to decrease close to 30% by both versions of the model. In the case of GRL blocking, duration is consistently projected to decrease around 6% and frequency around 10-20%. It is important to note that

part of this frequency and duration reductions can be due to the point-wise definition of these indices, and that this should be further explored to assess whether a box definition might be more appropriate for the assessment of future changes given the latitudinal changes projected for the storm track.

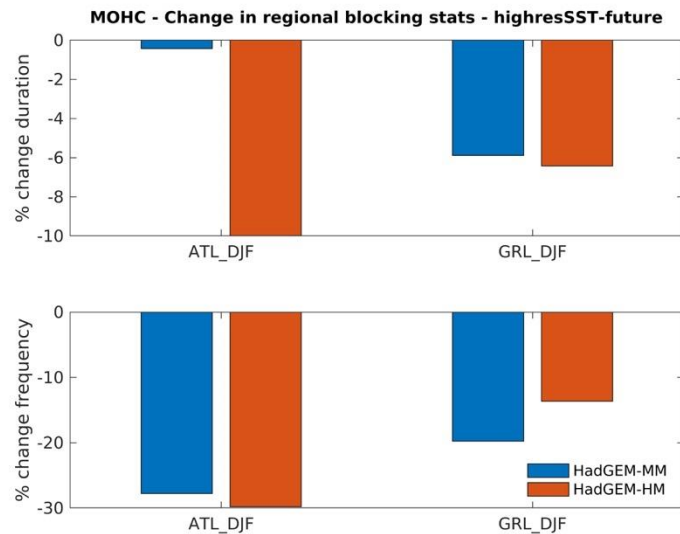


Figure 52: Projected changes in MOHC winter regional blocking statistics from the comparison of the highresSST-present and highresSST-future scenarios. Top panel presents percent changes in duration and bottom panel in frequency [%].

We then focus on the projected changes in the influence of blocking on the events of interest. Figure 53 shows the future probabilities of observing low wind days given winter blocking. In the case of ATL blocking, the main signal is a decrease in the probability of observing LW days centred in the region that had above climatological probabilities in the historical period (Figure 49, top panels). As a result, in the future period, only a smaller region including mainly the British Isles, France, Germany, Belgium and the Netherlands presents probabilities of these events higher than the climatology.

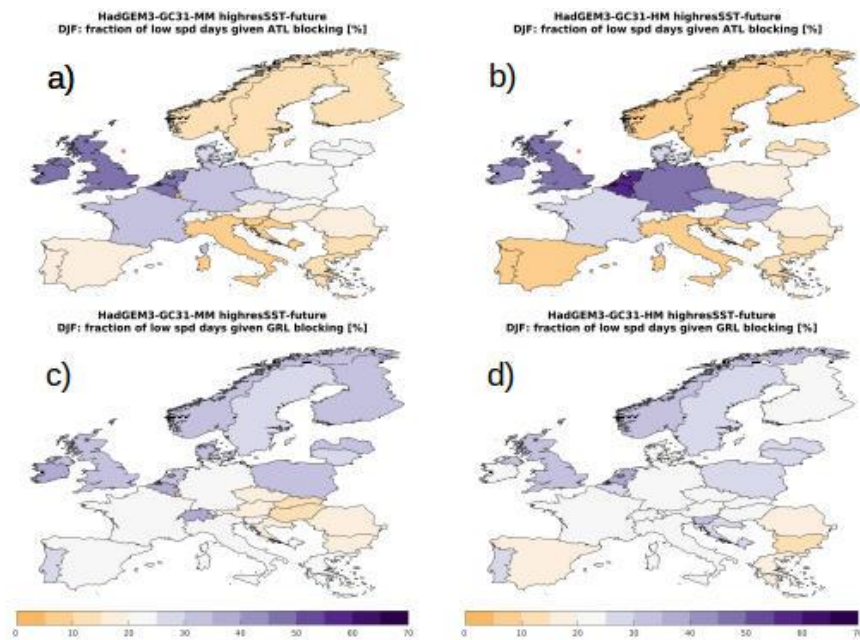


Figure 53: Projected probability of observing low wind days given the occurrence of winter regional blocking in MOHC under the highresSST-future scenario. a) ATL blocking in the LR version; b) ATL blocking in the HR version; GRL blocking in the LR version; d) GRL blocking in the HR version.

In the case of GRL blocking (panels c and d), the change pattern is more complex, showing slight decreases in some countries that had above climatological probabilities, such as the UK, and increases in other countries where the effect wasn't present, such as Italy or Austria (from comparison with Figure 49, bottom panels). Overall, the MOHC models project the increase frequency of LW days under GRL blocking to be marginally expanded geographically to the SE, though results for specific countries vary according to the model resolution.

Figure 54 presents analogous results but for the probability of observing cold days given winter blocking. Comparing this figure with Figure 50 it is possible to see that the probabilities associated with ATL blocking (top panels) change very little (for most countries, probability changes are smaller than 10%) and therefore there are no significant changes in the impact pattern. In the case of the impact of GRL (bottom panels) the results are very different for each model resolution. In the case of the LR version (panel c), the pattern is preserved but the probability increases are stronger than in the historical period. In the HR version (panel d) probabilities are severely reduced. For some countries like Germany, the probability change is of the order of 40%. As a result, only some northern countries show an increased probability of observing CE given GRL blocking in this model.

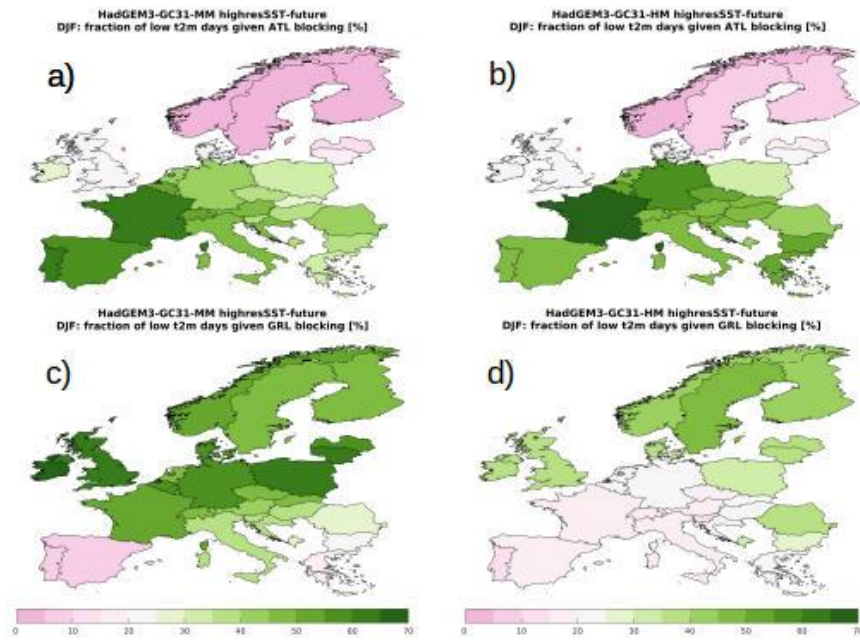


Figure 54: Projected probabilities of observing cold days given the occurrence of winter regional blocking in MOHC under the highresSST-future scenario. a) ATL blocking in the LR version; b) ATL blocking in the HR version; GRL blocking in the LR version; d) GRL blocking in the HR version.

Finally, Figure 55 presents the future probabilities of occurrence of joint low wind and cold events given winter blocking. In the case of the impact of ATL blocking (top panels), a comparison with Figure 51 reveals that the probabilities are generally reduced for the future period, but the pattern of increased occurrence of joint events in central Europe remains. In the case of GRL blocking (bottom panels), the probabilities are higher for the future period, indicating an enhancement in the joint impact over northern Europe and parts of central Europe, depending on the resolution.

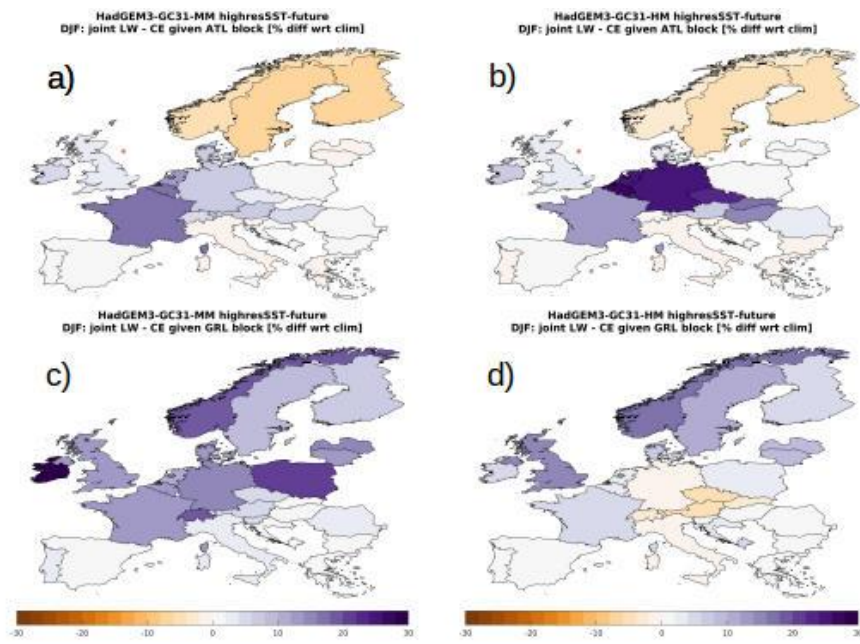


Figure 55: Projected probabilities of observing joint LW and CE days given the occurrence of winter regional blocking in MOHC under the highresSST-future scenario. a) ATL blocking in the LR version; b) ATL blocking in the HR version; GRL blocking in the LR version; d) GRL blocking in the HR version.

3.3.3.4 Preliminary discussion

We present here some initial results from the evaluation of the MOHC future projections regarding the impact of winter blocking on low wind, low temperature and joint events. For this specific model, the projections indicate a decrease in both the duration and frequency of winter blocking as identified by the ATL and GRL types. Moving to the impacts, in most cases the model projects a weakening of the impacts identified for the historical period, though this might change for some events and resolutions. Nonetheless, it holds that some large countries in central and northern Europe such as the UK, France and Germany are projected to experience more energy-relevant events (LW, CE and joint LW-CE) during winter blocking (both ATL and GRL) with respect to climatology. The fact that the frequency of blocking itself is projected to decrease might indicate an overall reduction of the number of these events.

It is important to note that the relevance of these results is limited by the current use of a single model. Nonetheless, a reduction in the frequency of winter blocking over Europe as presented here has been recently shown to be a robust projection in CMIP6 models (D'Andrea and Davini 2020). Even though we have assessed that the historical impact is captured by all models to some extent in the historical period, we are yet to address the future projections derived from other PRIMAVERA models.

Additionally, this analysis has only used the forced simulations, so including the coupled runs would also be advisable for robustness.

3.3.4 Discussion of sector impact

This section has introduced results from three research lines pursued within the context of PRIMAVERA with the common objective to explore different aspects of the future climate that will affect European wind power and more generally, the energy system.

The first subsection had a focus on exploring the influence of long term trends in the mean state as represented by the North Atlantic jet. It reveals that even within this next generation of GCMs large uncertainties remain in future projections for wind speeds. Even more so, as increases in horizontal resolution have led to opposing changes in the jet latitude, both at the large basin scale and at the regional European scale. Isolating in each model and resolution the influence of changes in the large scale variability did not reduce the uncertainty observed in regional European wind changes. A further investigation of these effects with a larger ensemble and looking further into the future is paramount for a robust assessment of the future of wind power resource over Europe, when its penetration in European energy systems continues to increase at a fast pace.

The second subsection focused on the use of a storyline approach to develop scenarios for the future of renewable energy generation over Europe, with a focus on NAO and its summer extension sNAO. These modes of variability dominate seasonal to interannual variability over Europe and are known to have a drastic impact on the energy sector. It was shown that even though climate change is likely to impact future renewable energy resources over Europe, these impacts are smaller than the variability induced by the change in NAO and sNAO, especially in the case of wind power. This implies that it is particularly important to plan for energy systems that are resilient to swings observed in current climate variability, even if future trends remain uncertain.

Finally, the third section presented an analysis of the impact of winter blocking and its projected changes on wind and temperature extreme events. Atmospheric blocking, a much shorter lived weather-scale phenomena, is known to have large impact on the European energy systems, by for instance promoting very cold events that further enhance winter peak demand. Furthermore, it is shown here that due to its impact on low wind events, it can lead to a double challenge in some large countries such as the UK and Germany with substantial – and increasing- wind power penetrations. The initial results presented here reveal that depending on the type of blocking and the specific country, the enhanced probability of occurrence of low wind, low temperature and compound extreme events is projected to be

reduced. Nonetheless, their probability of occurrence still exceeds the climatological odds in several countries in central Europe. Therefore, winter blocking conditions can still lead to anomalously high energy demand and low wind power generation, even if less frequently. Furthermore, the impact on the energy system can even be larger due to increasing penetrations of wind power.

Limitations in the analyses presented here were identified, related to different aspects such as ensemble sizes, projections periods and others. This, together with the strong impact that the processes covered here pose to the future of European energy systems, reinforces the need for further research into these and other aspects of the connection between weather and climate variability and energy. The rapid evolution of these systems and their increased sensitivity to weather and climate variability makes this research very timely to aid in the development of green and resilient energy future.

3.3.5 Key Points

- State-of-the art GCMs still present large uncertainties in the future projections of near-surface wind speeds over Europe and the relative contribution of large-scale circulation changes. Furthermore, large differences in the projections are observed between different resolutions of the same model, which further increases the uncertainty in the projections.
- Future changes in the mean state of renewable energy sources over Europe are small when compared to the shifts induced by the winter NAO and summer sNAO modes of variability, especially for wind power.
- An enhanced probability of occurrence of low wind, low temperature and compound events is linked to the occurrence of winter blocking over several countries in central and northern Europe. Preliminary results suggest that given a reduction in the frequency of winter blocking, the frequencies of these events are also projected to decrease, while still remaining above the climatological probability for several large countries such as Germany and the UK.
- The significant levels of uncertainty present in the future projections associated with these energy system-relevant processes suggest that for planning purposes, the focus should be put on designing systems that are resilient to current climate and weather variability. The impacts, however, are likely to be larger due to the enhanced sensitivity associated to increases in the penetration of renewable energy sources.

3.4 Precipitation and the water sector

Gustav Strandberg, SMHI

3.4.1 Introduction

The water sector consists of several different branches all of which, in different ways, are dependent on precipitation (see D10.1). Branches dealing with water availability and water resources are mostly interested in the overall precipitation sum over seasons, and less in how that precipitation amount is distributed over specific days. City planners and risk managers on the other hand are interested in the extreme precipitation. It makes a large difference if the same precipitation amount falls over one day or over a month since it's the extreme short-term precipitation that causes flash floods. Longer term precipitation could also cause problems when it leads to increased stream flow which could also lead to inundation. Agriculture, as well as production of food and drinking water are all dependent on water and on water quality. Water availability becomes scarce and water quality may deteriorate in a drier climate. Water quality may also deteriorate with increased precipitation, for example when dirty water floods agricultural land or penetrates water reservoirs. As a last example, hydro power is dependent on precipitation to fill the dams. How the precipitation is distributed over the year and if it falls as snow or rain is also important as that defines the conditions for how hydro power can be run.

The diverse water sector needs information about how precipitation is projected to change in the future. Depending on the branch of the sector it's interesting to know about seasonal average precipitation, extreme precipitation or how precipitation is distributed over a season. Thus, there is not one measure of how changes in precipitation impact the water sector. This section makes an attempt to cover some of them, which are considered general and interesting for more than one branch.

3.4.2 Method

This section looks at how precipitation in the relatively near future is simulated in some of the Primavera models, both low and high resolution versions of the models. The models used are: CNRM-CM6-1, CNRM-CM6-1-HR, EC-Earth3P, EC-Earth3P-HR, HadGEM3-GC31-LM, HadGEM3-GC31-MM, HadGEM3-GC31-HM, MPI-ESM1-2-HR, MPI-ESM1-2-XR. One member per model were used. Calculations of precipitation change are based on the difference between the periods 1981-2010 and 2021-2050. These two periods are only 40 years apart, which means that climate will not have time to change as much as if we would look at a period further in time. Furthermore, the natural variations in precipitations are large. Precipitation

varies significantly between days, seasons and years. In addition to that the simulated precipitation differs between models. The weak climate change signal in combination with large uncertainties and variability means that a significant trend may not be discernible. If the simulated precipitation change is small this could thus be an effect of one (or several) of the following: 1) the actual precipitation change is small 2) the change is small compared to the natural variability which makes it less significant 3) models disagree on the sign or magnitude of the change which makes the model ensemble mean small or uncertain. In the second case the climate change signal will get more significant as climate change continues. A more in-depth description of these different kinds of uncertainties is given in the Primavera fact sheet on uncertainties in climate projections (https://uiip.primavera-h2020.eu/sites/default/files/Uncertainty_Climate_Models.pdf). Despite the uncertainties mentioned above it is possible to draw some general conclusions about future precipitation in Europe.

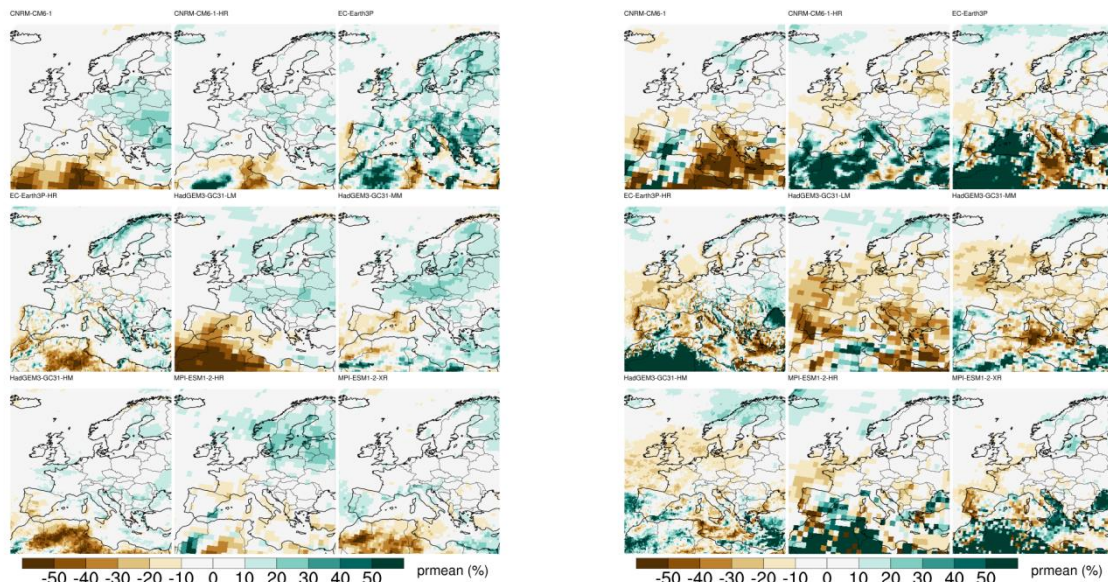


Figure 56. Change in average precipitation (%) 2021-2050 compared to 1981-2010 in winter (DJF, left) and summer (JJA, right) for 9 Primavera models.

3.4.3 Results

Figure 56 shows change in average precipitation in Europe. There are differences between models, but it's still possible to find similar patterns in all models. The differences between models are usually larger than the differences between resolutions for the same model. Even though the models give rather different absolute amounts of precipitation (see D10.2 and D10.3) the amplitude of the change signal is similar in all models, and for all resolutions. In general, precipitation is projected to increase in northern Europe and decrease in southern Europe. The

increase in the north is largest in winter (December, January, February; DJF), the decrease in the south is largest in summer (June, July, August; JJA). Changes are around $\pm 20\%$. The boundary between increasing and decreasing precipitation is shifted between seasons so that a larger part of Europe gets increased precipitation in winter, and a larger part get decreased precipitation in summer. The exact position of this boundary is a matter of discussion between models. Precipitation changes in central Europe must be considered to be more uncertain, but also smaller, than changes in southern and northern Europe. It should, however, be noted that in regions with no or very little precipitation, such as northern Africa, small changes can be very large when measured in percent; thus, these numbers should be interpreted with caution.

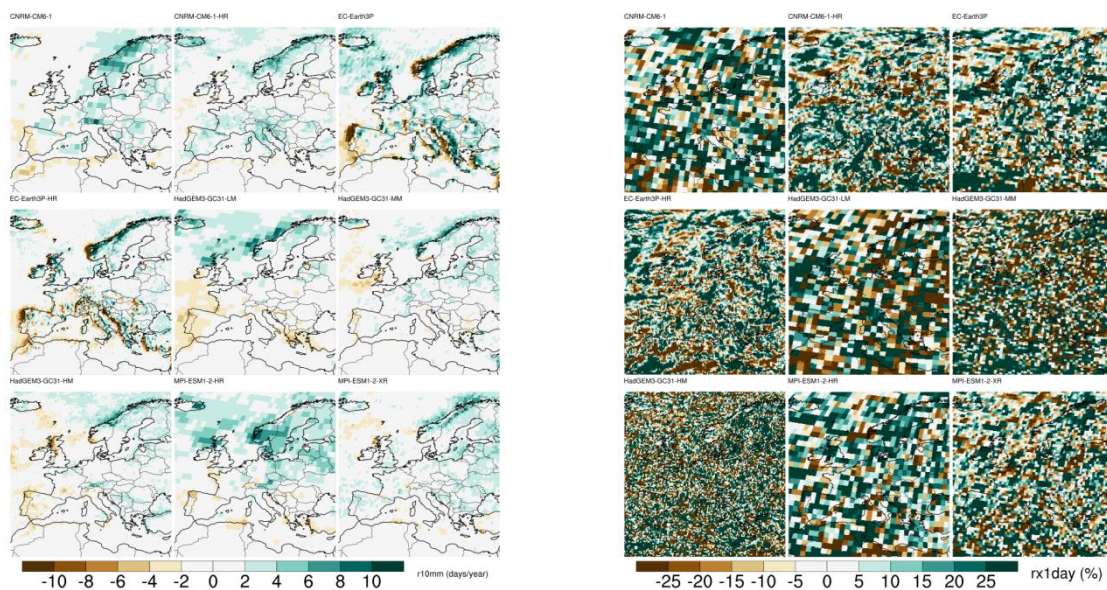


Figure 57. Change in the annual number of days with daily precipitation above 10 mm ($r10\text{mm}$, (days), left) and in the maximum one-day precipitation ($rx1\text{day}$ (%), right); 2021-2050 compared to 1981-2010 for 9 Primavera models.

With changing precipitation amounts the number of days exceeding certain thresholds of precipitation will also change. The change in days with precipitation amounts over 10 mm corresponds with the change in average precipitation (Figure 57 left), and so do the days with precipitation amounts above 20 mm (not shown). The change in the most extreme precipitation (maximum one-day precipitation, Figure 57 right) shows a more complex pattern. Extremes are per definition occurring seldom, which makes the change signal noisy with both decreases and increases scattered over Europe. On the local scale, one point may have had an extreme precipitation event in the current 30-year period. If this is a rare event it may not happen in the future 30-year period which will give a decrease in the maximum one-day precipitation (or the other way around). On the larger scale, however, the tendency is that extreme precipitation will increase in the future, also in regions with

decreasing average precipitation. This means that some regions may have increasing problems with both drought and extreme showers (Collins et al., 2013).

Both the amount and intensity of precipitation will thus change in the future. That the changes are different in different seasons also mean that the dynamics of water availability will change. Even regions with relatively unchanged precipitation amounts will be affected, since evaporation will increase in a warmer climate, and since extreme precipitation can change even if the average amount doesn't.

3.4.4 Conclusions

Precipitation will change in the future. The amount and sign of change varies between seasons and regions, but less with model resolution. Generally precipitation will increase in northern Europe and decrease in southern Europe. Extreme precipitation will also change, but in a different way. Any region may get extreme showers, and any region can get an increase in extreme precipitation, even regions where the average precipitation is projected to decrease.

This means that the water sector will face new problems. Depending on the region and season water availability will decrease or increase. In a warmer climate less precipitation will fall as snow which has an impact on runoff and stream flows (this section only looks at precipitation and not runoff, but it's worth noting). This means that hydro power will have to be managed in a different way compared to today. In southern Europe irrigation may have to be limited during the dry season to save water, while in northern Europe measures have to be taken to handle the increased amounts of water. On top of that, extreme precipitation may increase all over Europe, which means that all cities have to be prepared for more flash floods.

As always with climate adaptation it is difficult to give general, but specific guidelines. Depending on business sector and geographical region the challenges are different. For different sectors different indices are relevant. Some are sensitive to the seasonal sum of precipitation, while another is sensitive to intense precipitation; yet another may be sensitive to the number of dry days or precipitation days. Every sector must think about what their particular sensitivities are. The key message here is that precipitation will change and that we have to adapt to that. This section only looks at changes up until 2050, which may well reflect the time limit for many investments; however, climate change will continue also in the latter half of this century, which also means that adaptation measures will have to continue.

3.4.5 Key points

- The amount and change in precipitation vary with season, region and also index. Precipitation will change in many ways; it's important to know in what way you are sensitive to precipitation and precipitation change.

- Model resolution does not strongly impact simulated precipitation change. The difference between different models is larger.

3.5 Management of low-temperature and high-temperature conditions in the transport sector

Galina Guentchev and Erika Palin, Met Office; Paula Gonzalez and Reinhard Schiemann, UREAD; Antonello Squintu and Gerard van der Schrier, KNMI

3.5.1 Motivation

The transport sector is impacted by weather in a variety of ways (see e.g. Palin et al., 2018 and PRIMAVERA D10.1). Some examples (non-exhaustive) are:

- High temperatures – buckling of rails; road surface rutting and cracking; passenger and staff thermal comfort issues
- Low temperatures – icing of roads and runways, requiring de-icing treatment; railway overhead line equipment icing; railway tracks blocked by snow; tunnel icing; passenger and staff thermal comfort issues; increased personal injury risk (slips and falls) at stations
- Excess precipitation – flooding of roads, railway tracks and runways; flooding of depots; water ingress to locomotive electronics; landslides
- High winds – vehicle overturning; objects blown onto road/railway; disruption of port and airport operations
- Coastal hazards – storm damage to port infrastructure, and to coastal road, rail and airport infrastructure
- Lightning – road/tracksides vegetation fires; railway signalling disruption; disruption to aviation; risk to airport staff

In D10.1 several transport use cases were proposed:

- Information to support flood hazard assessment
- Managing wind hazards
- Transport operations during hot weather

These use cases were somewhat speculative because at the time of preparing D10.1, there had been limited engagement with the transport sector. In this deliverable we have chosen to focus on temperature-related hazards. As well as considering high temperatures, a low-temperature use case not put forward in D10.1 was also revealed during subsequent stakeholder engagement.

3.5.1.1 High temperature impacts on transport

Vajda et al. (2011) defined weather-related thresholds for transport disruption that were intended to be applicable across Europe. In practice such thresholds will vary, as transport assets will be sensitive in different ways and in different locations. However, these thresholds are a useful starting point for understanding the possible impacts of climate change on future weather-related transport disruption in Europe.

3.5.1.2 Low temperature impacts on transport

During stakeholder engagement with Transport Infrastructure Ireland (TII) a low-temperature use case emerged. Specifically, TII undertakes road salting activities when the road surface temperature is $\leq 1^{\circ}\text{C}$ and there is precipitation (or precipitation is forecast), at temperatures down to -5°C . When the road surface is below -5°C , treatment intensifies, with a greater spread rate of salt. LUAS (Dublin light rail system) platforms are also salted according to the same criteria.

Current resilience in Ireland is defined as each local authority having the capacity to undertake at least three treatments (25g/m^2) a day for 21 days. There are 370 salt spreaders around Ireland, and TII's medium-to-long-term plan is to replace the whole fleet, which would be a large investment. TII is therefore interested in obtaining information about the future frequency/severity of low temperature extreme events (e.g. those like the "Beast from the East" in February/March 2018). Design standards might need to be revised in the light of such information, and decisions around the future size of the salt spreader fleet would also need to be supported by this kind of information.

While results from PRIMAVERA cannot be used in isolation to guide this kind of decision, they can be used to demonstrate the sort of information that could be useful in future.

3.5.1.3 Threshold values and calculation of indices

Table 2 shows some relevant temperature thresholds for Europe chosen by Vajda et al. (2011). Because the thresholds were defined for Europe as a whole, they span a range of climatic conditions, not all of which will be relevant for a given European location. The "possible" and "likely" thresholds have been used to represent high-temperature impacts, as exceedance of the "virtually certain" threshold is likely to be very rare (and not applicable to the climate of the UK and Ireland, which are the main locations studied), and hence not a robust parameter to evaluate for this study.

Table 2: Temperature thresholds chosen by Vajda et al. (2011) as representative of hazardous conditions for European transport.

Hazard	Parameter	Possible adverse impacts	Likely adverse impacts	Virtually certain adverse impacts
High temperature / heatwave	Daily Tmax	>25 °C	>32 °C	>43 °C

Furthermore, in the Netherlands the government organization responsible for maintaining and extending the national railway network infrastructure (ProRail) indicates that a maximum temperature of 25°C is important to consider. Exceedance of this threshold leads to impacts such as expansion and buckling of the rails, signal and switch failures due to disruptions of electronic equipment, and heat related impacts on passengers and workers (ProRail, undated; ProRail, 2019). Having this in mind we decided to use the two heat-related thresholds in our analyses, specifically, the number of days with daily maximum temperatures higher than 25°C, and equal to or higher than 32°C in our analyses. The exceedance of the first threshold is also the well-known “summer days” (SU) ETCCDI index¹. Both indices are calculated for each year in a historical and future period and represent the annual number of days with maximum temperatures equal to or above the chosen threshold. The annual frequencies are summarized by calculating the period mean annual frequency of days with temperatures exceeding the thresholds for the historical (1950-2014 or 1980-2014) and the future period (2015-2050).

The low-temperature threshold was based on the discussions and operational activities which are usually undertaken when low temperatures affect Ireland and specifically Dublin, as outlined in Section 3.5.1.2. An illustrative threshold of daily minimum temperature less than 0°C was chosen as a starting point for our analyses. This is the ETCCDI “frost days” (FD) index¹. The frost days index represents the annual number of days with daily minimum temperature below 0°C. The calculation of this index is identical to the method discussed above for the high temperature extremes. The annual frequencies for a given period are again summarized by calculating the period mean of the index for the historical and the future periods.

Finally, the average change in the annual frequency of the days with temperatures above or below a threshold in the future is calculated as the difference between the period mean values for the future and historical periods.

3.5.2 Process

¹ http://etccdi.pacificclimate.org/list_27_indices.shtml

3.5.2.1 Blocking and low-temperature events

Work for the energy sector (see Section 3.3 of this deliverable) has explored the impact of blocking on the probability of low temperature days. In that work, a low temperature day was defined as a day with temperature below the monthly climatological 20th percentile per grid point; i.e. a different definition from that used here, and five models from the following modelling centres were used – MOHC, MPI, ECMWF, EC-Earth Consortium and CMCC. The pattern of regional variation of cold day probability during winter blocking events (according to two different blocking indices, representing Atlantic and Greenland blocking) was found to be captured quite well by the models, albeit with biases in the magnitude.

The same study explored the future changes in the probability of cold days during blocking events (2015-2050 cf. 1950-2015). Only the low- and high-resolution HadGEM3 projections were utilized for this part of the study and they indicated a decrease in both the duration and frequency of winter blocking as identified by the two indices. For Atlantic blocking, only small projected changes in the probability of cold days were projected (typically <10% for most countries) with no significant changes in the regional pattern. For Greenland blocking there were very different results for different resolutions (i.e., the low- and high-resolution simulations). The projected future decreases in winter blocking are consistent with the tendency of reduction in these events found in CMIP6 as a whole.

3.5.2.2 Weather patterns associated with high and low temperatures in the UK and Ireland

The occurrence of extreme high or low temperatures over Ireland is generally related to the relative positions of anticyclones and cyclones near or over the British Isles. When blocking occurs, these weather systems can remain in the same relative positions for a long period, thereby facilitating the build-up of heat/cold day by day, and/or advecting hot/cold air from elsewhere. In summer, the highest temperatures typically occur as a result of southerly or south-easterly air flows. In winter, the lowest temperatures typically occur as a result of northerly or easterly air flows, as well as under the influence of high-pressure systems located over the British Isles.

The days ($n = 2534$) with a minimum temperature below 0°C occurring in Dublin, Ireland, were calculated from v12 of the EOBS dataset² (Haylock et al., 2008) for the

² Acknowledgement: We acknowledge the E-OBS dataset from the EU-FP6 project UERRA (<http://www.uerra.eu>) and the Copernicus Climate Change Service, and the data providers in the ECA&D project (<https://www.ecad.eu>).

period 1950-2014. The weather pattern on each day was identified using the 30 weather patterns developed for the Met Office Decider tool (Neal et al., 2016). Eight patterns occur with a frequency greater than 5% when low minimum temperatures were recorded (6, 14, 17, 19, 24, 25, 27 and 28, Figure 58).

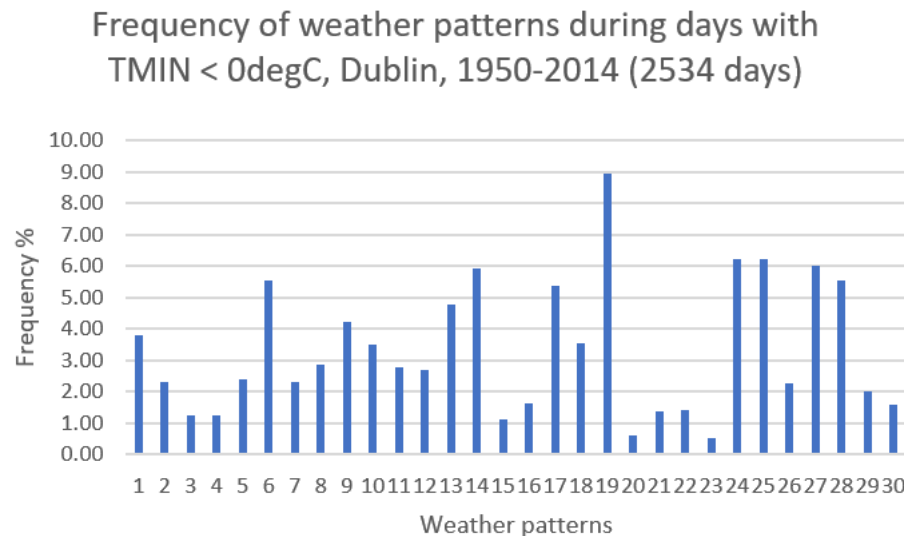


Figure 58 Frequency of weather patterns during days with minimum temperatures below 0°C; 30 weather patterns defined by Robert Neal.

Mean sea level pressure characteristics of these eight patterns are presented on the maps below - Figure 59. The maps represent weather patterns with a predominantly northerly flow (14, 19, 24, 25), a high-pressure system located over the British Isles (6), and predominantly easterly flow (17, 27 and 28).

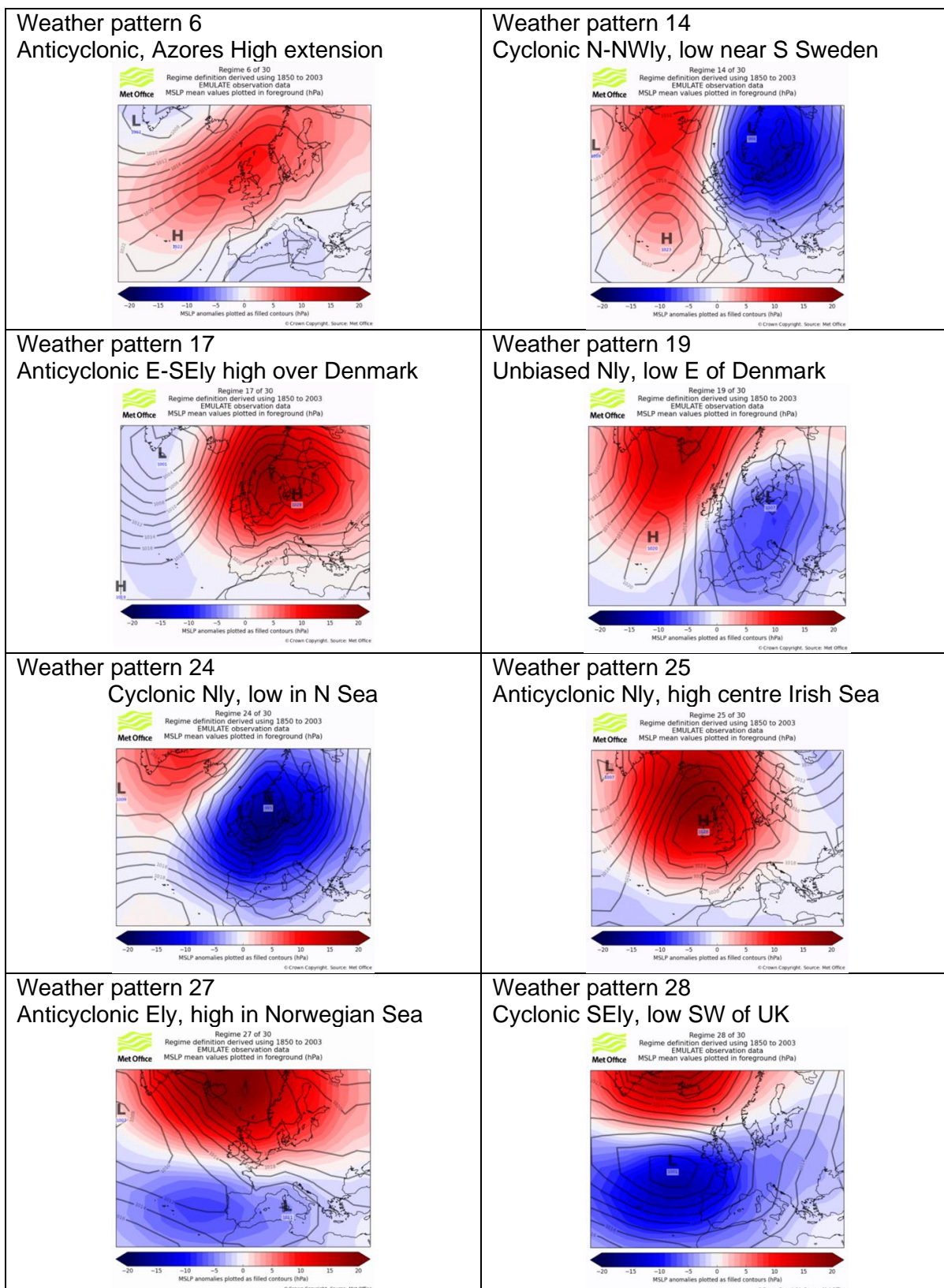


Figure 59 Weather patterns occurring most frequently during days with minimum temperatures below 0°C in Dublin, Ireland.

The weather patterns on days with daily maximum temperatures greater than 25°C for Dublin (“summer days” (SU) index) were identified for the period 1950-2014. Four patterns (numbers 3, 5, 6 and 12) occurred with frequencies larger than 10%, and 3 and 6 have frequencies of about 20% (Figure 60). All of these patterns are characterized by a high pressure system located in the vicinity of the British Isles or extending towards the British Isles leading to southerly or south-westerly flow bringing warm air over Dublin (Figure 61).

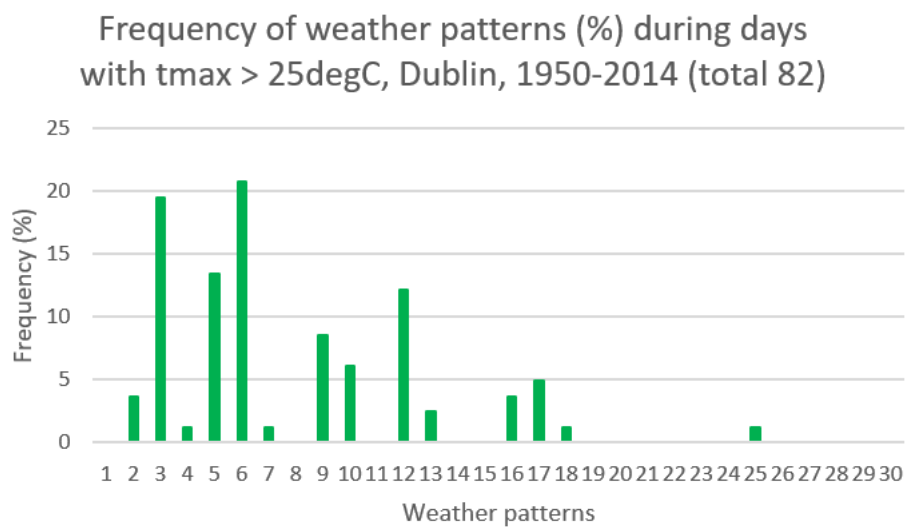


Figure 60 Frequency of weather patterns during days with maximum temperature above 25°C in Dublin.

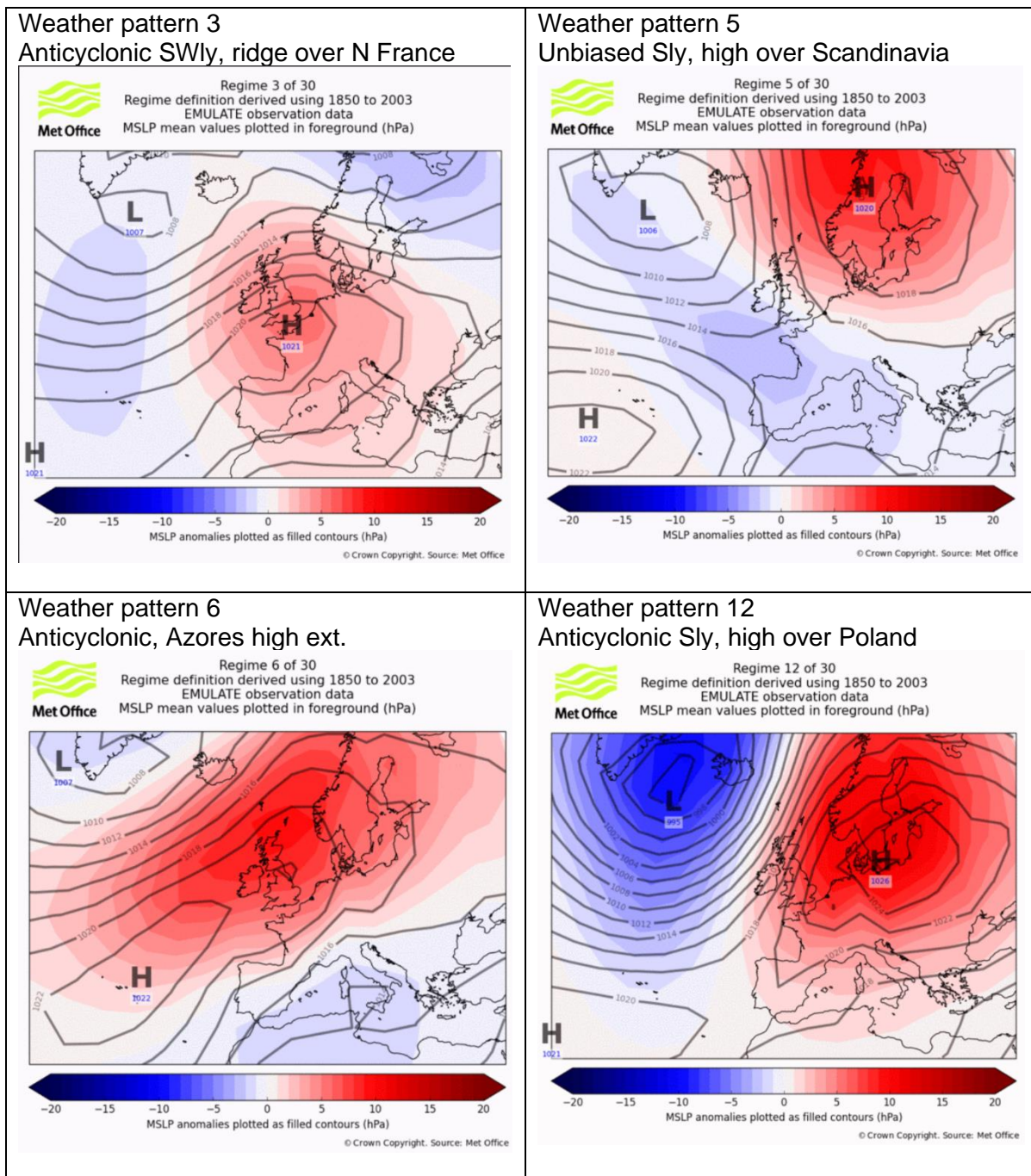


Figure 61 Weather patterns occurring most frequently during days with maximum temperatures above 25°C in Dublin, Ireland.

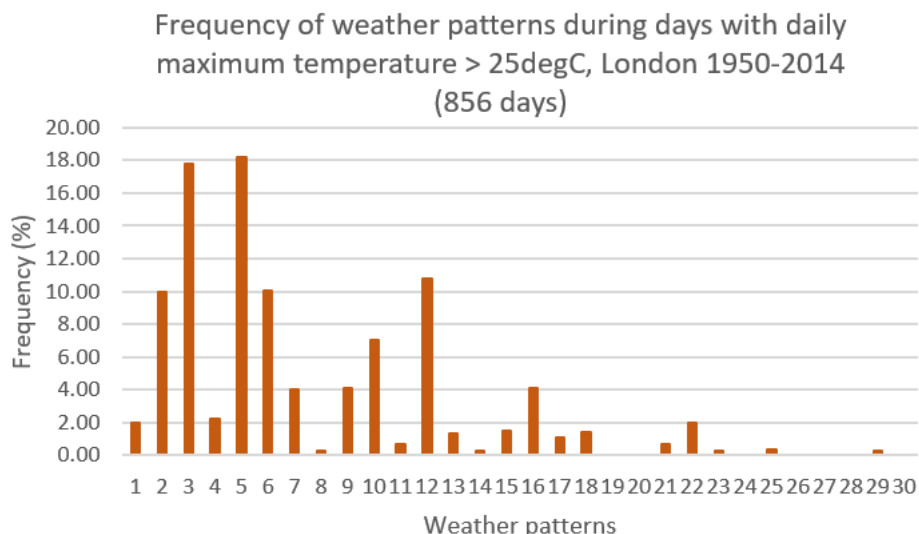


Figure 62 Frequency of weather patterns during days with maximum temperature above 25°C in London.

The number of days with daily maximum temperatures above 25°C in London (856) is greater than that in Dublin (82). There is similarity between the weather patterns that impact Dublin and those that affect London with weather patterns 3, 5, 6 and 12 (Figure 61) also occurring most frequently (Figure 62). Patterns 3 and 5 have frequencies of about 18%. In addition, weather pattern 2 is also more frequent for London (10%) than Dublin (4%). Weather pattern 2 (Figure 63) is characterized by polar maritime air approaching the British Isles from the south-west; this pattern exhibits slack flow over the south east of the UK, indicating that this would be the only area likely to experience any significant build in temperature if it were to persist. In turn this explains why this pattern occurs for warm days in London but not Dublin.

Weather pattern 2
Cyclonic SWly, returning Pm airmass

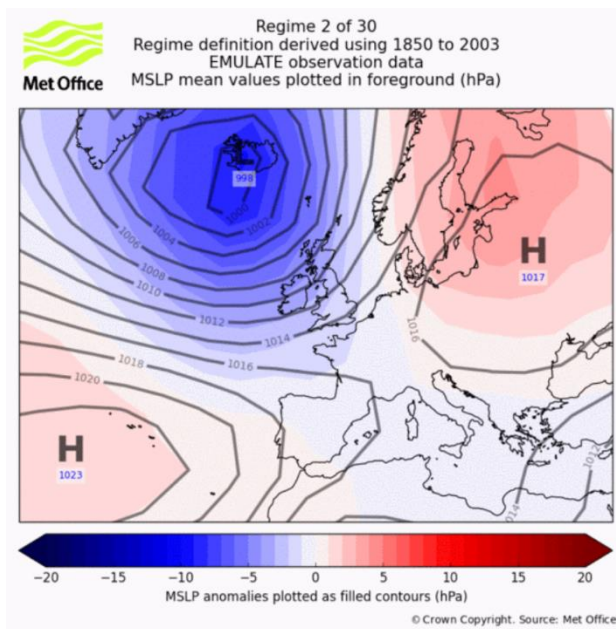


Figure 63 Weather pattern 2 occurring frequently during days with maximum temperatures above 25°C in London, Great Britain.

3.5.2.3 Representation of daily minimum temperatures below 0°C (“frost days” by the low- and high-resolution PRIMAVERA models during the historical period 1950-2014

The simulations from the sets of low- and high-resolution PRIMAVERA models were examined to assess how well they represent the occurrence of low minimum temperature events in Dublin, Ireland and in the UK. The comparison period was 1950-2014 and both the forced (AMIP) as well as the coupled simulations were used. The model simulations were compared to the EOBS ~25km gridded dataset v12 (Cornes et al. 2018). The model simulations were compared with gridded data from v12 of the EOBS dataset (Haylock et al., 2008). The models included in the historical analyses are shown below (Table 3).

Table 3 Summary of models analysed with approximate native horizontal resolutions at mid latitudes (50°N).

Modelling centre	PRIMAVERA high-resolution models	PRIMAVERA low-resolution models
CMCC	CMCC-CM2-VHR4 (18km)	CMCC-CM2-HR4 (64km)
ECEARTH	ECEARTH3-HR (36km)	ECEARTH3 (71km)
MOHC	HadGEM3-GC31-HM (25km)	HadGEM3-GC31-LM (135km)
MPI	MPIESM-1-2-XR (34km)	MPIESM-1-2-HR (67km)

ECMWF	ECMWF-IFS-HR (25km)	ECMWF-IFS-LR (50km)
-------	------------------------	---------------------

3.5.2.3.1 AMIP low- and high-resolution simulations

The frost days (FD) metric was computed at every grid point using the low-resolution atmosphere-only simulations (AMIP) from the five models listed above.

Bias in annual number of Frost Days, $t_{min} < 0C$ vs EOBS, 1950-2014, AMIP

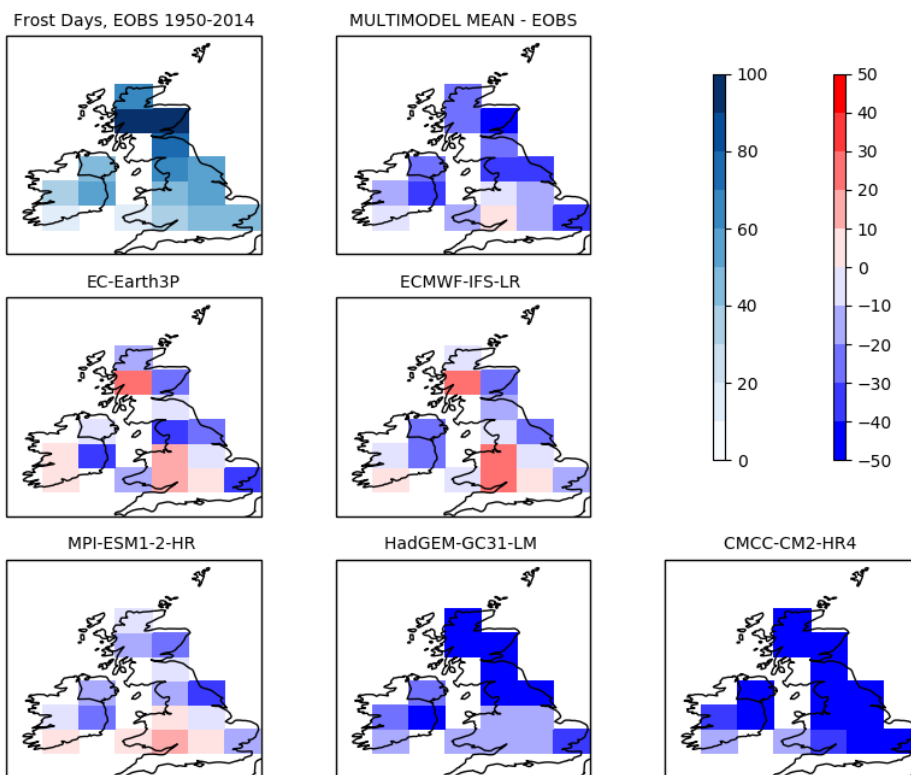


Figure 64 Biases in annual number of Frost Days (FD) as indicated by a set of AMIP low-resolution PRIMAVERA models for 1950-2014, compared to EOBS. All models and observations re-gridded to the HadGEM3-GC31-LM model grid. Negative values indicate areas where modelled numbers of frost days are smaller than those observed.

The largest number of frost days in the UK and Ireland is seen in the Grampian mountains of Scotland. Frost days are rarer in Ireland owing to its milder, maritime-influenced climate. The HadGEM3 and the CMCC model underestimate to a greater extent the number of frost days during the historical period while the rest of the models from this group demonstrate regionally specific positive or negative biases (Figure 64). The overall multi-model mean indicates an underestimation of the number of frost days (between 10 and 40 days) over Ireland and most of Great Britain for the historical period.

The high-resolution models demonstrate greater spatial detail in the number of frost days (Figure 65). For instance, the greater number of observed frost days over the high ground in parts of northern England and the Southern Uplands of Scotland is now visible, as well as a better resolution of the Grampian region. While the numbers of frost days are underestimated by the HadGEM3 and the CMCC models, the EC-Earth and the ECMWF models demonstrate an overestimate these numbers. The multi-model mean exhibits slightly different biases compared with the low-resolution models, varying between +10 and up to -30 days for Ireland. Positive multi-model mean biases are seen in the southernmost parts of Ireland, and mostly in the western parts of Scotland.

Bias in annual number of Frost Days, $t_{min} < 0C$ vs EOBS, 1950-2014, AMIP

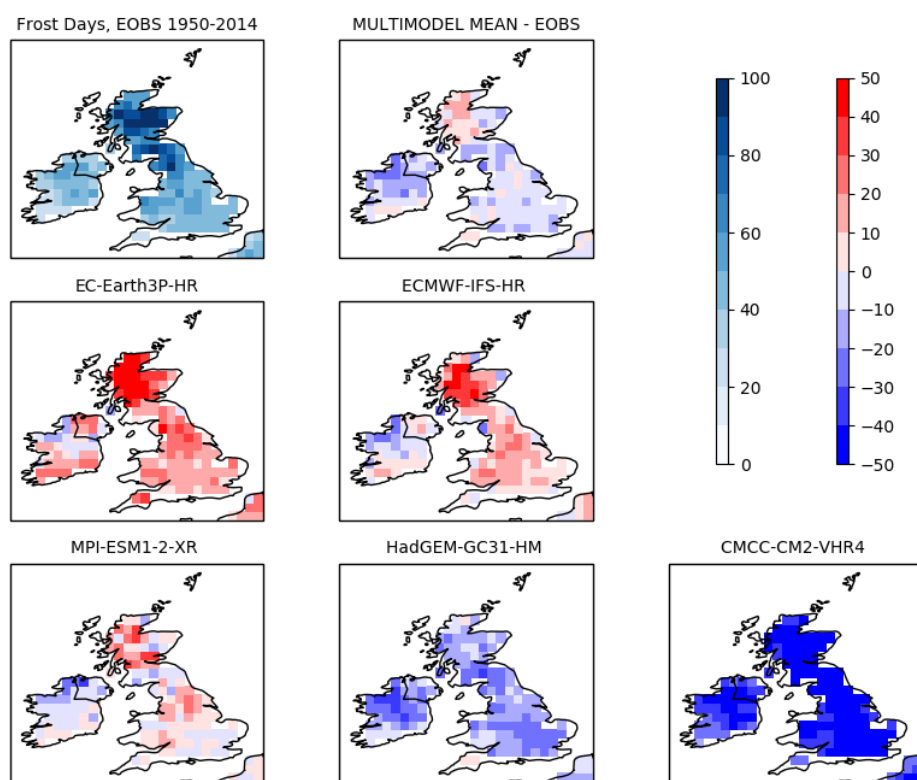


Figure 65 Biases in annual number of Frost Days (FD) as indicated by a set of AMIP high-resolution PRIMAVERA models for 1950-2014, compared with EOBS. All models and observations re-gridded to the MPI-ESM1-2-XR model grid.

3.5.2.3.2 Coupled low- and high-resolution simulations and comparison to the AMIP simulations

The annual numbers of frost days were also calculated from the low- and high-resolution coupled model simulations. The biases in the modelled numbers of frost

days in the low-resolution simulations are shown in Figure 66. The ECMWF model has a large positive bias (overestimation) in the numbers of frost days, whereas the CMCC model has a large negative bias (underestimation). The other three models feature regionally distributed positive and negative biases. The multi-model mean indicates slight overestimation in the southern areas of Ireland and Great Britain and slight underestimation in other areas.

The coupled high-resolution models generally overestimate the numbers of frost days (Figure 67). The exception is the CMCC model, which simulates too few frost days. The multi-model mean indicates a slight overestimation (by about 10 days) over the majority of Great Britain, as well as over the southern areas of Ireland (Figure 67). A larger positive bias (up to 30 days) is seen over Scotland, and slight underestimation over the northern areas of Ireland (up to 20 days).

Bias in annual number of Frost Days, $t_{min} < 0C$ vs EOBS, 1950-2014, Coupled

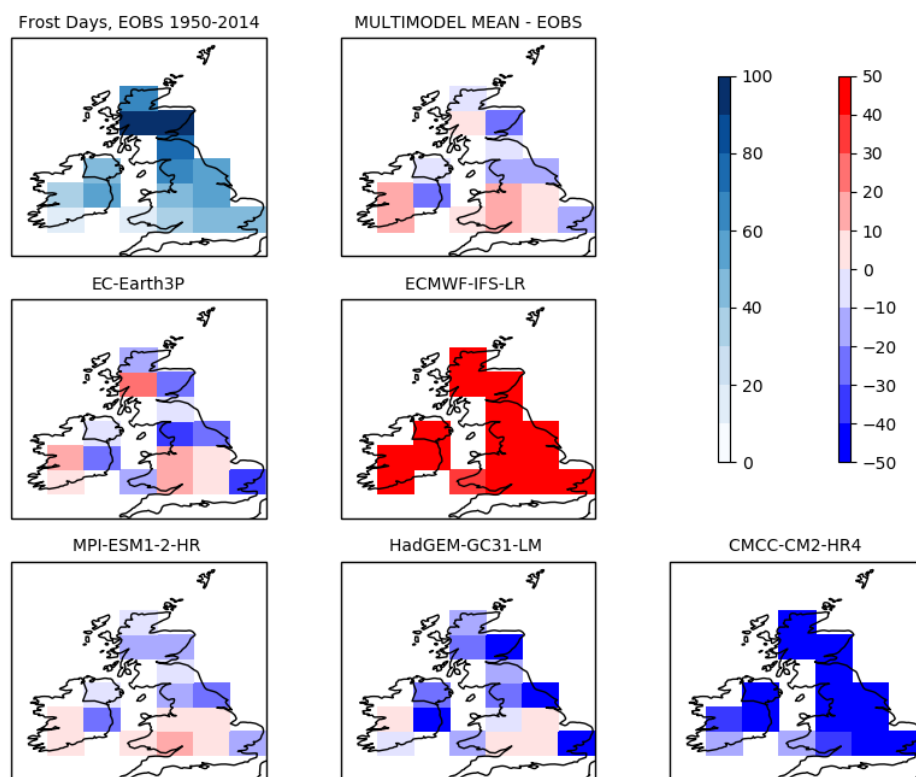


Figure 66 Biases in annual number of Frost Days (FD) as indicated by a set of coupled low-resolution PRIMAVERA models for 1950-2014, compared to EOBS. All models and observations re-gridded to the HadGEM3-GC31-LL model grid.

Bias in annual number of Frost Days, $t_{min} < 0C$ vs EOBS, 1950-2014, Coupled

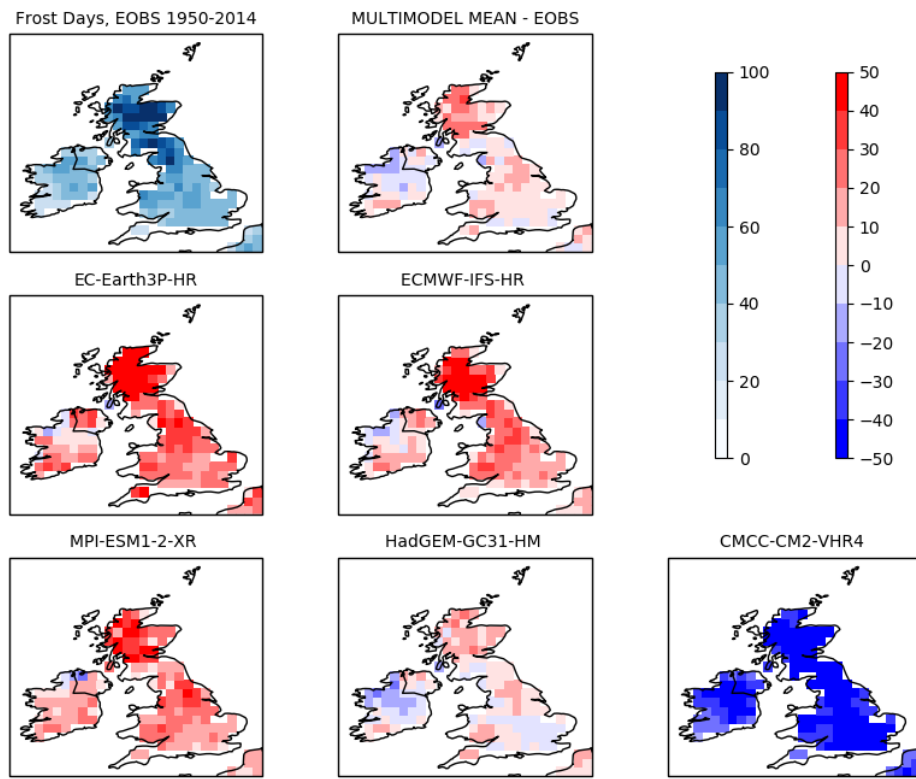


Figure 67 Biases in annual number of Frost Days (FD) as indicated by a set of coupled high-resolution PRIMAVERA models for 1950-2014, compared with EOBS. All models and observations re-gridded to the MPI-ESM1-2-XR model grid.

Figure 68 and Figure 69 show the differences between the absolute AMIP and coupled models biases as compared to the EOBS dataset. The differences are calculated as follows: $|AMIP \text{ biases}| - |coupled \text{ biases}|$ and a positive value (red colour in these maps) indicates an improvement in the coupled models, while a negative value (blue colour in the maps) indicates that the coupled models have larger biases compared to the AMIP simulations.

The results show that, overall, the coupled models have larger biases than the forced simulations (Figure 68). The multi-model mean is affected by the larger biases demonstrated by the ECMWF model, while the rest of the models either indicate improvement as in the case of the HadGEM3 model, or show regional improvements and deteriorations as in the rest of the models, except for the CMCC which demonstrates small deterioration in the coupled simulations.

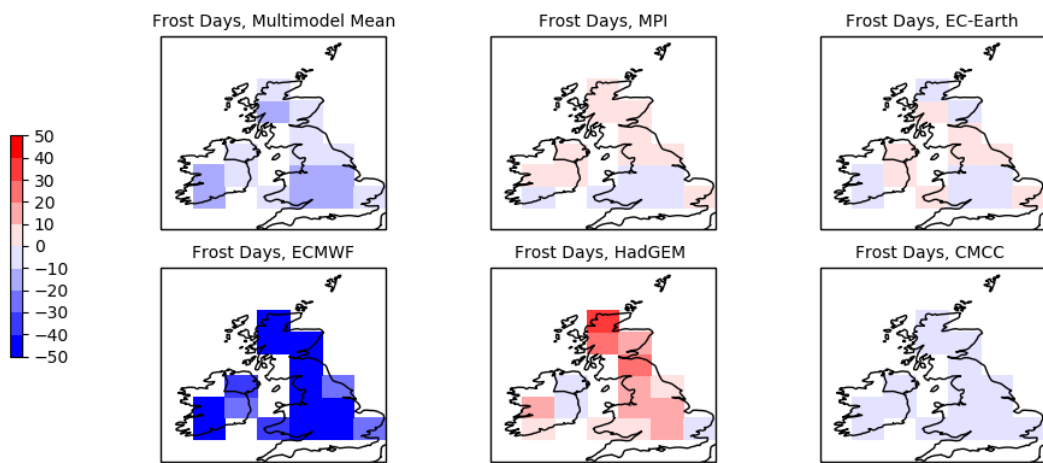


Figure 68 Bias improvement between AMIP and coupled low-resolution simulations for 1950-2014; positive values indicate that the coupled models have smaller biases when compared with EOBS; models re-gridded to HadGEM3-GC31-LL

The high resolution simulations (Figure 69) show that for three of the five models the coupled simulations demonstrate larger biases compared to the forced (AMIP) simulations (MPI, EC-Earth and ECMWF), while for two models the coupled simulations are an improvement in terms of bias in the annual number of frost days compared to EOBS (HadGEM3 and CMCC). The multi-model mean again shows slight deterioration in the representation of that index in the coupled simulations over the British Isles, with the exception of the north-western areas of Ireland where there is slight improvement. The multi-model means calculated from the high-resolution models generally have smaller biases than the low-resolution models.

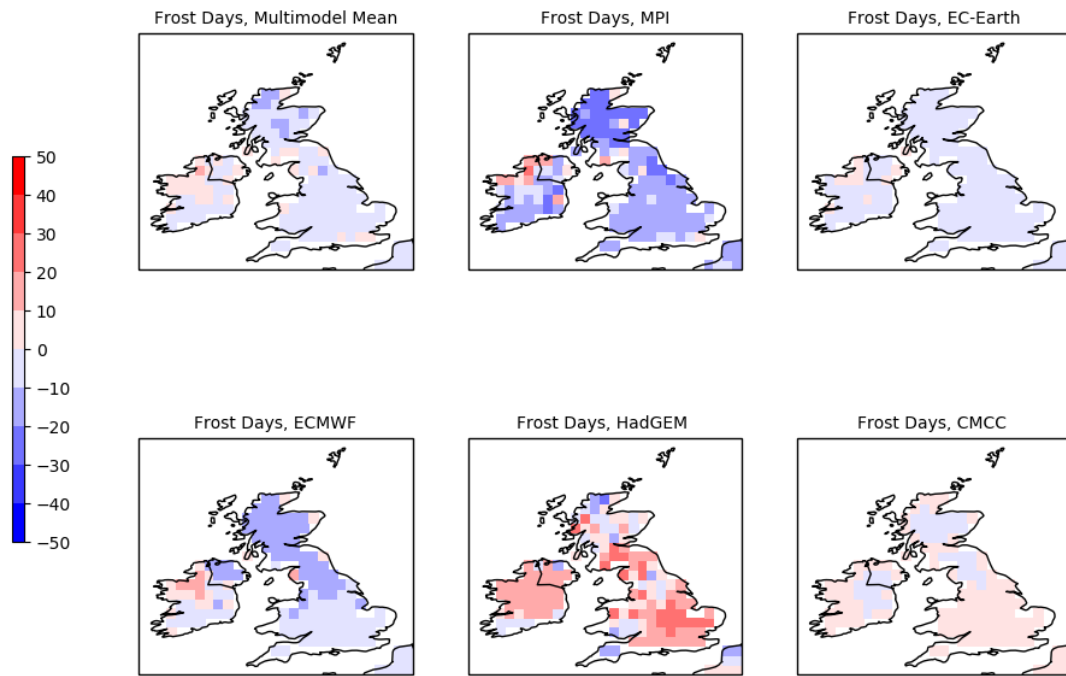


Figure 69 Bias improvement between AMIP and coupled high-resolution simulations for 1950-2014; positive values indicate that the coupled models have smaller biases when compared with EOBS; models re-gridded to HadGEM3-GC31-LL

3.5.2.4 Future projected changes in occurrence of daily minimum temperatures below 0°C (“frost days”) as simulated by the low- and high-resolution PRIMAVERA models

Figure 70 shows how future frost day numbers are projected to change 1980-2014 and 2015-2050, in both the low- and high-resolution models. The top left panel shows the observed annual frequency of frost days during the period 1980-2014. Both of the low- and high-resolution models indicate a decrease of up to 10 days in the number of frost days for the future period (2015-2050) compared to the historical (1980-2014) for Ireland. The decreases projected by the high-resolution models are generally larger than the decreases in the low-resolution models. The exception is the MPI model (bottom panels in Figure 70), which shows more moderate decreases in the high-resolution than in the low-resolution (lighter colours for HR than for LR).

The high-resolution multi-model mean (right-hand column of Figure 70, top panel) depicts almost the entire country as experiencing such a decrease, while the low-

resolution map shows only a limited area of Ireland being affected by a larger decrease of up to 10 days. A reduction of up to 15 frost days is projected over almost all of England, Wales and Scotland. An even greater reduction (of up to 20 days) is evident in central Scotland.

Future changes in Frost Days for 2015-2050

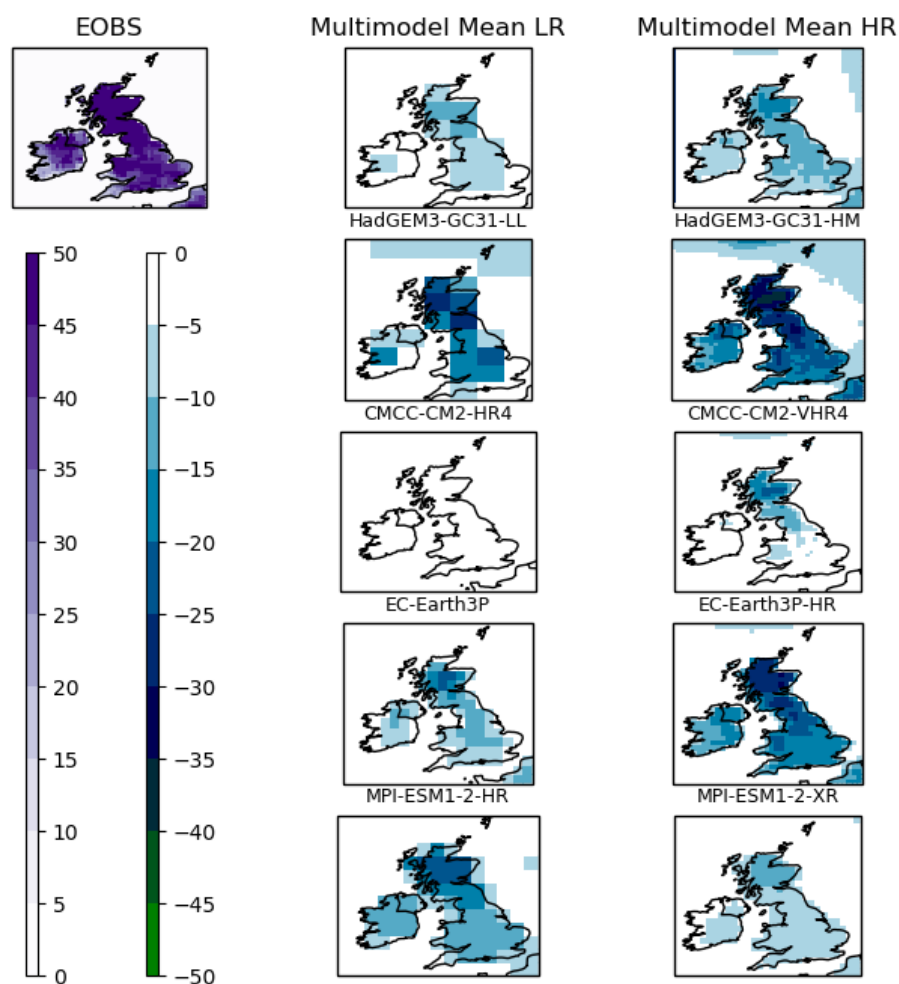


Figure 70 Future changes in annual frequency of Frost Days (2015-2050 minus 1980-2014) for coupled simulations from the low- and high-resolution PRIMAVERA models. The EOBS frost days are calculated for the period 1980-2014.

3.5.2.5 Representation of hot days with maximum temperature $\geq 32^{\circ}\text{C}$ over Europe

The frequency of hot days (daily maximum temperature greater or equal to 32°C (TX32)) in the models was analysed. The threshold 32°C is a useful for surface transport activities and infrastructure, and is one of the thresholds highlighted by Vajda et al. (2011) in their work for Europe. Only the coupled model simulations were analysed, and comparisons with the EOBS data are performed for the historical period, 1950-2014. Projected changes in hot days are calculated for the period 2015-2050 while the historical frequencies are estimated for the 1980-2014 period which allowed for a fairer comparison where the historical and the future period are almost equal-sized.

During the historical period (1950-2014) TX32 values were highest in southern Europe and the Mediterranean region. The analysis indicated that the coupled models generally slightly overestimate the frequency of TX32 in Italy and south-eastern Europe, and underestimate it in Spain, based on the multi-model mean (Figure 71 and Figure 72). The biases are generally greater in the low-resolution coupled models compared to the high-resolution coupled models.

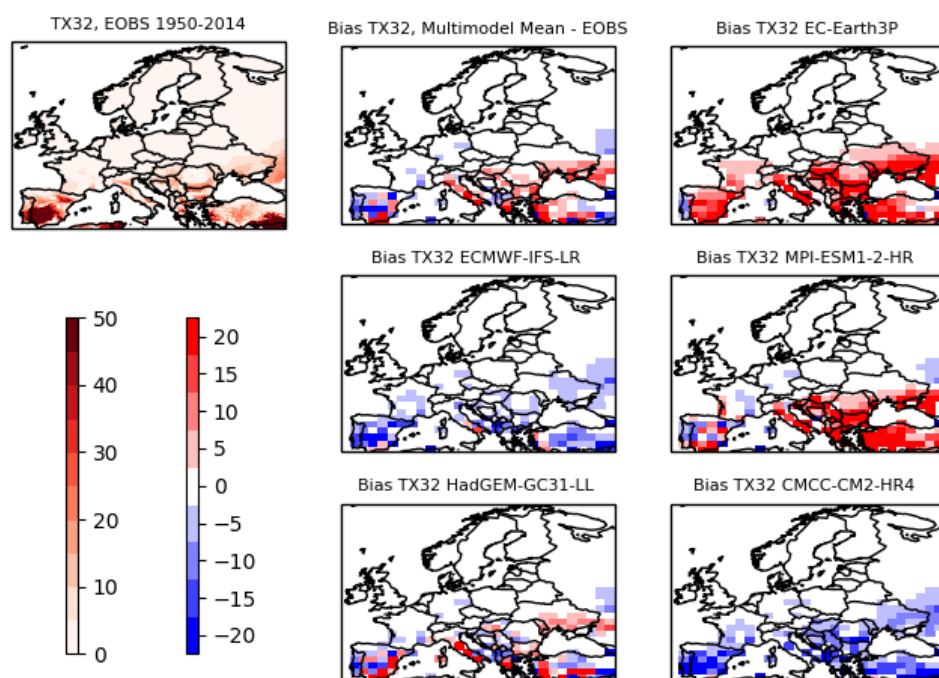


Figure 71 Biases in the frequency of TX32 in PRIMAVERA low-resolution coupled models for 1950-2014 compared with EOBS; Models re-gridded to HadGEM3-GC31-LL grid.

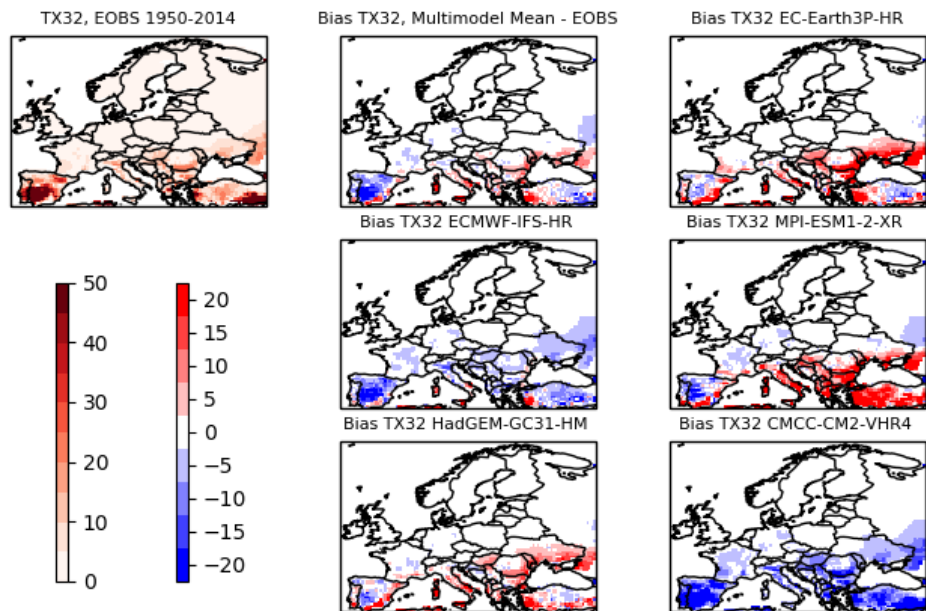


Figure 72 Biases in the frequency of TX32 in PRIMAVERA high-resolution coupled models for 1950-2014 compared with EOBS; Models re-gridded to MPI-ESM1-2-XR grid.

3.5.2.6 Future changes in hot days with maximum temperature $\geq 32^{\circ}\text{C}$ over Europe

Simulations of the future period (2015-2050) are available from four of the low-resolution models. These models project that the annual frequency of hot days would increase, on average, by 20-25 days in southern and south-eastern Europe (Figure 73). The CMCC model generally simulates cooler temperatures, and projects smaller increases in the number of hot days in the future compared to the other three models.

Future changes in TX32 for 2015-2050 Coupled models

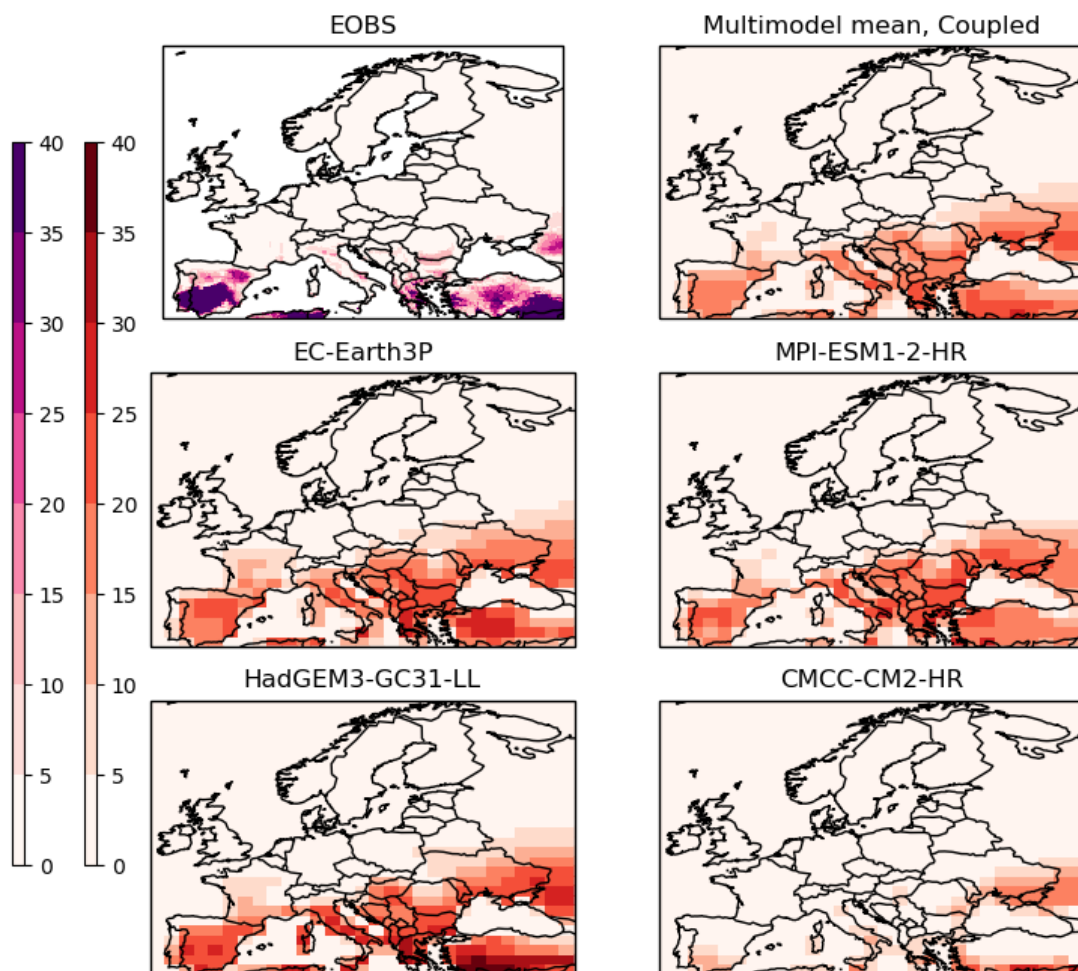


Figure 73 Future changes in frequency of TX32 days as represented by low-resolution PRIMAVERA models, 2015-2050 minus 1980-2014. The EOBS frequency of hot days is also included for comparison (1980-2014)

Changes in the numbers of hot days in the high resolution coupled models were also calculated. Increases in frequency of hot days (between 10 and 30 days) and in the areas affected by such hot days are evident in the EC-Earth, HadGEM3 and MPI models (Figure 74). The CMCC model simulates only small increases for the future period. The high-resolution models demonstrate the importance of resolving orography, with key mountain ranges and highland areas in Southern Europe (e.g. the Pyrenees, Carpathian Mountains, Alps and Massif Central) showing up as regions with, not surprisingly, small or negligible changes in TX32. Both the low- and the high-resolution simulations indicate that areas located further to the north compared to the historical period will be affected by hot days in the future.

Future changes in TX32 for 2015-2050 Coupled models

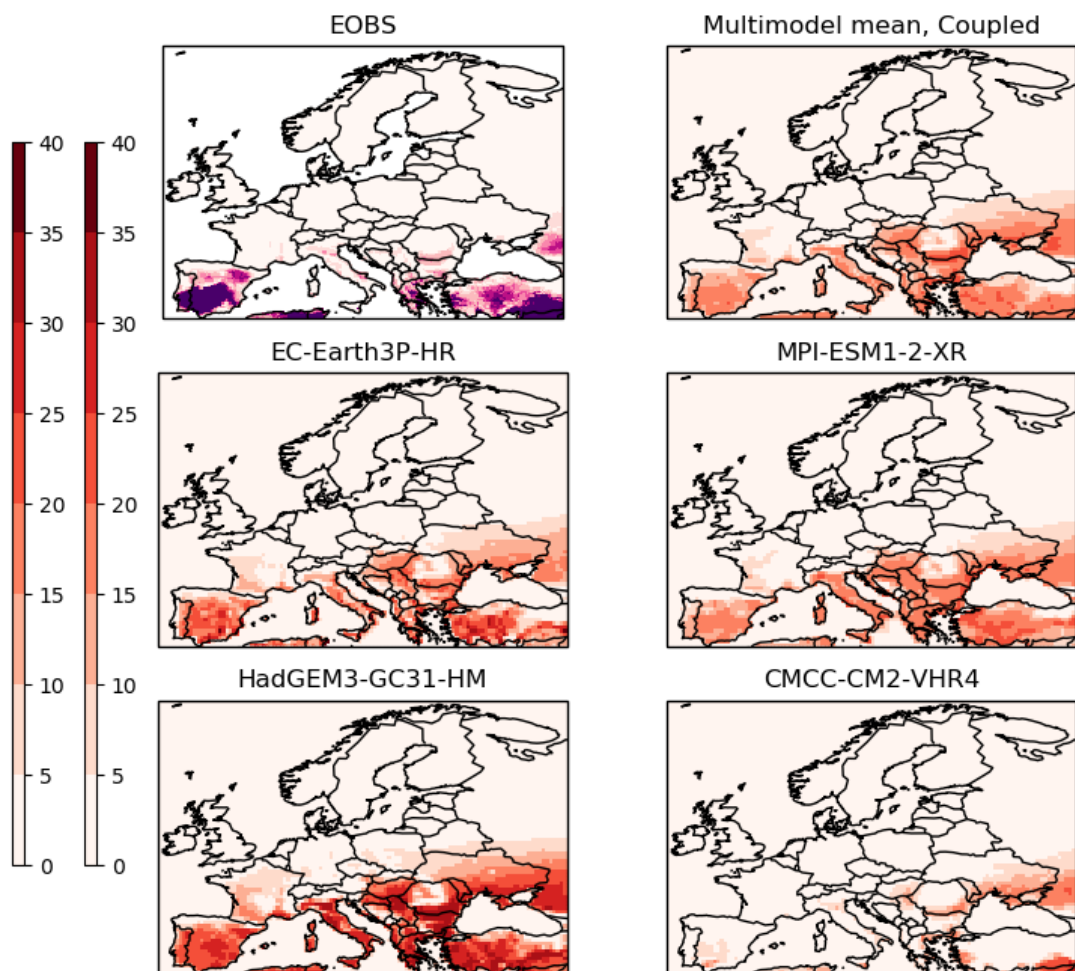


Figure 74 Future changes in frequency of TX32 days as represented by high-resolution PRIMAVERA models, 2015-2050 minus 1980-2014. The EOBS frequency of hot days is also included for comparison (1980-2014)

3.5.2.7 Representation of Summer days (SU) with maximum temperature > 25°C over UK and Ireland

The EOBS data (aggregated to the resolution of the HadGEM3-GC31-LL model) shows that summer days occur, on average, up to 8 days a year during 1950-2014. The low-resolution coupled model simulations generally underestimate the frequency of summer days in the southern UK (Figure 75).

Bias in Summer days, Low res coupled models - EOBS, 1950-2014

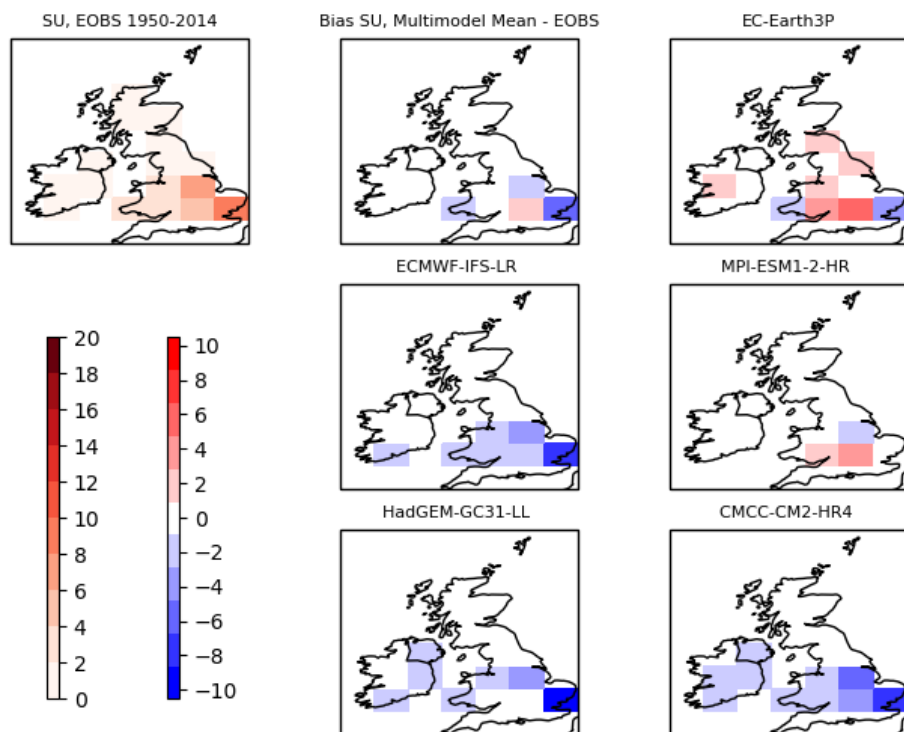


Figure 75 Biases in the frequency of SU in PRIMAVERA low-resolution coupled models for 1950-2014 compared with EOBS; Models re-gridded to HadGEM3-GC31-LL grid.

The high-resolution coupled model simulations also slightly underestimate the frequency of summer days predominantly in southeast England (Figure 76). The EC-Earth model slightly overestimates that frequency.

Bias in Summer days, High res coupled models - EOBS, 1950-2014

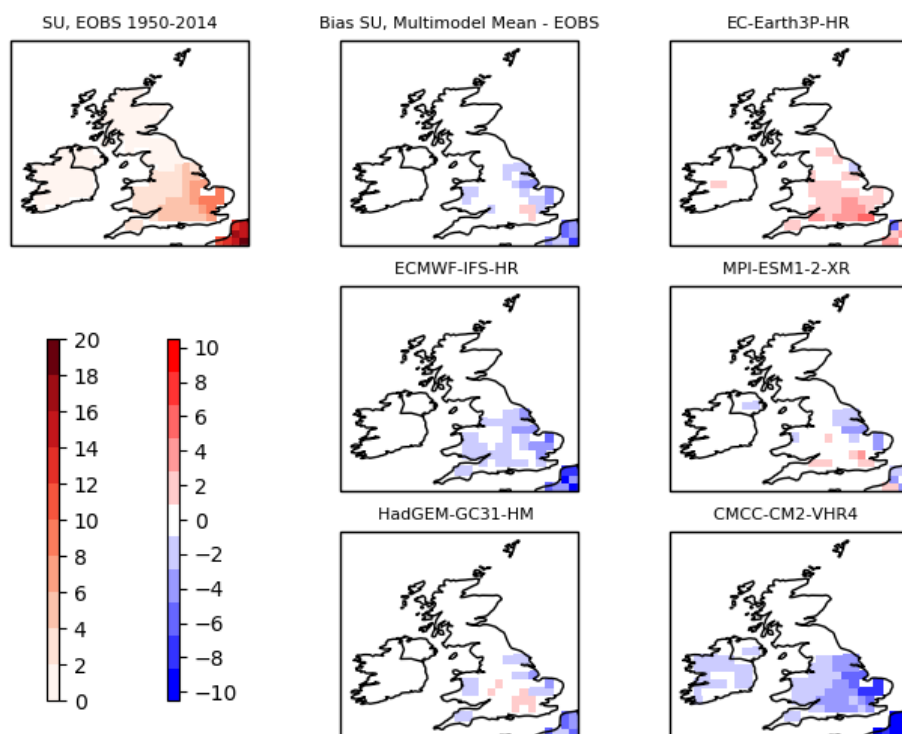


Figure 76 Biases in the frequency of SU in PRIMAVERA high-resolution coupled models for 1950-2014 compared with EOBS; Models re-gridded to MPI-ESM1-2-XR grid.

3.5.2.8 Future changes in Summer days with maximum temperature > 25°C over UK and Ireland

The future changes in this index projected by the low-resolution coupled models are shown in Figure 77, and by the high-resolution models in Figure 78. In the southern areas of England and in Wales, the annual frequency of summer days is projected to increase by up to 8 days in the low-resolution simulations (Figure 77) and by up to 10 days in the high-resolution simulations (Figure 78). The MPI and CMCC models project somewhat smaller increases in the frequency of summer days, whereas the EC-Earth and particularly HadGEM3 project large increases.

Future changes in SU for 2015-2050 Coupled models

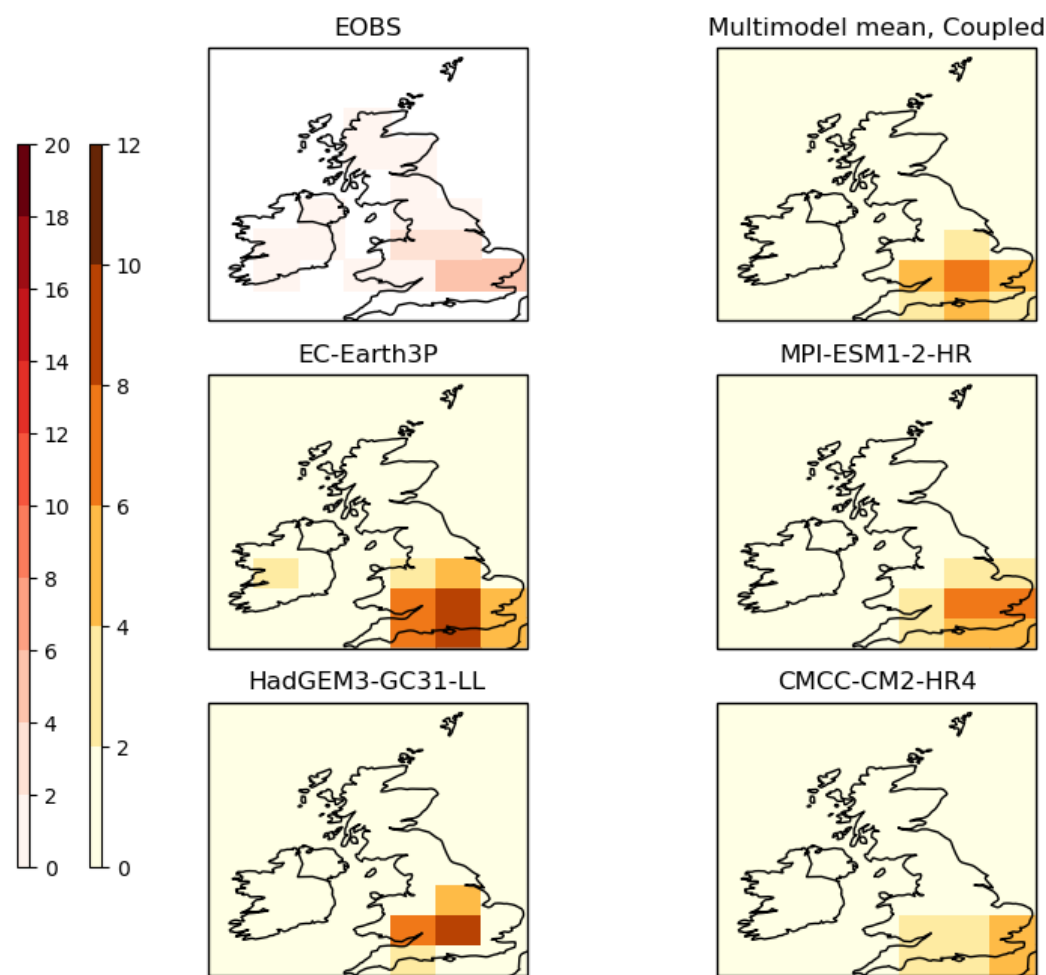


Figure 77 Future changes in frequency of SU as represented by low-resolution PRIMAVERA models, 2015-2050 minus 1980-2014; The EOBS frequency of these days is also included for comparison (1980-2014)

Future changes in SU for 2015-2050 Coupled models

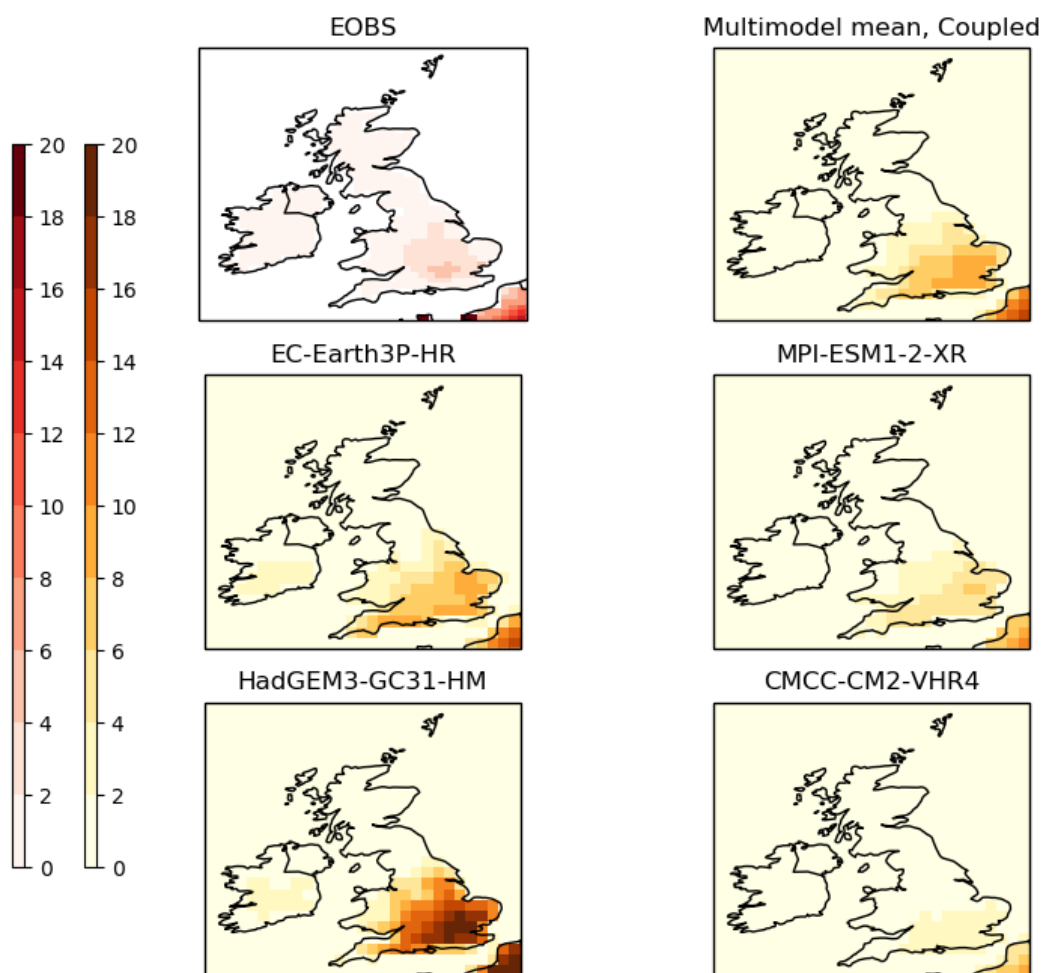


Figure 78 Future changes in frequency of SU as represented by high-resolution PRIMAVERA models, 2015-2050 minus 1980-2014; The EOBS frequency of these days is also included for comparison (1980-2014)

3.5.3 Benefits of PRIMAVERA

The occurrence of extreme temperature conditions is often linked to the relative positions of different large-scale weather systems (areas of relatively high or low pressure) controlling the flow of comparatively hot or cold air masses over the location in question. Evaluating the ability of the climate models to represent these systems could help establish the credibility of the model data regarding extreme heat

and cold events governed by these weather systems. High-pressure blocking systems which impede the normal west to east air flow in the mid-latitudes may persist for many days over some areas, and can lead to very impactful weather episodes. These events are of special interest in relation to hot and cold extreme temperature episodes. PRIMAVERA colleagues have explored the representation of various characteristics of blocking in (a) PRIMAVERA (CMIP6) models vs. CMIP5, and in (b) the high-resolution vs. low resolution PRIMAVERA models (Schiemann et al. 2020).

They found a clear improvement in simulated blocking in the CMIP6 model ensemble compared with CMIP5:

- The improvement is robust, occurring in both the Euro-Atlantic and Pacific regions; in winter and summer; for both the frequency and persistence of blocking; and for two different measures of blocking
- The improvement is sizeable (for example, a bias in one DJF blocking metric in CMIP5 models of -33% was reduced to -18% in the CMIP6 models)

With regard to the relative performance of the PRIMAVERA low-resolution and high-resolution models for blocking:

- An improvement in the simulation of blocking frequency was observed for the Atlantic region in both summer and winter, and for the Pacific region in summer
- This improvement was predominantly seen in the spatial pattern of blocking frequency; there was no evidence for the improved simulation of blocking persistence
- These results were considered conservative, as models are not re-tuned at higher resolution

From this they concluded that:

- Their results are consistent with previous findings that the successful simulation of blocking in climate models depends on a range of factors and their interactions
- Increased horizontal atmospheric resolution, from ~100km to ~20km, is one of these factors, and benefits the simulation of blocking
- An increase in resolution alone will not completely remedy blocking biases in models, notably in the persistence of blocking events
- The most recent generation of GCMs continues to be affected by long-standing blocking biases, albeit at a smaller magnitude in CMIP6 models than in CMIP5 models – implying that, overall, CMIP6 models strike a better balance of the different factors affecting blocking simulation

These findings are relevant for the representation of extreme low and high temperatures, as their occurrence in the UK and Ireland is contingent on adequate

representation of (a) blocking generally, and (b) its persistence (the most extreme temperatures require a build-up of heat or cold). Since there is no improvement in the simulation of persistence, it could be that PRIMAVERA models do not improve the representation of hot or cold spells, but we have not explored this in detail, having evaluated only daily temperature exceedance in this work, not the spell duration thereof.

3.5.4 Consequence on sector

The balance between high and low temperature extremes is relevant for the management of the associated transport risks. For example, in the UK, salt spreaders – normally seen in action only in cold weather – are sometimes used during extremely hot weather to spread material (usually a dust made from stone) on the roads, to help with surface melting³ by stabilising the bitumen. It is possible that in future this unusual use of salt spreaders could increase even if their use in winter becomes less frequent. In any case, frost days are projected to continue to occur into the future in the UK and Ireland, so some size of salt spreading fleet will continue to be needed.

Similarly, the relative risks of rail buckling in hot weather vs. rail breaks/cracks in cold weather is managed by engineering the “stress-free temperature” (SFT) of the rail. This is the temperature at which the rail is under neither tensile nor compressive stress. In other countries, different rail stressing regimes are used depending on the frequency of cold vs. hot conditions (Dobney et al. 2009, 2010; Nemry and Demirel 2012, Palin et al. 2013), with different countries using different SFTs (Nemry and Demirel 2012).

Finally, transport providers will need to consider behavioural changes that in turn influence transport demand and result from the occurrence of heat waves and cold spells. For example, warmer conditions tend to result in increased demand for leisure travel, and cycling and walking can be less popular in colder conditions as people switch to the safer and/or warmer option of cars or public transport.

3.5.5 Caveats

3.5.5.1 Representation of blocking

³ e.g. <https://www.bbc.co.uk/news/uk-england-leeds-44611800>

As discussed above in Sections 3.5.2.1 and 3.5.3, there is improvement in some of the aspects of the representation of blocking in PRIMAVERA models, but no improvement in other aspects, particularly persistence.

3.5.5.2 Representation of trends in winter and summer averages and extremes

Squintu et al. (2020) analysed atmosphere-only simulations at low- and high-resolution from several PRIMAVERA models from the following modelling centres: CMCC, CNRM, EC-Earth Consortium, ECMWF, MOHC and MPI. They evaluated the representation of winter and summer average temperatures, trends in these seasonal averages and also trends in some extremes (TN10p – % of days with daily minimum temperatures below the 10th percentile in winter, TX90p – % of days with daily maximum temperatures above the 90th percentile in summer) over the 1970-2014 period in these AMIP simulations. The model simulations were compared with gridded temperatures in the EOBS – homogenized dataset.

The authors established that the AMIP model-simulated trends in averages and extremes in winter are “too warm over western Europe and too cold over eastern Europe”, which means that the models do not simulate as many cold winter extremes as observed over western Europe and simulate a much greater number of cold winter extremes over eastern Europe compared to the EOBS dataset. These results correspond well to our findings of general underestimation of the number of frost days over the UK and Ireland in the AMIP low- and high-resolution simulations.

In addition, the AMIP models tended to underestimate the summer maximum temperature averages in northern Europe, while overestimating them in the Mediterranean. Furthermore, the model simulated trends were too warm in the north-west (leading to greater high temperature extremes) and too cold in the south-east areas of Europe (underestimating the high temperature extremes). Comparing the results from PRIMAVERA to CMIP5 the authors found that the new high-resolution models demonstrate a slight improvement in the simulation of winter minimum temperatures but no such improvement in the simulation of summer maximum temperatures.

3.5.6 Key points

- Extreme temperatures – both hot and cold – have impacts for the transport sector.
- The occurrence of these conditions is often linked to the relative positions of different large-scale weather systems (areas of relatively high or low

pressure) controlling the flow of comparatively hot or cold air masses over the location in question. For example, blocking high-pressure systems which impede the normal west to east air flow in the mid-latitudes and may persist for a long time over some areas can lead to very impactful weather episodes and are of special interest in relation to hot and cold extreme events.

- There are improvements in the representation of some aspects of blocking in the PRIMAVERA models compared with CMIP5, and in the high-resolution PRIMAVERA models compared with the low-resolution PRIMAVERA models. However, there is no improvement in the representation of blocking persistence, which is likely to be important for the occurrence of extreme temperatures within prolonged hot or cold spells.
- **Frost days in the UK and Ireland** – in general, the low- and high-resolution **AMIP** simulations underestimate the frequency of frost days compared to the EOBS data for 1950-2014, while their counterpart **coupled** models show a slight underestimation only in the north in the low-resolution simulations. The rest of the areas for the low-, and the entire islands for the high-resolution simulations, display an overestimation of the frequency of frost days.
- The general underestimation of the frequency of frost days (an absolute threshold extreme) by the **AMIP** simulations during the historical period is corroborated by the findings of Squintu et al (2020) using a percentile metric (TN10p), where they found that these simulations display warmer trends in the winter extremes leading to simulation of not as many low extremes as in the EOBS dataset.
- The comparison of the biases between the **AMIP** and the **coupled** models showed that for both the low- and high-resolution simulations the coupled models suffer from slightly larger biases for this index.
- Both sets of low- and high-resolution **coupled** models indicate a projected decrease of up to 15 days in the number of frost days for the future period (2015-2050) compared to the historical (1980-2014) for Ireland and a much greater decrease (between 5 and 35 days in the high-resolution simulations) for Scotland and the northern areas of England.
- **Hot days (TX32) across Europe** – The **coupled** models generally slightly overestimate the frequency of TX32 in Italy and south-eastern Europe and underestimate it in Spain based on the multi-model mean. The biases are greater in the low-resolution coupled models compared to the high-resolution coupled models. Both the low- and high-resolution models indicate an increase (between 10 and 30 days) in the frequency of hot days during 2015-2050, especially in southern and south-eastern Europe.
- **Summer days (SU) in the UK and Ireland** – During the historical period (1950-2014), summer days were experienced, on average, up to 8 days a year in the United Kingdom as represented in the EOBS dataset. The multi-model mean biases indicate that the frequency of these days is generally

underestimated by the low- and high-resolution PRIMAVERA **coupled** model simulations; The future changes in this index show that, in the southern areas of England and in Wales, the frequency of summer days will increase by up to 8 days a year on average in the low-resolution simulations and by up to 10 days a year in the high-resolution simulations.

4 Lessons Learnt

A central concern of this deliverable has been to construct scientific narratives or storylines linking physical climate processes and PRIMAVERA model outputs to specific use cases and sectors. The specific findings for each use-case are varied and sector-dependent and are thus not recapitulated here. The following general observations can, however, be drawn:

- In several cases, there are strong suggestions that enhanced horizontal resolution may have great value for the simulation of climate phenomena relevant to Europe. Improved representation of blocking and cyclones (tropical, extratropical and post-tropical translation) may, for example, offer significant benefits to users of climate data, particularly where the detailed simulation of meteorological phenomena and their compound impacts is critical such as in insurance, energy and transport. The availability of high-frequency, high-resolution output data (particularly pertaining to surface meteorological variables) is often highly valued by many of these users and should therefore be considered as a high priority output in future modelling exercises.
- There are intriguing suggestions that increased horizontal resolution may itself have consequences for European climate projections. For example, the more rapid slowdown of the AMOC in higher resolution models associated with changes in drought severity (Section 3.1). Set against this, however, is the recurrent difficulty of detecting relatively modest “signals” (associated with climate change and/or the effects of resolution) against very high levels of “noise” associated with inter-model spread (e.g., different model responses to identical climate forcings) and natural climate variability. This suggests that increased ensemble size and/or longer simulations are likely to remain critical for climate impact assessment for some time.

On a project level, it is noted that the PRIMAVERA climate model “output” data (i.e., the Stream 1 and 2 simulations) was itself an “input” from the WP10/11 perspective of constructing end-user use-cases and risk assessment. Delays in the availability of the PRIMAVERA simulations – associated with delayed formulation of suitable climate forcing scenarios by groups external to the PRIMAVERA community - therefore impacted on the timing of the user case-study analyses and, in particular, limited the opportunity for a more inclusive and comprehensive engagement with users. This risk (the delayed climate forcing scenarios) was not identified at the start of the project, and suitable work-arounds for WP10/11 analyses were difficult to formulate (in effect, WP10/11 was forced to rely on non-PRIMAVERA climate datasets for a much longer period than anticipated). In future projects, more time

could be allowed for the climate data production process (i.e., further offsetting the end-user engagement work which requires the climate model output) or else giving higher priority to ensuring the timely delivery of the climate model outputs for onward user-engagement activities (even if this comes at the cost of using less-than-ideal climate forcing inputs).

The storylines which are at the heart of this Deliverable are targeted at specific sectors and the impact of the simulations of future climate on these sectors is typically assessed by onward translation through “impact models”. However, the running of impact models and the feeding-in of large data volumes from the PRIMAVERA simulations requires a considerable effort for both the climate data producer (here, the PRIMAVERA team) and the climate data user (here, organisations and groups within the impacted sector). In the PRIMAVERA project, sectoral users are not directly involved in the consortium and, as a consequence, any effort on the side of the sectoral users for this Deliverable is not covered financially. This therefore limits the extent to which the data can be taken on into impacts-oriented use cases.

Somewhat related to this, the diverse requests from the initial user-engagement phase (outlined in Deliverable D10.1) arguably led to some dilution of project resources by attempting to respond to too many different use-cases (i.e., producing research and output for too many different interested parties). Establishing a small number of core case studies (either as ‘champion users’ or more generalised ‘representative sectoral applications’) earlier in the project may help to better focus user engagement and project resources, allowing more rapid research progress and, ultimately, better tailoring of output to sectoral needs.

5 Links Built

5.1 Outside PRIMAVERA

An important effort of WP10 and 11 was enabling knowledge coproduction, by: (i) engaging stakeholders through knowledge sharing using diverse communication channels, such as the UIP, factsheets and primavera mailing list updates; (ii) involving users in knowledge exchange, through surveys, interviews, meetings and webinars; and (iii) knowledge co-development through close collaboration between users and WP10/11 impact researchers. The latter developed strong links and true partnerships between scientists and the user community. Such a strong collaboration resulted in new shared knowledge and capacities. The project scientists received valuable feedback about the usability of project's results, while the users were supported to apply this novel knowledge in their sectoral and decision-making contexts. The trust is also built among the project scientists from other WPs, for some of whom this was the first closer interaction with the user community. The new partnerships will continue after the project ends, bringing scientific knowledge ever closer to real-world decision making processes.

Other, more specific links include:

- Section 3.1 contributes to the KNMI Climate Scenario's for 2023.
- Observational data on temperature and precipitation, used in section 3.1, has been compiled in Copernicus Climate Change Service contract C3S_311a_Lot4 and the impact information was compiled under the ERA4CS project INDECIS.
- Results from Section 3.2.2 were presented at GEOMAR (Germany).
- Section 3.2.4 liaised with the Windstorm Information Servce (WISC, a Copernicus Climate Change Service) to ensure compatibility between these projects. Strong links with several (re)insurance companies/brokers were built which will continue after the project. One company has agreed to contribute to an academic paper describing the event set production and analysis (in prep). It is also expected that the insurance event set work described in Section 3.2.4 will be presented to the insurance sector as a webinar in the final stages of the project.
- Section 3.3 motivated the convening of an international virtual workshop “Next Generation Challenges in Energy-Climate modelling” (22nd – 23rd June 2020; hosted by UREAD). Approximately 70-80 participants took part each day including attendees from across Europe, Australia, and North America. Participants were predominantly from academia (though with several industrial researchers present), attracting a strong presence from “energy science” research. Many of the links will be continued (including exploitation

of legacy PRIMAVERA high-frequency surface climate output datasets) beyond the end of the project.

- The engagement activity reported in Section 3.5 enabled the Met Office to build links with TII and representatives of the Irish Government, and to strengthen existing links with Met Éireann.

5.2 Between PRIMAVERA workpackages

- WP10 and WP11 are closely connected. The WP10-11 link is bi-directional: following D10.2 and D10.3, the scientific studies undertaken for this deliverable aim to address at least some of the use cases from D10.1, which were, in turn, compiled based on methods and information from the WP11 interviews/survey (D11.6). These user cases informed the priorities for cross-partner collaborations on relevant topics and helped define the scope of this deliverable report.
- Section 3.2.2 had strong links with WP6 (simulations used were performed as part of that WP), WP1 (TCs were detected and tracked using the vortex tracker integrated in the ESMValTool infrastructure) and WP2 (impact of resolution on IKE).
- Section 3.2.4 used the ETC tracks provided by WP1. This work also has links with WP2 (impact of resolution on North Atlantic climate system processes).
- Section 3.5 relied on results from the analysis performed by Paula Gonzalez in relation to blocking and low temperature extremes, as well as on results from the work of Antonello Squintu and Gerard van der Schrier who focused on the representation of low and high temperature extremes in the AMIP simulations of the PRIMAVERA models. In addition, this deliverable benefited from the work of Reinhard Schiemann and colleagues from WP2 on representation of blocking by the high- and low-resolution PRIMAVERA models.
- WP11 intends to give at least one further user-focused webinar, based on the content of D10.4. The work described in D10.4 has also contributed to the reporting of end-user evaluation of PRIMAVERA in D11.5 and D11.7 through the use of existing user relationships, and the development of new ones, in constructing the storylines presented.

6 References

Archer, C. L., Colle, B. A., Delle Monache, L., Dvorak, M. J., Lundquist, J., Bailey, B. H., ... & Lee, S. (2014). Meteorology for coastal/offshore wind energy in the United States: Recommendations and research needs for the next 10 years. *Bulletin of the American Meteorological Society*, 95(4), 515-519.

Baatsen, M. et al., 2015: Severe Autumn storms in future Western Europe with a warmer Atlantic Ocean. *Climate Dynamics* **45**, 949-964

Baker, A. J. et al., 2020: Historical variability and lifecycles of North Atlantic midlatitude cyclones originating in the tropics. Under review, *Geophysical Research Letters*.

Baker, A. J., Schiemann, R., Hodges, K. I., Demory, M. E., Mizielinski, M. S., Roberts, M. J., ... & Vidale, P. L. (2019). Enhanced Climate Change Response of Wintertime North Atlantic Circulation, Cyclonic Activity, and Precipitation in a 25-km-Resolution Global Atmospheric Model. *Journal of Climate*, 32(22), 7763-7781.

Bao, S, D Stark and L Bernadet (2013) USERS' GUIDE for the Community release of the GFDL Vortex Tracker.
https://dtcenter.org/HurrWRF/users/downloads/Tracker_releases/V3.5b/stand_alone_tracker_UG_v3.5b.pdf

Bell, G. D., Halpert, M. S., Schnell, R. C., Higgins, R. W., Lawrimore, J., Kousky, V. E., Tinker, R., Thiaw, W., Chelliah, M. & Artusa, A. (2000): Climate assessment for 1999. *Bulletin of the American Meteorological Society*, 81.6, S1-S50.

Bieli, M. et al., 2019: A Global Climatology of Extratropical Transition. Part I: Characteristics across Basins. *Journal of Climate* **32**, 3557-3582

Blake, E. S. et al., 2013: Hurricane Sandy (AL182012). *National Hurricane Center Tropical Cyclone Report*, https://www.nhc.noaa.gov/data/tcr/AL182012_Sandy.pdf

Bloomfield, H. C., Brayshaw, D. J., Shaffrey, L. C., Coker, P. J., & Thornton, H. E. (2018). The changing sensitivity of power systems to meteorological drivers: a case study of Great Britain. *Environmental Research Letters*, 13(5), 054028.

Cannon, D. J., Brayshaw, D. J., Methven, J., Coker, P. J., & Lenaghan, D. (2015). Using reanalysis data to quantify extreme wind power generation statistics: A 33 year case study in Great Britain. *Renewable Energy*, 75, 767-778.

Cherchi, A., Ambrizzi, T., Behera, S., Freitas, A. C. V., Morioka, Y., & Zhou, T. (2018). The response of subtropical highs to climate change. *Current Climate Change Reports*, 4(4), 371-382.

Collins, M., R. Knutti, J. Arblaster, J.-L. Dufresne, T. Fichefet, P. Friedlingstein, X. Gao, W.J. Gutowski, T. Johns, G. Krinner, M. Shongwe, C. Tebaldi, A.J. Weaver and M. Wehner, 2013: Long-term Climate Change: Projections, Commitments and Irreversibility. In: Climate Change 2013: The Physical Science Basis. Contribution of Working Group I to the Fifth Assessment Report of the Intergovernmental Panel on Climate Change [Stocker, T.F., D. Qin, G.-K. Plattner, M. Tignor, S.K. Allen, J. Boschung, A. Nauels, Y. Xia, V. Bex and P.M. Midgley (eds.)]. Cambridge University Press, Cambridge, United Kingdom and New York, NY, USA.

Copernicus Climate Change Service, 2017: ERA5: Fifth generation of ECMWF atmospheric reanalyses of the global climate.

Cornes, R., G. van der Schrier, E.J.M. van den Besselaar, and P.D. Jones. 2018: An Ensemble Version of the E-OBS Temperature and Precipitation Datasets, *J. Geophys. Res. Atmos.*, 123. doi:10.1029/2017JD028200.

Craig, M. T., Carreño, I. L., Rossol, M., Hodge, B. M., & Brancucci, C. (2019). Effects on power system operations of potential changes in wind and solar generation potential under climate change. *Environmental Research Letters*, 14(3), 034014.

D'Andrea, F. & Davini P. (2020) Northern Hemisphere atmospheric blocking simulation in present and future climate. EGU General Assembly. <https://doi.org/10.5194/egusphere-egu2020-18294>.

Dee, D. P., Uppala, S. M., Simmons, A. J., Berrisford, P., Poli, P., Kobayashi, S., ... & Bechtold, P. (2011). The ERA-Interim reanalysis: Configuration and performance of the data assimilation system. *Quarterly Journal of the royal meteorological society*, 137(656), 553-597.

Dekker, M. M. et al., 2018: Characteristics and development of European cyclones with tropical origin in reanalysis data. *Climate Dynamics* **50**, 445-455.

Dobney K, Baker CJ, Quinn AD, Chapman L (2009) Quantifying the effects of high summer temperatures due to climate change on buckling and rail related delays in south-east United Kingdom. *Meteorological Applications*, 16, 245–251.

Dobney K, Baker C, Chapman L, Quinn AD (2010) The future cost to the United Kingdom's railway network of heat-related delays and buckles caused by the predicted increase in high summer temperatures owing to climate change. *Proceedings of the Institution of Mechanical Engineers Part F – Journal of Rail and Rapid Transit*, 224, 25–34.

Donelan, M., Haus, B. K., Reul, N., Plant, W., Stiassnie, M., Gruber, H. C., Brown, O. & Saltzman, E. (2004): On the limiting aerodynamic roughness of the ocean in very strong winds. *Geophysical Research Letters*, 31.18.

Emanuel K (2005): Increasing destructiveness of tropical cyclones over the past 30 years. *Nature*, 436.7051, 686-688.

Emanuel, K. (2017). Assessing the present and future probability of Hurricane Harvey's rainfall. *Proceedings of the National Academy of Sciences*, 114(48), 12681-12684.

European Commission. The European Green Deal. (2019) https://ec.europa.eu/info/strategy/priorities-2019-2024/european-green-deal_en

Evans, C. et al., 2017: The Extratropical Transition of Tropical Cyclones. Part I: Cyclone Evolution and Direct Impacts. *Monthly Weather Review* **145**, 4317-4344

Fabiano, F., Christensen, H.M., Strommen, K. et al. (2020) Euro-Atlantic weather Regimes in the PRIMAVERA coupled climate simulations: impact of resolution and mean state biases on model performance. *Climate Dynamics*. <https://doi.org/10.1007/s00382-020-05271-w>

Gao, J., Minobe, S., Roberts, M. J., Haarsma, R. J., Putrasahan, D., Roberts, C. D., ... & Vidale, P. L. (2020). Influence of model resolution on bomb cyclones revealed by HighResMIP-PRIMAVERA simulations. *Environmental Research Letters*.

Gonzalez, P. L., Brayshaw, D. J., & Zappa, G. (2019). The contribution of North Atlantic atmospheric circulation shifts to future wind speed projections for wind power over Europe. *Climate Dynamics*, 53(7-8), 4095-4113.

Grams, C. M., Beerli, R., Pfenninger, S., Staffell, I., & Wernli, H. (2017). Balancing Europe's wind-power output through spatial deployment informed by weather regimes. *Nature climate change*, 7(8), 557-562.

Haarsma, R. J. et al., 2013: More hurricanes to hit western Europe due to global warming. *Geophysical Research Letters* **40**, 1783-1788

Hahmann, A. N., Peña, A., Pryor, S.C. ,& Luzia, G. (2020). Future wind energy resources in the North Sea as predicted by CMIP6 models. EGU General Assembly. <https://doi.org/10.5194/egusphere-equ2020-9093>

Hart, R. E., 2003: A Cyclone Phase Space Derived from Thermal Wind and Thermal Asymmetry. *Monthly Weather Review* **131**, 585-616

Hart, R. E., and J. L. Evans, 2001: A Climatology of the Extratropical Transition of Atlantic Tropical Cyclones. *Journal of Climate* **14**, 546-564

Haylock, M., N. Hofstra, A. M. G. Klein Tank, E. J. Klok, P. D. Jones, M. New (2008), A European daily high-resolution gridded dataset of surface temperature, precipitation and sea-level pressure, *J. Geophys.Res.*, 113, D20119, doi:10.1029/2008JD010201

Hodges, K. I., 1995: Feature Tracking on the Unit Sphere. *Monthly Weather Review* **123**, 3458-3465

Hodges, K. I., 1999: Adaptive Constraints for Feature Tracking. *Monthly Weather Review* **127**, 1362-1373

Hodges, K. I. et al., 2017: How Well Are Tropical Cyclones Represented in Reanalysis Datasets? *Journal of Climate* **30**, 5243-5264

Jones, S. C. et al., 2003: The Extratropical Transition of Tropical Cyclones: Forecast Challenges, Current Understanding, and Future Directions. *Weather and Forecasting* **18**, 1052-1092.

Kantha, L. (2006): Time to replace the Saffir-Simpson hurricane scale? *Eos, Transactions American Geophysical Union*, 87.1, 3-6.

Karnauskas, K. B., Lundquist, J. K., & Zhang, L. (2018). Southward shift of the global wind energy resource under high carbon dioxide emissions. *Nature Geoscience*, 11(1), 38-43.

Keller, J. H. et al., 2019: The Extratropical Transition of Tropical Cyclones. Part II: Interaction with the Midlatitude Flow, Downstream Impacts, and Implications for Predictability. *Monthly Weather Review* **147**, 1077-1106

Klawa, M. and Ulbrich, U., 2003: A model for the estimation of storm losses and the identification of severe winter storms in Germany, *Nat. Hazards Earth Syst. Sci.*, **3**, 725–732, <https://doi.org/10.5194/nhess-3-725-2003>

Knutson, T. R. et al, 2015. Global projections of intense tropical cyclone activity for the late twenty-first century from dynamical downscaling of CMIP5/RCP4.5 scenarios. *J. Clim.* **28**, 7203–7224.

Kobayashi, S. et al., 2015: The JRA-55 Reanalysis: General Specifications and Basic Characteristics. *Journal of the Meteorological Society of Japan. Ser. II* **93**, 5-48.

Kozar, M. E. & Misra, V. (2019): Integrated Kinetic Energy in North Atlantic Tropical Cyclones: Climatology, Analysis, and Seasonal Applications". Hurricane Risk. Springer, pp. 43-69.

Laurila, T. K. et al., 2019: The Extratropical Transition of Hurricane Debby (1982) and the Subsequent Development of an Intense Windstorm over Finland. *Monthly Weather Review* **148**, 377-401

Lee, C. Y., Tippett, M. K., Sobel, A. H., & Camargo, S. J. (2018). An environmentally forced tropical cyclone hazard model. *Journal of Advances in Modeling Earth Systems*, **10**(1), 223-241.

Liu, M. et al., 2017: The Present-Day Simulation and Twenty-First-Century Projection of the Climatology of Extratropical Transition in the North Atlantic. *Journal of Climate* **30**, 2739-2756.

Liu, M., Vecchi, G.A., Smith, J.A. et al, 2019. Causes of large projected increases in hurricane precipitation rates with global warming. *npj Clim Atmos Sci* **2**, 38.

Mahendran, M. (1998): Cyclone intensity categories. *Weather and forecasting*, **13**.3, 878-883.

Met Office (2017) Ex-hurricane Ophelia 16 October 2017.
<https://www.metoffice.gov.uk/binaries/content/assets/metofficegovuk/pdf/weather/learn-about/uk-past-events/interesting/2017/ex-hurricane-ophelia-16-october-2017---met-office.pdf>

Michaelis, A. C., and G. M. Lackmann, 2019: Climatological Changes in the Extratropical Transition of Tropical Cyclones in High-Resolution Global Simulations. *Journal of Climate* **32**, 8733-8753

Molod, A. et al., 2015: Development of the GEOS-5 atmospheric general circulation model: evolution from MERRA to MERRA2. *Geosci. Model Dev.* **8**, 1339-1356

Munich Re (2018): The natural disasters of 2018 in figures.
<https://www.munichre.com/topics-online/en/climate-change-and-natural-disasters/natural-disasters/the-natural-disasters-of-2018-in-figures.html>

Neal R, Fereday D, Crocker R, Comer RE (2016) A flexible approach to defining weather patterns and their application in weather forecasting over Europe. *Meteorological Applications* **23**:389-400.

Nemry F, Demirel H (2012) *Impacts of climate change on transport: a focus on road and rail transport infrastructures*. JRC Scientific and Policy Reports. Report EUR 25553 EN. European Commission, Joint Research Centre, Institute for Prospective Technological Studies. Office of the European Union, Luxembourg. Retrieved from <ftp://ftp.jrc.es/pub/EURdoc/JRC72217.pdf>.

Onogi, K. et al., 2007: The JRA-25 Reanalysis. *Journal of the Meteorological Society of Japan. Ser. II* **85**, 369-432

Ostermeier, G. M., and J. M. Wallace (2003) Trends in the North Atlantic Oscillation–Northern Hemisphere Annular Mode during the Twentieth Century. *J. Climate*, **16**, 336–341.

Palin EJ, Thornton HT, Mathison CT, McCarthy RE, Clark RT, Dora J (2013) Future projections of temperature-related climate change impacts on the railway network of Great Britain. *Climatic Change*, **120**, 71-93.

Palin EJ, Guentchev GS, Lockwood J (2018) Exploring user needs for climate risk assessment in the transport sector: how could global high-resolution climate models help? Proceedings of 7th Transport Research Arena TRA 2018, April 16-19, 2018, Vienna, Austria. <http://doi.org/10.5281/zenodo.1962772>

Pfahl, S., O'Gorman, P. A., & Fischer, E. M. (2017). Understanding the regional pattern of projected future changes in extreme precipitation. *Nature Climate Change*, 7(6), 423-427.

Pinto, J. G. et al., 2013: Development of a novel Pan-European Windstorm Model, *EGU General Assembly 2013, held 7-12 April, 2013 in Vienna, Austria*, id. EGU2013-10995, <https://ui.adsabs.harvard.edu/abs/2013EGUGA..1510995P/abstract>

Powell, M. D. & Reinhold, T. A. (2007): Tropical cyclone destructive potential by integrated kinetic energy. *Bulletin of the American Meteorological Society*, 88.4, 513-526.

Powell, M. D., Vickery, P. J. & Reinhold, T. A. (2003): Reduced drag coefficient for high wind speeds in tropical cyclones. *Nature*, 422.6929, 279-283.

ProRail (undated) Lente en zomer. Retrieved from <https://www.prorail.nl/reizigers/weersinvloeden/lente-en-zomer>. (In Dutch.)

ProRail (2019) ProRail neemt hittemaatregelen in hete week. Retrieved from <https://www.prorail.nl/nieuws/prorail-neemt-hittemaatregelen-in-hete-week>. (In Dutch.)

Rappaport, E. N. (2014). Fatalities in the United States from Atlantic tropical cyclones: New data and interpretation. *Bulletin of the American Meteorological Society*, 95(3), 341-346.

Ravestein, P., Van der Schrier, G., Haarsma, R., Scheele, R., & Van den Broek, M. (2018). Vulnerability of European intermittent renewable energy supply to climate change and climate variability. *Renewable and Sustainable Energy Reviews*, 97, 497-508.

Rienecker, M. M. et al., 2011: MERRA: NASA's Modern-Era Retrospective Analysis for Research and Applications. *Journal of Climate* **24**, 3624-3648

Risser, M. D., & Wehner, M. F. (2017). Attributable human-induced changes in the likelihood and magnitude of the observed extreme precipitation during Hurricane Harvey. *Geophysical Research Letters*, 44(24), 12-457.

RMS (2000) Windstorms Lothar and Martin. https://forms2.rms.com/rs/729-DJX-565/images/ws_1999_windstorms_lothar_martin.pdf

RMS (2007) The Great Storm of 1987: 20-year retrospective.
https://forms2.rms.com/rs/729-DJX-565/images/ws_1987_great_storm_20_retrospective.pdf

Roberts JF, Champion AH, Dawkins LC, Hodges KI, Shaffrey LC, Stephenson DB, Stringer MA, Thornton HE, Youngman BD (2014) The XWS open access catalogue of extreme European windstorms from 1979 to 2012. *Natural Hazards and Earth System Science* 14 2487-2501

Roberts, M. J. et al., 2020: Impact of Model Resolution on Tropical Cyclone Simulation Using the HighResMIP–PRIMAVERA Multimodel Ensemble. *Journal of Climate* **33**, 2557-2583

Roberts, M., Camp, J., Seddon, J., Vidale, P. L., Hodges, K., Vanniere, B., Mecking, J., Haarsma, R., Bellucci, A., Scoccimarro, E. et al. (2020): Projected Future Changes in Tropical Cyclones using the CMIP6 HighResMIP Multi-model Ensemble. Submitted.

Saha, S. et al., 2010: The NCEP Climate Forecast System Reanalysis. *Bulletin of the American Meteorological Society* **91**, 1015-1058

Saha, S. et al., 2014: The NCEP Climate Forecast System Version 2. *Journal of Climate* **27**, 2185-2208

Schiemann, R., Demory, M. E., Shaffrey, L. C., Strachan, J., Vidale, P. L., Mizielinski, M. S., ... & Jung, T. (2017). The resolution sensitivity of Northern Hemisphere blocking in four 25-km atmospheric global circulation models. *Journal of Climate*, 30(1), 337-358.

Schiemann, R., Athanasiadis, P., Barriopedro, D., Doblas-Reyes, F., Lohmann, K., Roberts, M. J., ... & Vidale, P. L. (2020). The representation of Northern Hemisphere blocking in current global climate models. In open review for Weather and Climate Dynamics. *Weather and Climate Dynamics*.

Scoccimarro, E., Gualdi, S., Villarini, G., Vecchi, G. A., Zhao, M., Walsh, K., & Navarra, A. (2014). Intense precipitation events associated with landfalling tropical cyclones in response to a warmer climate and increased CO₂. *Journal of climate*, 27(12), 4642-4654.

Semmler, T. et al., 2008: Regional model simulation of North Atlantic cyclones: Present climate and idealized response to increased sea surface temperature. *Journal of Geophysical Research: Atmospheres* **113**, D02107

Shepherd, T. G. (2014). Atmospheric circulation as a source of uncertainty in climate change projections. *Nature Geoscience*, 7(10), 703-708.

Shepherd, T. G. (2019). Storyline approach to the construction of regional climate change information. *Proceedings of the Royal Society A*, 475(2225), 20190013.

Squintu, A., G. van der Schrier, E. van den Besselaar, E. van der Linden, E. Scocciamarro, C. Roberts, A. Klein Tank, (2020) Evaluation of trends in extreme temperatures simulated by HighResMIP models across Europe. *Climate Dynamics*, under review.

Steptoe, H. (2017) C3S WISC Event set description, *Copernicus Climate Change Service technical report: C3S_441_Lot3_WISC_SC2-D3.2.1-CGI-RP-17-0080*, https://wisc.climate.copernicus.eu/wisc/documents/shared/C3S_WISC_Event%20Set_Description_v1.0.pdf

Stewart, S. R., 2018: Hurricane Ophelia (AL172017). *National Hurricane Center Tropical Cyclone Report*, www.nhc.noaa.gov/data/tcr/AL172017_Ophelia.pdf

Studholme, J. et al., 2015: Objective determination of the extratropical transition of tropical cyclones in the Northern Hemisphere. *Tellus A: Dynamic Meteorology and Oceanography* **67**, 24474

Thornton, H. E., Scaife, A. A., Hoskins, B. J., & Brayshaw, D. J. (2017). The relationship between wind power, electricity demand and winter weather patterns in Great Britain. *Environmental Research Letters*, 12(6), 064017.

Trenberth, K. E., Fasullo, J. T., & Shepherd, T. G. (2015). Attribution of climate extreme events. *Nature Climate Change*, 5(8), 725-730.

UNFCCC (2015) The Paris Agreement. <https://unfccc.int/process-and-meetings/the-paris-agreement/the-paris-agreement>

Vajda A, Tuomenvirta T, Jokinen P, Luomaranta A, Makkonen L, Tikanmaki M, Groenemeijer P, Saarikivi P, Michaelides S, Papadakis M, Tymvios F, Athanastos S (2011) Probabilities of adverse weather affecting transport in Europe: climatology and scenarios up to the 2050s. Finnish Meteorological Institute. Reports 2011:9. Helsinki.

van den Hurk, B., van Meijgaard, E., de Valk, P., van Heeringen, K. J., & Gooijer, J. (2015). Analysis of a compounding surge and precipitation event in the Netherlands. *Environmental Research Letters*, 10(3), 035001.

van der Linden, E., R. Haarsma, G. van der Schrier, (2019). Impact of climate model resolution on soil moisture projections in central-western Europe. *Hydrol. Earth Syst. Sci.*, 23, 191-206. <https://doi.org/10.5194/hess-23-191-2019>.

Van Oldenborgh, G. J., Van Der Wiel, K., Sebastian, A., Singh, R., Arrighi, J., Otto, F., ... & Cullen, H. (2017). Attribution of extreme rainfall from Hurricane Harvey, August 2017. *Environmental Research Letters*, 12(12), 124009.

Vanniere, B., M. J. Roberts, P. L. Vidale, K. I. Hodges, M.-E. Demory, L.-P. Caron, E. Scocciamarro, L. Taurent, R. Senan, The moisture budget of tropical cyclones in

HighResMIP models : large-scale environmental balance and sensitivity to horizontal resolution. *Journal of Climate, under review.*

Vecchi, G. A. et al., 2019: Tropical cyclone sensitivities to CO₂ doubling: roles of atmospheric resolution, synoptic variability and background climate changes. *Climate Dynamics* **53**, 5999-6033

Veers, P., Dykes, K., Lantz, E., Barth, S., Bottasso, C. L., Carlson, O., ... & Laird, D. (2019). Grand challenges in the science of wind energy. *Science*, 366(6464), eaau2027.

Volodire, A., Saint-Martin, D., Senesi, S., Decharme, B., Alias, A., Chevallier, M., Colin, J., Gueremy, J.-F., Michou, M., Moine, M.-P. et al., (2019): Evaluation of CMIP6 DECK Experiments With CNRM-CM6-1. *Journal of Advances in Modeling Earth Systems*, 11.7, 2177-2213.

Welker, C. et al., 2020 (in review): Comparing an insurer's perspective on building damages with modelled damages from pan-European winter windstorm event sets: a case study from Zurich, Switzerland, *Nat. Hazards Earth Syst. Sci. Discuss.*, <https://doi.org/10.5194/nhess-2020-115>

Williams, KD, van Niekerk, A, Best, MJ, et al. (2020) Addressing the causes of large-scale circulation error in the Met Office Unified Model, *QJR Meteorol Soc.*, 1–17.

Youngman, B. D and Stephenson, D.B., 2016: A geostatistical extreme-value framework for fast simulation of natural hazard events, *Proc. R. Soc. A.47220150855*, <http://doi.org/10.1098/rspa.2015.0855>

Zappa, G., Hoskins, B. J., & Shepherd, T. G. (2015). The dependence of wintertime Mediterranean precipitation on the atmospheric circulation response to climate change. *Environmental Research Letters*, 10(10), 104012.

Zarzycki, C. M. et al., 2017: Objective tropical cyclone extratropical transition detection in high-resolution reanalysis and climate model data. *Journal of Advances in Modeling Earth Systems* **9**, 130-148

Zappa, G. et al., 2013: The ability of CMIP5 models to simulate North Atlantic extratropical cyclones. *Journal of Climate*, **26** (15), 5379-5396. ISSN 1520-0442 doi: <https://doi.org/10.1175/JCLI-D-12-00501.1>

Zappa, G. (2019). Regional Climate Impacts of Future Changes in the Mid-Latitude Atmospheric Circulation: a Storyline View. *Current Climate Change Reports*, 5(4), 358-371.

Zhai, A. R. & Jiang, J. H. (2014): Dependence of US hurricane economic loss on maximum wind speed and storm size. *Environmental Research Letters*, 9.6.